Gating mechanisms underlying deactivation slowing by atrial fibrillation mutations and small-molecule activators of KCNQ1

Gary Peng

Submitted in partial fulfillment of the
requirements for the degree of
Doctor of Philosophy
under the Executive Committee
of the Graduate School of Arts and Sciences

COLUMBIA UNIVERSITY
2017

ABSTRACT

Gating mechanisms underlying deactivation slowing by atrial fibrillation mutations and small-molecule activators of KCNQ1

Gary Peng

Ion channels are membrane proteins that facilitate electrical signaling in important physiological processes, such as the rhythmic contraction of the heart. KCNQ1 is the pore-forming subunit of a voltage-gated potassium channel that assembles with the β-subunit KCNE1 in the heart to generate the I_{Ks} current, which is critical to cardiac action potential repolarization and electrical conduction in the heart. Mutations in I_{Ks} subunits can cause potentially lethal arrhythmia, including long QT syndrome, short QT syndrome, and atrial fibrillation. Each channel consists of four voltage-sensing domains and a central pore through which ions permeate. Voltage-dependent gating occurs when movement of voltage sensors cause pore opening/closing through coupling mechanisms. Although KCNQ1 by itself is able to form a voltage-dependent potassium channel, its assembly with KCNE1 is essential to generating the physiologically critical cardiac I_{Ks} current, characterized by a delay in the onset of activation, an increase in current amplitude, and a depolarizing shift in the current-voltage relationship. KCNE1 is thought to have multiple points of contact with KCNQ1 that reside within both the voltage-sensing domain and the pore domain, allowing for extensive modulation of channel function.

Atrial fibrillation is the most common cardiac arrhythmia and affects more than 3 million adults in the United States. Much rarer, genetic forms of atrial fibrillation have been associated with gain-of-function mutations in KCNQ1, such as two adjacent mutations, S140G and V141M.

Both mutations drastically slow channel deactivation, which underlies their pathophysiology. Deactivation slowing causes accumulation of open channels in the context of repeated stimulation, which abnormally increases the repolarizing K^+ current, excessively shortens the action potential duration, and predisposes to re-entry arrhythmia such as atrial fibrillation. Although both mutations are located in the voltage-sensing domain, their mechanisms of action remain unknown. Understanding the gating mechanisms underlying deactivation slowing may provide key insights for the development of mechanism-based pharmacologic therapies for arrhythmias associated with KCNQ1 mutations.

In addition to gain-of-function mutations, molecular activators of KCNQ1 can slow deactivation and increase channel activity. An existing problem in the pharmacologic treatment of arrhythmia is that many antiarrhythmic drugs do not have specific targets and cause undesired side effects such as additional arrhythmia. Thus, developing mechanism-based therapies may optimize clinical treatment for patients with specific forms of channel dysfunction. Two KCNQ1 activators, ML277 and R-L3, have been previously shown to slow current deactivation, but the underlying gating mechanisms remain known. Although these modulators are unlikely to serve directly as antiarrhythmic therapy, investigating their mechanisms will likely provide fundamental insights on channel modulation and guide future efforts to develop personalized therapies for arrhythmia, such as congenital long QT syndrome.

Given the central importance of deactivation slowing in both pathophysiology and pharmacology, we focused on investigating gating mechanisms that underlie deactivation slowing. To this end, we utilized voltage clamp fluorometry, a technique that simultaneously assays for voltage sensor movement and ionic current through the channel pore. In Chapter 1, we begin our study by examining the gating mechanisms of KCNQ1 atrial fibrillation mutations

in the absence of KCNE1. We show that S140G slows voltage sensor deactivation, which indirectly slows current deactivation. On the other hand, V141M neither slows voltage sensor nor current deactivation. This is followed by Chapter 2, where we examine the gating mechanisms underlying deactivation slowing by atrial fibrillation mutations in the presence of KCNE1. We show that both S140G and V141M slow I_{Ks} deactivation by slowing pore closing and altering voltage sensor-pore coupling. Based on these findings, we proposed a molecular mechanism in which both mutations disrupt the orientation of KCNE1 relative to KCNQ1 and thus impede pore closing, implying that future efforts to modulate KCNQ1 function can benefit from targeting the β-subunit. Finally, in Chapter 3, we explore the gating mechanisms underlying deactivation slowing for two small-molecule activators of KCNQ1. We show that ML277 predominantly slows pore transitions, whereas R-L3 slows voltage sensor deactivation, which indirectly slows current deactivation. Taken together, these studies guide future efforts to develop mechanism-based therapies for arrhythmia.

Table of Contents

List of Charts, Graphs, Illustrations

List of Abbreviations

APD – action potential duration

AKAP-9 – A-kinase anchoring protein 9 (also known as yotiao)

ciVSP - voltage-sensing phosphatase from *Ciona intestinalis*

CTD – C-terminal domain

EAD – early afterdepolarization

DAD – delayed afterdepolarization

I_{Ks} – slow delayed rectifier potassium current

I_{Ks}^{S140G} and I_{Ks}^{V141M} – mutant KCNQ1 co-expressed with KCNE1

JLNS – Jervell and Lange-Nielsen syndrome

K_V – voltage-gated potassium channel

$KCNQ1^{S140G}$ and $KCNQ1^{V141M}$ – mutant KCNQ1 in the absence of KCNE1

LQTS – long QT syndrome

PIP_2 – phosphatidylinositol 4,5-bisphosphate

PKA – protein kinase A

SQTS – short QT syndrome

VCF – voltage clamp fluorometry

VSD – voltage-sensing domain

Acknowledgments

First and foremost, I would like to thank my thesis advisor Robert Kass for allowing me to pursue my research interests in his laboratory and teaching me electrophysiology. It has been an honor being his Ph.D. student. He provided a supportive and collaborative environment that fostered growth in my scientific abilities. I am deeply grateful for his continuous support and guidance.

I cannot thank enough all members of the Kass Lab for their help during my graduate studies. Working with them has been superbly fun, exciting, and informative. I want to thank Kevin Sampson, Lei Chen, Vivek Iyer, and Cecile Terrenoire for their immense support and encouragement. They have taught me so much. I am grateful to have the support of fellow graduate students Seth Robey, Mia Shandell, and Michael Bohnen, who continue to motivate and inspire me with their own wonderful work. Thank you to Jenny Rao for keeping the lab in order and for all your technical expertise.

I am deeply grateful for H. Peter Larsson for allowing me to come to his lab in Miami and learn VCF. More importantly, I treasure my scientific discussions with him throughout my graduate studies. I also thank Rene Barro-Soria for kindly lending his time and teaching me VCF. His help was instrumental to my project. In addition, I want to thank Marta Elena Perez for additional technical help.

My thesis work would not be possible without the support and guidance of my thesis committee: Henry Colecraft, Richard Robinson, and Steven Marx. I also want to thank Jian Yang for partaking in my defense committee. A special thanks to Zaia Sivo for guiding my graduate studies every step of the way and organizing incredibly fun and educational retreats for the Integrated Program. I also thank Karen Allis, Felisha Young, Rozanna Yakub, and Jeffrey

Brandt for all of their help and support. I would like to acknowledge Alexandra Bussek, Kristi Van Den Berghe and others at Ecocyte Bioscience US LLC for providing great oocytes that made the VCF experiments possible. In addition, I want to thank the mentorship of the MD/PhD directors Steven Reiner, Ronald Liem and Patrice Spitalnik.

My time at Columbia has been largely been made enjoyable by friends and colleagues, whose talents and skills continue to inspire me. I am grateful that my time in New York City has allowed me to forge new friendships and strengthen old ones. Last but not least, I want to thank my wonderful parents for their wisdom, encouragement, and unconditional love. They have been there for me since day one, and too often I forget how incredibly lucky I am to be their son. I cannot ever thank them enough.

DEDICATION

To the memory of my grandmother, Kuang Qingshu (1926 - 2015),

for her love and care.

INTRODUCTION

The Cardiac Action Potential

Electrical signals propagate through the heart to cause the coordinated and rhythmic contraction of cardiac muscles, allowing efficient pumping of blood into the vasculature[1]. Normal electrical activity in the heart originates in the sinoatrial node, propagates through the atria to reach the atrioventricular node, and then travels through the bundle of His, the bundle branches, and the Perkinje fibers to reach the ventricles. Electrical stimulation of cardiomyocytes results in a sequence of changes in the cellular membrane potential over time known as the cardiac action potential. These changes in the membrane potential are driven by the summation of a variety of cellular ionic currents with different time-dependent profiles (Fig. I1). Ionic currents flow through membrane proteins known as ion channels, whose unique structural, gating, and pharmacologic properties give rise to distinct types of currents.

The action potential in a normal ventricular cardiomyocyte begins at a resting potential of approximately -85 mV[2]. This potential is close to the potassium equilibrium potential because of open inwardly rectifying potassium channels. Upon electrical stimulation, voltage-gated sodium channels, predominantly $Na_V1.5$, open to allow influx of sodium ions. This depolarizes the cell to approximately +30 mV in a rapid upstroke. The rate of upstroke correlates with the speed of electrical propagation across the cardiac tissue and can be modulated. This is followed by the inactivation of sodium currents and activation of transient outward potassium currents, which briefly repolarize the cell and give rise to a notch in the action potential. Next is the plateau phase, where there is concomitant activation of L-type calcium channels (predominantly $Ca_V1.2$) and the delayed rectifier potassium currents (I_{Ks} and I_{Kr}). The delicate balance between inward calcium currents and outward potassium currents maintain the plateau potential. Calcium influx

also triggers the release of calcium from the sarcoplasmic reticulum into the cytosol, a process known as calcium-induced calcium release. This process is critical to excitation-contraction coupling. Released calcium binds to troponin-C, allows myosin to interact with actin, and causes cardiomyocytes to contract. Eventually, inactivation of calcium channels causes potassium currents to dominate and repolarize the membrane potential back to resting level. There is a refractory period in which sodium channels have yet to recover from inactivation and thus is unresponsive to stimulation. The cell remains at the resting potential for some time, during which cardiomyocytes relax and allow heart chambers to fill with blood before the next cycle of contraction.

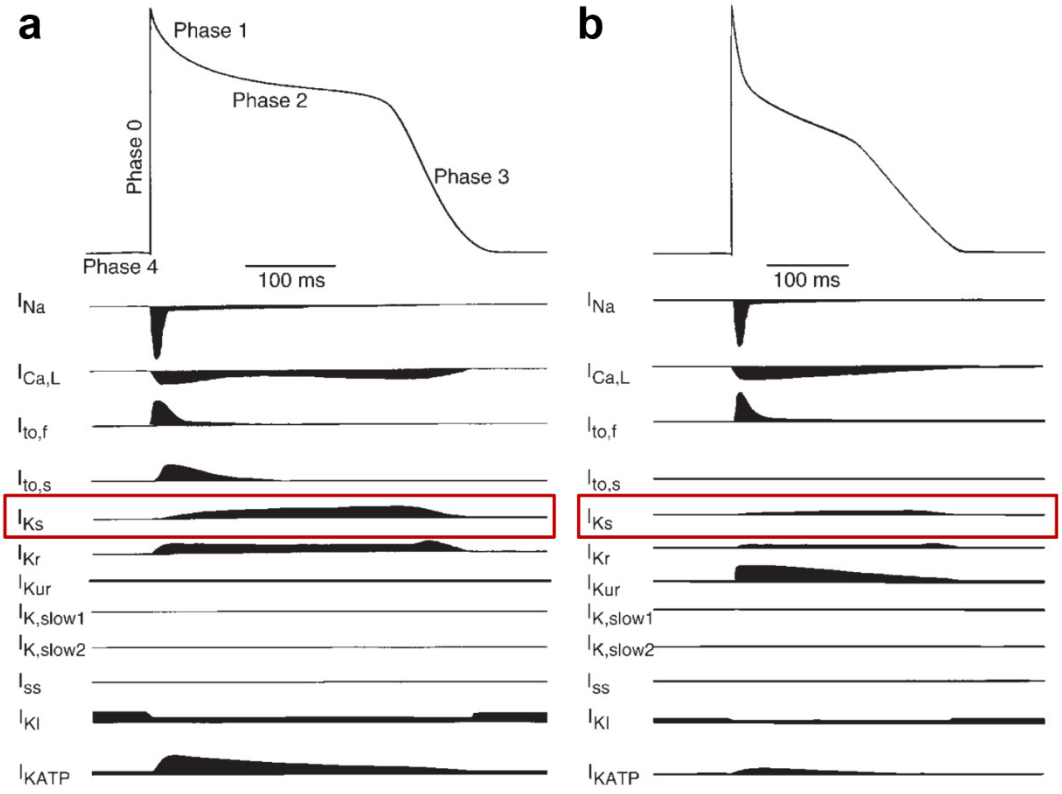

Figure I1. The cardiac ventricular and atrial action potential. The ventricular (a) and atrial (b) action potential are depicted as membrane potential vs. time. The time-dependent profiles of ionic currents that contribute each action potential are shown underneath. I_{Ks}, the slow delayed rectifier potassium current, is an outward current that contributes to both the plateau phase and the repolarization phase of the ventricular action potential, but contributes less to the action potential of atrial cardiomyocytes. Figure from Nerbonne, J. M. & Kass, R. S., 2005.

The action potential duration (APD) varies between cells from different regions of the heart. For example, atrial cardiomyocytes have shorter APD than ventricular cardiomyocytes due to differences in underlying ionic currents[1]. In particular, $I_{K(ultrarapid)}$ is an atrial-specific outward potassium current that is thought to contribute to larger repolarizing currents and shorter APD in atrial cardiomyocytes[1]. Although I_{Ks} is also present in atrial cardiomyocytes, it is thought to play a smaller role in atrial repolarization.

Control of the APD is critical to normal cardiac function. Excessive prolongation or shortening of the APD can predispose individuals to potentially lethal arrhythmia[2]. Action potential prolongation can manifest on an electrocardiogram (EKG) as a prolonged QT interval, such as in patients with long QT syndrome (LQTS)[2]. Drug-induced LQTS results from drugs which inadvertently inhibit ionic currents (particularly I_{Kr}), whereas congenital LQTS often results from disease mutations in ion channels that underlie cardiac currents such as I_{Ks}, I_{Kr}, and I_{Na}. When the action potential is prolonged, sodium and calcium currents may recover from inactivation prior to termination of the action potential, leading to an abnormal pattern of depolarization known as early afterdepolarization (EAD). EADs can cause degeneration of cardiac rhythm into a sinusoidal wave pattern known as *torsades de pointes,* which may lead to ventricular fibrillation and sudden cardiac death. An alternative mechanism for arrhythmic events is delayed afterdepolarization (DAD), which results from intracellular calcium overload that occurs under prolonged action potentials. On the other hand, pathological shortening of the action potential can decrease the refractory period of cardiomyocytes and predispose to re-entry arrhythmia such as atrial fibrillation. This mechanism is also thought to underlie arrhythmic events seen in patients with short QT syndrome (SQTS). Given the association between

abnormal APD and disease, maintenance of normal APD is critically important to normal cardiac function.

I_{Ks}, the slow delayed rectifier potassium current

I_{Ks}, an outward current with unique kinetic and voltage-dependent properties, plays a key role in the repolarization of the cardiac action potential[1]. In 1969, the delayed rectifier potassium current was studied in sheep Purkinje fibers and shown to possess two kinetically distinct components[3]. These currents were later pharmacologically dissected in guinea pig ventricular myocytes into I_{Ks} and I_{Kr}[4]. I_{Ks} is slowly-activating and most prominent during the plateau and repolarizing phases of the cardiac action potential, where it contributes to counterbalancing calcium influx and repolarizing the action potential. Expression of I_{Ks} has been demonstrated in both human atrial and ventricular myocytes[5-7]. In addition, it has also been measured in cardiomyocytes from non-human mammalian species including dogs[8-12] and rabbits[13]. On the other hand, I_{Ks} is expressed at very low levels or absent in mouse hearts[14].

The central role of I_{Ks} in normal cardiac conduction became more evident when it was discovered that mutations causing loss of I_{Ks} function leads to congenital LQTS (Fig. I2). Jervell and Lange-Nielsen syndrome (JLNS), the autosomal recessive form of congenital LQTS, has so far only been associated with mutations causing loss of I_{Ks} function[15,16]. An additional feature of JLNS is sensorineural deafness, which is consistent with the finding that I_{Ks} is expressed in the inner ear and facilitates K^+ secretion into the endolymph[17]. Nonetheless, the majority of LQTS arising from I_{Ks} mutations are autosomal dominant in a condition known as Romano-Ward syndrome, which is not associated with deafness[18,19].

Importantly, I_{Ks} is subject to upregulation by β-adrenergic stimulation to control APD in the face of sympathetic nerve activity[20,21]. During sympathetic activation such as in exercise, adrenergic stimulation augments I_{Ks}, which counterbalances the concomitant increase in calcium currents, prevents prolongation of the cardiac APD, and allows for adequate diastolic filling times between heart beats[22]. However, insufficient I_{Ks} activation such as in LQT1 results in failure to counterbalance the calcium influx, prolonging the APD and increasing susceptibility to arrhythmia. This is consistent with exercise being a key trigger of cardiac events in LQT1 patients[23]. Normal I_{Ks} function is therefore critical to maintaining normal electrical activity of the heart, especially under stressful conditions. Given this, understanding the properties of ion channels that underlie physiologically important currents such as I_{Ks} would be an important step to investigating mechanisms of disease.

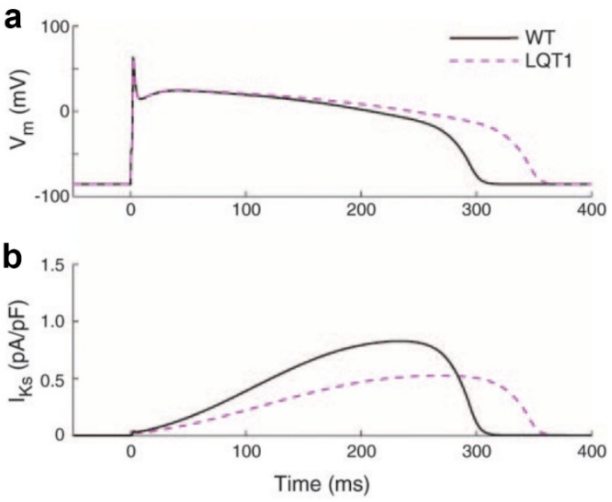

Figure I2. Simulating the effect of I_{Ks} loss-of-function on action potential duration. (a) Simulated steady-state action potential waveform for control (WT) and following I_{Ks} loss-of-function (LQT1). (b) Corresponding I_{Ks} current profile for wildtype and in loss-of-function. LQT1 mutations reduce the amplitude of the outward I_{Ks}, thus prolonging the APD. Figure from Nerbonne, J. M. & Kass, R. S., 2005.

General Properties of Ion Channels

Ion channels are proteins on the plasma membrane that underlie many ionic currents in the heart. Coordination among ion channels facilitates the ionic balance necessary for the generation of an action potential and normal electrical propagation through excitable membranes. These channels create specialized pores in the membrane through which ions may passively

diffuse down their electrochemical gradient at high rates. The channel pore contains a selectivity filter with distinctive atomic components to allow for selective permeation of ions[24-26].

The ion channel pore can open and close in response to a variety of signals. Some ion channels exhibit voltage-dependent gating, in which changes in membrane potential cause conformational changes in voltage-sensing domains and lead to pore opening or closing[27]. Examples include voltage-gated sodium and potassium channels, whose gating properties make them useful in the propagation of action potentials. In contrast, ligand-gated ion channels undergo conformational changes upon binding to signaling molecules[28]. These channels are particularly important in neuronal synaptic transmission and signaling at the neuromuscular junction. On the other hand, mechanosensitive channels are opened by physical stretch and play important roles in touch and hearing[29]. A group of ion channels known as inward rectifier potassium channels allow influx potassium ions but do not conduct outward currents. Rectification is not an intrinsic property of these ion channels; instead, it is due to intracellular magnesium ions that plug the pore at depolarized voltages. Thus, although these channels lack intrinsic gating mechanisms, conductance of ions appears voltage-dependent[30]. To add even greater diversity, some channels display combinations of the abovementioned gating properties.

Diversity in ion channel function also depends on a variety of molecular entities that contribute to their trafficking, stabilization, signaling, and function[1]. For example, accessory subunits are proteins that can associate with ion channels to modify their properties and generate physiologically significant currents[31,32]. Mutations in accessory subunits are implicated in genetic diseases, underscoring their physiological importance[33]. In addition, accessory subunits can alter ion channel response to activators and inhibitors and therefore are important to consider in designing drugs that target physiologically relevant ion channels[34]. In addition to accessory

subunits, cytoskeleton-associated proteins such as ankyrin and syntrophin are known to interact with and stabilize ion channels in the plasma membrane[2]. Mutations in ankyrin and syntrophin are known to disrupt ion channel function and are associated with LQTS. Thus, ion channels interact with surrounding proteins to fulfill their varied physiological roles. The nature of these interactions are oftentimes informed by structural information.

Structure of Voltage-gated Potassium Channels

The superfamily of voltage-gated potassium (K_V) channels plays central roles in physiology, particularly in repolarizing action potentials in excitable tissue. In general, each voltage-gated potassium channel consists of four identical subunits, and each subunit contains six transmembrane helices (Fig. I3 a). The S1-S4 helices comprise the voltage-sensing domain (VSD) and includes the positively charged S4 that respond to changes in membrane potential. The helices S5, S6, and the linker in-between comprise the pore domain and line the pathway of ion permeation. This linker is known as the P-loop and contains the selectivity filter. Between the VSD and the pore domain is the S4-S5 linker, which physically couples the VSD to the pore. Structural insights on the K_V superfamily are mainly derived from crystal structures of the Shaker channel, which was the first cloned K_V channel and is considered the prototype of the K_V family[35,36]. These structural insights shed light on channel function and are summarized below.

The pore of the K_V1.2 (Shaker) channel is located at the center and is formed by the pore domains of four channel subunits[26] (Fig. I3 b). The structure of the pore is similar to that of KcsA, a previously crystallized voltage-independent potassium channel[37]. The selectivity filter is located near the extracellular side of the channel and allows for the selective permeation of

potassium ions (Fig. I3 c). It contains rings of electronegative oxygen atoms arranged in specific atomic dimensions that coordinate with potassium ions and provides the necessary stabilization energy to remove water molecules[38]. As water molecules are stripped away, potassium ions pass through the filter. Larger ions do not pass through the filter as easily because of geometric constraints. On the other hand, smaller ions (ex. Na^+) do not coordinate with the oxygen atoms in the selectivity filter as tightly as K^+ and therefore are less energetically favored to lose water molecules. As a result, the Na^+-H_2O complex is too large to pass through the selectivity filter. The selective permeation of K^+ ions allow K_V channels to effectively repolarize the cell membrane to negative potentials.

Beneath the selectivity filter is a water-filled central cavity whose properties can influence ion conduction[37] (Fig. I3 c). For example, a higher density of negative charges lining the central cavity is thought to attract K^+ ions and contribute to increased K^+ conductance in BK channels[39]. Underneath the central cavity, the intracellular ends of four S6 helices cross

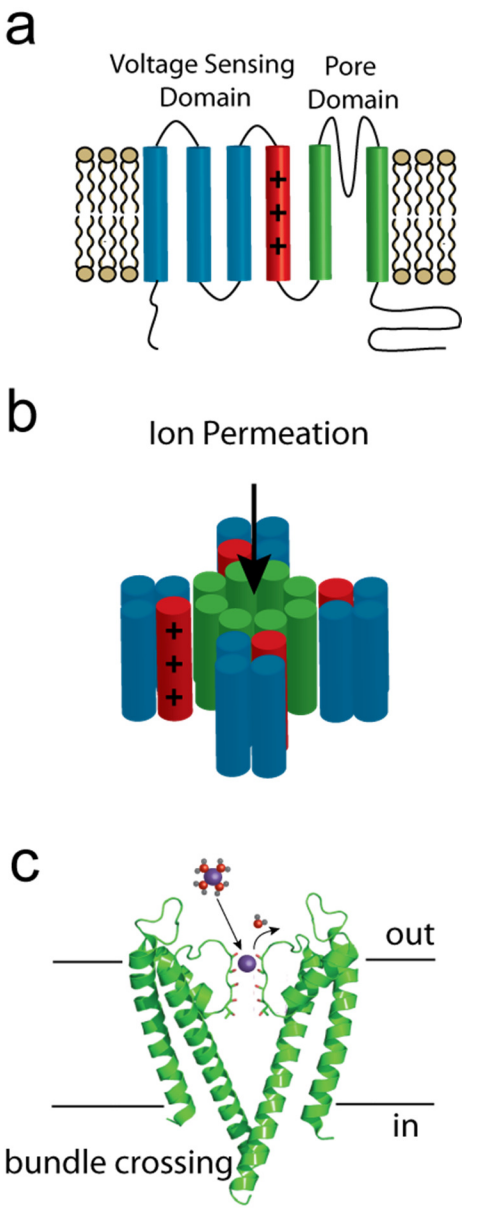

Figure I3. Structure of voltage-gated potassium channels. (a) Topology of a generic voltage-gated potassium channel. (b) Cartoon representation of the 3-dimentional structure of a generic voltage-gated potassium channel. (c) The 3-D crystal structure of a potassium channel pore. Only two subunits are shown for clarity. The precise geometry of the selectivity filter provides energetic stabilization for potassium ions (purple), resulting in selective permeation. Figure from Jeremiah Osteen.

each other to form the inner helix-bundle, which constricts and dilates to close and open the channel respectively. This is thought to be the activation gate of the channel. Gating can be controlled by movement of the VSD, which is coupled to the gate.

Each K_V1.2 (Shaker) channel contains four VSDs located at the perimeter of the channel pore[26] (Fig. I3 b). The VSDs appear to be structurally independent from the pore with only few points of contact. In fact, chimeric channels containing VSDs of one protein and the pore domains of another can undergo voltage-dependent gating, supporting the modular nature of VSDs[40,41]. The S4-S5 linker provides a physical connection between the VSD and the channel gate, thereby coupling voltage sensor movement to pore opening/closing. Domain-swapping is observed in K_V1.2, such that the voltage-sensing domain of one subunit is spatially juxtaposed to the pore-forming helices of an adjacent subunit. The domain-swapping leads to a geometric orientation that is thought to be important in VSD-pore coupling[42].

Pore domains and voltage-sensing domains are shared features among voltage-dependent ion channels. As such, crystallographic studies of K_V1.2 have provided a critically important framework for interpreting structural and functional information on other channels in the K_V superfamily[43], including KCNQ1. They have been particularly useful for describing the structural underpinnings of voltage-dependent gating processes, helping to align previously obtained functional data while guiding further investigation of gating mechanisms in K_V channels.

Mechanisms of Gating in Voltage-Dependent Channels

In 1952, Hodgkin and Huxley published a series of seminal studies on voltage-dependent potassium and sodium currents in the squid giant axon using the voltage-clamp technique[44-49].

Based on kinetic analyses, they developed kinetic models that postulated the presence of "gating particles" which undergo transitions in response to changes in membrane potential and cause current activation. Their prediction of 4 gating particles for the potassium current turned out to be remarkably consistent with the stoichiometry of 4 voltage sensors per channel. Their contributions created a framework of voltage-dependent gating that exerted widespread influence on the field of electrophysiology and would remain relevant in modern views of channel gating mechanisms.

S4 as the voltage sensor

Since the early studies of Hodgkin and Huxley, extensive efforts have been devoted to understanding how voltage-sensing occurs in ion channels. The gating particle proposed by Hodgkin and Huxley is now understood to be the S4 helix in voltage-gated ion channels, which contains positively charged residues that allow it to sense changes in membrane potential. The number of gating charges can be measured by blocking ionic currents through the channel pore and integrating the remaining gating current over time. Using this technique, the number of gating charges in the Shaker channel has been measured to be approximately $13e_0$[50-52]. Charge neutralization experiments show that the first four arginines on S4 are responsible for these gating charges. While some of the arginines are stabilized by electrostatic interactions with negatively charged residues on the S2 transmembrane helix[53,54], others face toward membrane lipids[27]. The balance of electrostatic and hydrophobic interactions is thought to be important in shaping the energetic landscape of voltage sensors[27].

Movement of the S4 through the plasma membrane has been demonstrated through a variety of experiments, though the extent of movement has been controversial. For example, S4

residues accessible to cysteine modification reagents from the intracellular side of the Shaker channel becomes accessible from the extracellular side following outward displacement of the S4[55], suggesting a large movement (>10 Å) of the S4 during activation. Similarly, experiments examining the rate of cysteine modification at a site close to the S4 suggest that the S4 translocates by >12 Å relative to the pore[56]. However, other studies of the Shaker channel suggest that the S4 undergoes small displacement within a concentrated electric field[57-60] created by aqueous crevices that penetrate into the voltage-sensing domain. This model is supported by data suggesting the presence of a hydrophilic permeation pathway across the VSD that is normally blocked by native channel residues[61-63]. Despite evidence from biophysical and biochemical studies, insight on the degree and nature of S4 movement has been hindered by a lack in crystallographic evidence. Because proteins are crystallized in the absence of an external electric field, nearly all crystal structures of potassium channels contain activated conformations of S4[43]. While molecular dynamic simulations have been useful in elucidating details of S4 movement[64], future studies may be required to provide conclusive answers.

S4 coupling to the channel pore

Whether large or small, S4 movement is coupled to the channel pore to control pore opening/closing. In the Shaker channel, voltage sensor-pore coupling is achieved by the S4-S5 linker, an amphipathic helix on the intracellular side of the plasma membrane that physically connects the S4 to the inner-helix bundle, also known as the channel gate[65]. Yet, coupling mechanisms vary between channels. The hERG channel, in contrast to Shaker, does not require an intact S4-S5 linker for voltage-dependent gating[66]. Instead, coupling may be mediated by domain-domain electrostatic interactions requiring membrane phospholipids. In addition, the

HCN channel is a cationic channel that is opened by hyperpolarization rather than depolarization, and generates the "funny current" that underlies the automaticity of cardiac pacemaker cells. Interestingly, the voltage sensors of HCN, like those of K_V channels, still move outward in response to depolarization, suggesting that an altered voltage sensor-pore coupling mechanism underlies its reversed voltage-dependence[67]. Variations in coupling mechanisms therefore contribute to diversity in gating behavior that exists among voltage-dependent channels.

Inactivation

Some voltage-gated ion channels can inactivate and become non-conducting during sustained depolarization. Inactivation is therefore distinct from deactivation, where the channel gate closes upon repolarization. There are several types of inactivation with different underlying mechanisms. Clay Armstrong noticed that for potassium channels that do not inactivate, the addition of a TEA^+ molecule covalently bonded to a carbon chain to the intracellular solution can mimic channel inactivation[68]. Based on this result and others, Armstrong and Bezanilla proposed the "ball and chain" model of inactivation, in which a peptide "ball" linked to the channel by a peptide "chain" swings over to physically obstruct the channel pore[69]. After the Shaker channel was cloned, its N-terminus was found to contain multiple hydrophobic residues that are thought to plug the channel pore and cause inactivation[70]. This gave rise to the term N-type inactivation. This model was confirmed by the crystal structure of $K_V1.2$ in which the N-terminal peptide can fit snugly inside the pore to block conduction[26]. The other well studied form of inactivation in K_V channels is C-type inactivation, which is slower than N-type inactivation and is caused by a rearrangement of the channel pore and selectivity filter[71,72]. Interestingly, C-type inactivation is slowed by increasing extracellular K^+ concentration, which

may be attributed increased rate of K^+ binding to the mouth of the pore and stabilization of the open conformation[73]. C-type inactivation endows the hERG channel with an inward rectifying property[74,75], which is important physiologically. The hERG channel underlies the I_{Kr} current, which is relatively small at depolarized potentials during the plateau phase of the cardiac action potential. However, as repolarization begins, hERG channels recover from inactivation, prominently increasing I_{Kr} and quickly restoring cells to the resting potential.

Kinetic models of voltage-dependent gating

Kinetic processes such as S4 movement, pore opening/closing and inactivation can be represented in Markov models to simulate ion channel function. These kinetic models use a set of channel states and transitions defined by rate constants to describe gating. Kinetic models are always simplifications of reality, but the advantages of modeling are multifold. First, a good model provides a framework for interpreting electrophysiological data and sheds light on channel gating mechanisms. Second, models can be used to infer the mechanisms of effect of channel mutations and drugs that perturb channel gating. Third, models of individual ion channels can be incorporated into larger, *in silico* cellular models of action potential to study arrhythmogenesis.

When Hodgkin and Huxley studied the kinetics of voltage-dependent sodium and potassium currents in the squid giant axon, they proposed kinetic models to describe their observations and infer gating mechanisms. In order to simulate the potassium current, they utilized a model containing four identical gating particles that can activate or deactivate in response to changes in voltage. Activation and deactivation are transitions governed by rate constants[49]. In their kinetic scheme, the potassium currents turn on once all four particles are activated. On the other hand, sodium currents can be simulated if one of the four gating particles

was substituted by an inactivation particle. These models provided an early picture of channel gating that aligns remarkably well with present understanding. Kinetic models are therefore a useful tool to understanding gating processes that underlie channel function.

The accuracy of a kinetic model depends on the amount and accuracy of data used to constrain it. In addition to the kinetics of activation and deactivation, other biophysical properties such as steady-state activation and gating currents can used to constrain a kinetic model[76]. Furthermore, mutagenesis can be used to dissect state transitions that are otherwise difficult to distinguish in the wildtype channel[77]. These techniques led to a kinetic model of the Shaker channel in which four voltage sensors activate independently of one another. Furthermore, the model describes a two-step activation for each voltage sensor. Once all voltage sensors are fully activated, a final cooperative step leads to channel opening. As new constraining data are obtained from functional experiments, kinetic models can undergo further refinement and improvement.

Variations in kinetic gating schemes reflect the functional diversity of voltage-gated channels. Whereas the Shaker channel requires full activation of all voltage sensors prior to channel opening, functional data for the BK channel mSlo are consistent with an allosteric model of gating. In this gating scheme, independent activation of each voltage sensor increases the open probability[78,79]. An additional property of BK channels is calcium-dependent activation, which mediates important physiological processes such as spike frequency adaptation in neurons[80]. The allosteric model of mSlo accounts for calcium-dependent activation and suggests that calcium binds to open states to stabilize activation[81]. In addition to BK channels, the gating properties of HCN is also consistent with an allosteric gating scheme[82]. However, in the case of HCN, voltage sensor activation promotes channel closing, not opening, resulting in a reversed

voltage-dependence. Thus, differences in voltage-dependent gating schemes reflect the diversity of ion channels which are unique adapted to their physiological roles.

In addition to elucidating diversity of gating processes between different ion channels, kinetic models have provided insights on how accessory subunits modulate channel gating. For example, the β-subunit KCNE1 drastically alters the biophysical properties of KCNQ1 to generate the slowed delayed rectifier current, I_{Ks}. Multiple studies have utilized kinetic modeling to elucidate the effects of KCNE1 on KCNQ1 gating, in particular the alteration in coupling between voltage sensors and pore[83,84]. Below is a summary of the molecular and biophysical properties of channel subunits underlying I_{Ks} before an in-depth review of I_{Ks} gating mechanisms.

Molecular and biophysical properties of KCNQ1 and I_{Ks}

A pioneering step in identifying the ion channel underlying the I_{Ks} current was the discovery that the *KCNQ1* (*KvLQT1*) gene is linked to long QT syndrome type 1 and encodes a voltage-gated potassium channel[85]. The current conducted by this channel is minimally inactivating and its activation is relatively fast compared with any previously known current in the heart. However, soon it was shown that KCNQ1 together with the accessory protein KCNE1 (minK) generates I_{Ks}[31,32]. While KCNE1 had previously been thought to independently form a potassium channel[86,87], it was confirmed that KCNQ1 is actually the α- or pore-forming subunit of I_{Ks} while KCNE1 is a critical β- or modulatory subunit. Co-expression of KCNQ1 with KCNE1 generates the hallmark I_{Ks} current with slow activation. KCNQ1 and KCNE1 are expressed in all four chambers in the heart[88], as well as the inner ear[89,90], where I_{Ks} is thought to play a role in K^+ secretion into the endolymph[17]. This explains the observation that congenital

deafness is a key feature of JLNS. In addition, KCNQ1 and KCNE1 are expressed elsewhere in the body, including the pancreas, the kidneys, and the brain[91].

KCNQ1, the pore-forming subunit

Four subunits of KCNQ1 come together to form a channel that is capable of voltage-dependent gating (Fig. I4 b). Each KCNQ1 subunit, like most voltage-gated potassium channels, consists of six transmembrane helices[85] (Fig. I4 a). The helices S1-S4 comprise the voltage-sensing domain. In particular, the S4 helix contains positive charges and moves outward in response to membrane depolarization similar to other K_V channels[92-94]. Following the voltage-sensing domain is the pore domain, which consists of the S5, P-loop, and S6. Furthermore, the cytoplasmic linker between S4 and S5 plays important roles in voltage sensor-pore coupling and voltage-dependent gating[95-97], similar to other voltage-gated channels[98-100]. The C-terminal domain (CTD) of KCNQ1 is large and contains 4 intracellular α-helices referred to as A-D. A wide range of functions has been attributed to the CTD including calmodulin binding, interaction with β-subunits and scaffolding proteins, as well as channel assembly and trafficking[101,102]. Other members of the KCNQ family (KCNQ2-5) share between 40-60% sequence homology with KCNQ1. Their transmembrane regions are highly conserved, but other regions such as the C-terminal domains are relatively variable[103]. In particular, KCNQ2 and KCNQ3 are widely expressed in the brain and can harbor mutations associated with neonatal epilepsy[104-107].

KCNQ1 voltage-dependent gating

In the absence of β-subunits, KCNQ1 generates time-dependent currents in response to depolarization. Its kinetics of activation and deactivation are slow compared with most voltage-

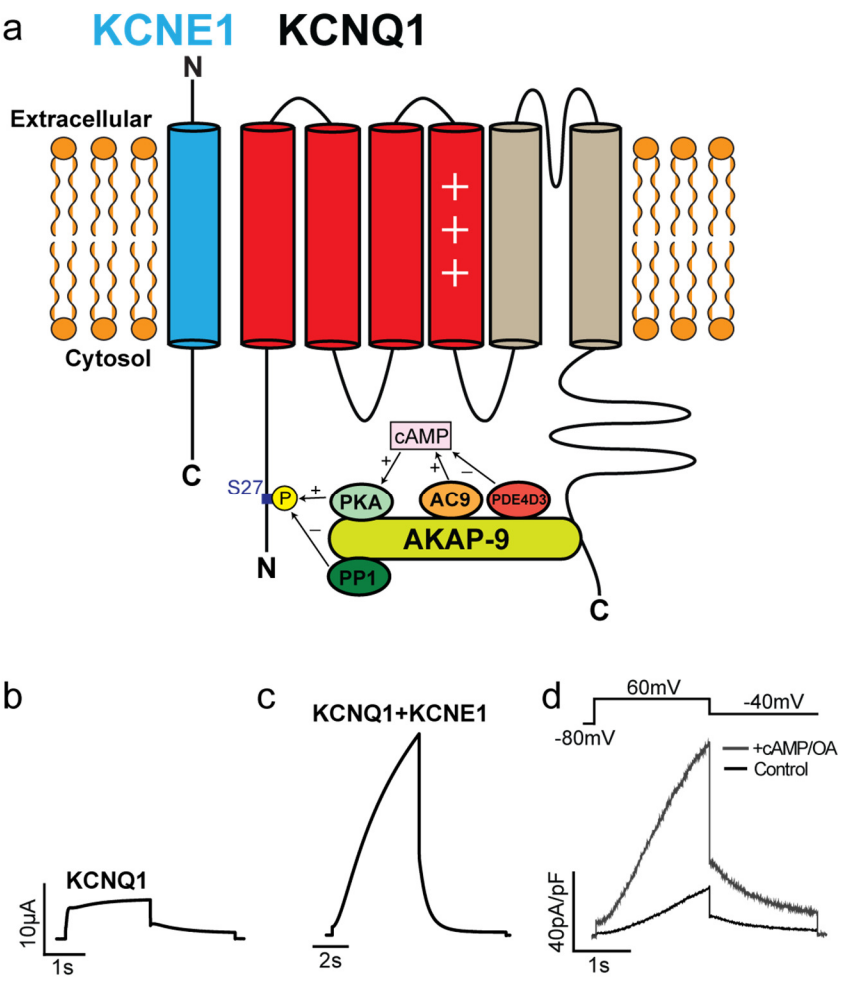

Figure I4. The I_{Ks} macromolecular complex and PKA-mediated regulation. (a) Topology of KCNQ1, KCNE1, and associated proteins that participate in adrenergic regulation. (b-c) Single pulse recordings of KCNQ1 either expressed alone (b) or co-expressed with KCNE1 (c) in *Xenopus* oocytes. (d) Dialysis with 200 μM cAMP and 0.2 μM okadaic acid (OA) slows deactivation and increases I_{Ks} amplitude. I_{Ks} was heterologously expressed in CHO cells. Panel (d) from Chen, L. *et al.* 2005.

gated potassium channels. For instance, wildtype KCNQ1 expressed in *Xenopus* oocytes reaches near steady state on the order of seconds at +40 mV[31] (Fig. I4 b). In comparison, at the same voltage, the prototypical Shaker channel reaches maximal activation on the order of 10's of milliseconds and then rapidly inactivates[108]. Gating currents in KCNQ1 are small and difficult to measure, suggesting that KCNQ1 voltage sensor movement is also relatively slow compared with other channels[83,109]. In addition, KCNQ1 displays a relative paucity of positively charged

residues on its S4 compared with other channels, further contributing to small gating currents. This relative paucity in gating charges may contribute to the gating flexibility that KCNQ1 exhibits when modulated by β-subunits. For instance, KCNE3 converts KCNQ1 into a constitutively active channel to facilitate intestinal chloride secretion[110]. Previous studies have shown that KCNE3 stabilizes voltage sensor activation through electrostatic interactions between positive charges on S4 and negative charges at the extracellular end of the KCNE3 transmembrane region[111]. Such a constitutive mode of gating contrasts greatly with the voltage-dependent behavior of KCNQ1 alone and is altogether different from the slowly activating I_{Ks} generated by co-expression with KCNE1.

Remarkable insight into the gating processes of KCNQ1 comes from voltage clamp fluorometry (VCF), a technique that allows for simultaneous measurement of ionic current with voltage sensor movement. This fluorescence-based technique is particularly useful as it overcomes the issue of small gating currents that makes it otherwise difficult to study S4 movement in KCNQ1. Initially, the technique was developed to study S4 movement in the Shaker channel and helped confirm S4 as the voltage sensor[112,113]. The technique involves engineering a cysteine residue at a particular site of interest and covalently attaching a fluorophore. Conformational changes involving the labeled site alters the hydrophobicity of the surrounding environment, leading to changes in fluorescence intensity. Fluorescence changes can be measured in real time together with ionic currents. Although cysteine accessibility experiments also assay for protein conformational changes, they require alteration of channel function during the course of the experiment, whereas VCF often imposes minimal changes to protein function. Since its initial development, VCF has been utilized to study S4 movement in a variety of ion channels, including $Na_V1.5$[114,115], $Ca_V1.2$[116], hERG[117-119], and HCN[120].

Previous VCF studies demonstrate an allosteric gating mechanism for KCNQ1[121]. To report S4 movement in KCNQ1, Osteen *et al.* attached a fluorophore to an engineered cysteine residue at the S3-S4 linker of KCNQ1. By altering S4 movement using mutations and selectively labeling channel subunits, Osteen *et al.* showed that the four S4's of KCNQ1 move independently of one another. Furthermore, locking two of four voltage sensors in the activated state enhances constitutive activation, suggesting that KCNQ1's pore can open without complete activation of all voltage sensors. In addition, the mutation L251A alters the coupling between the voltage sensor and the pore such that voltage sensor activation precedes pore opening, resulting in a slowly activating current that resembles I_{Ks}. These results can be explained by an allosteric model where independent activation of each voltage sensor increases the open probability of the channel. Furthermore, the model does not require activation of all four voltage sensors for channels to open. In addition, the model suggests that voltage sensor-pore coupling in KCNQ1 is relatively weak compared with Shaker and may underlie dramatic changes in the channel gating behavior caused by modulatory subunits such as KCNE1[122].

Voltage sensor-pore coupling mechanisms allow voltage sensor movements to induce pore motions and have been studied in great detail for KCNQ1. The S4-S5 linker physically interacts with the activation gate and is thought to be a critical mediator of coupling in KCNQ1. Choveau *et al.* showed that the S4-S5 linker can reversibly bind to the S6 C-terminus, which is the activation gate of the channel[97]. In a different study, Labro *et al.* used double mutant cycle analysis to demonstrate interactions between residues in the S4-S5 linker and those in the S6 C-terminus[96]. In addition to mechanical coupling mediated by the S4-S5 linker, the lipid molecule phosphatidylinositol 4,5-bisphosphate (PIP_2) is necessary for voltage sensor-pore coupling in KCNQ1. PIP_2 is found in the inner leaflet of plasma membranes[123] and can regulate a variety of

ion channels[124-129]. PIP_2 mainly binds to KCNQ1 at its cytoplasmic loops and at the C-terminal region near S6[95,130,131], regions that define the interface between the VSD and the pore domain[97,132]. PIP_2 binding is mediated by electrostatic interactions between its anionic lipid headgroup and positively charged channel residues[133]. Zaydman *et al.* devised a VCF experiment to show that PIP_2 is necessary for voltage sensor-pore coupling[95]. He first showed that the pore-opening mutation L353K stabilizes voltage sensors in the activated conformation. This is because coupling between voltage sensors and the pore is bidirectional, such that a pore effect can influence voltage sensor movement. However, depletion of PIP_2 abolishes L353K's effect on voltage sensors, indicating that PIP_2 is necessary for coupling. Furthermore, rundown of PIP_2 in the cell membrane reduces the current amplitude of KCNQ1 both in the presence and absence of KCNE1[134] as a result of uncoupling the pore from voltage sensors. Additional molecular dynamics studies suggest that in KNCQ1, voltage sensor-pore coupling mediated by the S4-S5 linker is relatively weak compared to other channels[130]. As such, PIP_2 plays a more prominent role in coupling for KCNQ1 compared with other channels. Whether PIP_2-dependent function represents a physiological mechanism to control or modulate I_{Ks} remains to be demonstrated.

KCNE1, the β-subunit

Co-expression of KCNE1 with KCNQ1 drastically alters channel function to generate I_{Ks}. Most prominently, assembly with KCNE1 leads to a delay in the onset of activation (Fig. I4 c), an increase in channel amplitude, as well as a depolarizing shift in the current-voltage relationship[31,32]. This results in a channel that, compared with most other voltage-gated potassium channels, activates at more positive voltages and with slower kinetics. These

properties allow I_{Ks} to be most activated toward the end of the plateau phase of the action potential, where it critically contributes to repolarization. KCNE1 contains 129 amino acids and consists of a single transmembrane helix, an extracellular N-terminus and an intracellular C-terminus[86]. A number of positively charged residues in the C-terminus are positioned closely to the cell membrane and recruit PIP_2 through electrostatic interactions, thereby augmenting current amplitude[134]. KCNE1 is thought to have extensive contact with KCNQ1 including the voltage-sensing domain[83,135-139], the pore domain[135,140,141], the S4-S5 linker[142], as well as the CTD[143,144]. Residues on KCNE1 can crosslink with both S1 and S6 of KCNQ1, suggesting that it is located in a cleft between the voltage-sensing domain and pore domain of different KCNQ1 subunits[135,139] (Fig. I5). From this position, KCNE1 can potentially modulate multiple aspects KCNQ1 gating, including voltage sensor movement, pore transitions, and coupling. With respect to the stoichiometry of KCNE1 to KCNQ1, some studies suggest a fixed 2:4 ratio[145,146] while others suggest a flexibility in stoichiometry up to 4:4 that contributes to modulation of assembled channels[147-149]. Although three other members of the KCNE family, KCNE2-KCNE4, are also expressed in the heart[88] and are capable of modulating KCNQ1 activity[88,110,150,151], whether they associate with KCNQ1 *in vivo* in the heart to contribute potassium currents remains to be explored.

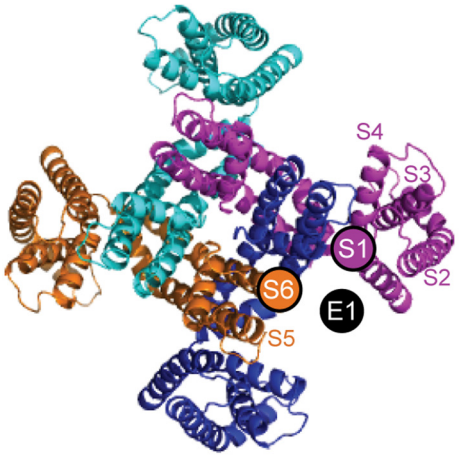

Figure I5. The location of KCNE1 relative to KCNQ1 according to cysteine crosslinking. Previous crosslinking studies are consistent with location of KCNE1 (black circle) in a cleft between the S1 and S6 helix of two different subunits. Figure modified from Chung, D. Y. *et al.* 2009.

I_{Ks} voltage-dependent gating

The ability for KCNE1 to drastically alter the ionic current of KCNQ1 is important to generating the slowly activating I_{Ks} in the heart. Yet, a number of questions arose regarding the underlying gating modifications imposed by KCNE1. For example, it was previously unclear whether the delay in the onset of I_{Ks} activation is due to a slowing in voltage sensor activation. Initial cysteine modification studies showed that the voltage-dependent modification of a cysteine residue introduced to the S4 (A226C) was slowed 13 times when KCNE1 was co-expressed[94], suggesting that KCNE1 slows voltage sensor activation. In addition, a VCF study that labelled the V221C residue in the S3-S4 linker with the fluorophore Tetramethylrhodamine-5-maleimide (TMRM) showed that KCNE1 slows S4 activation[109]. However, additional studies showed that S4 activation is actually minimally slowed by KCNE1. Rocheleau *et al.* showed that cysteine modification of the S4 occurs even when I_{Ks} is depolarized at short pulses of 0.1 s, suggesting that S4 activation is relatively fast[93]. The previously observed slowing of cysteine modification rate in the presence of KCNE1 can be explained by hindered accessibility of the modification reagent to its target site.

Additional VCF measurement of S4 movement demonstrated that voltage sensor activation is faster than current activation[83,138]. In these studies, the G219C residue in the S3-S4 linker was labelled with the fluorophore Alexa 488-maleimide to assay for voltage sensor movement. By measuring the voltage-dependence of activation for fluorescence and conductance, the studies showed that KCNE1 splits fluorescence activation into two distinct components. The first component occurs at more hyperpolarized potentials and represents voltage sensor movement while the pore remains closed. The second component at more depolarized potentials is thought to represent S4 conformational change occurring

simultaneously with gate activation and exhibits slower activation kinetics compared with the first component. Subsequent gating charge measurement showed that the majority of charge movement occurs during the first component of S4 activation[83]. Movement of the S4 in the absence of channel opening explains the Cole-Moore shift that occurs in the presence of KCNE1, in which a hyperpolarizing prepulse while channels are closed slows subsequent current activation upon depolarization. Because voltage sensors deactivate more fully during the hyperpolarizing prepulse, more time is required for subsequent activation and channel opening during the depolarizing pulse. In addition, the second component of fluorescence observed in these studies is consistent with previous VCF results using the TMRM fluorophore, suggesting that TMRM labelling misses the first component of S4 activation but shows the second, slower component.

Based on the two-component S4 activation observed, Barro-Soria *et al.* proposed a kinetic model in which four voltage sensors first independently activate while the pore remains closed before a second concerted movement that opens the pore[83]. Kinetic simulations from this gating scheme are consistent with experimental data. Compared with the allosteric gating scheme of KCNQ1 in the absence of KCNE1, these results suggest that KCNE1 has a major effect on voltage sensor-pore coupling. Whereas KCNQ1 in the absence of KCNE1 can open when some of its voltage sensors activate, KCNE1 suppresses channel opening until all four voltage sensors have activated.

Molecular interactions between the S4 and surrounding transmembrane helices can impede or guide its movement during channel activation. For example, Nakajo and Kubo showed that in the presence of KCNE1, steric collisions between the bulky residues F232 on S4 and F279 on S5 impede S4 activation and right-shift the voltage-dependence of channel

activation. This steric interaction between S4 and S5 is only prominent in the presence of KCNE1, suggesting that in KCNQ1 alone there is flexibility in S4 motion such that during activation it avoids collision with S5. The presence of KCNE1 may restrict the flexibility of S4 motion such that it collides with S5 and thereby destabilizes activation.

Additional evidence suggests that S4 arginines form state-dependent electrostatic interactions with the negatively charged residue E160 on the neighboring S2 helix. The particular charge-pair formed depends on the conformational state of S4. For example, E160 interaction with R228 stabilizes the resting state, whereas E160-R237 stabilizes the activated state[152]. Furthermore, the R231 residue, located between R228 and R237, interacts with E160 to stabilize what is considered the intermediate voltage sensor state[84,153]. These three distinct S4 interactions can explain the two-component S4 activation in I_{Ks}: voltage sensors first activate to the intermediate state, then enter the fully activated state. In addition, channels locked in distinct S4 states exhibit distinct pore properties such selective permeability[84], illustrating that S4 motion influences the pore. Given these insights, Zaydman *et al.* proposed a kinetic model to explain gating processes in both KCNQ1 alone and KCNQ1+KCNE1[84]. For KCNQ1 alone, the pore opens when some voltage sensors enter the intermediate state. Co-assembly with KCNE1 has minimal effect on S4 movement itself, but changes voltage sensor-pore coupling such intermediate S4 activation no longer opens the channel. This model agrees with the model of Barro-Soria *et al.* in that KCNE1 has a critical impact on the coupling between S4 movement and the channel pore. While the exact molecular interactions that mediate KCNE1's effect remain to be explored, mechanistic understanding of channel gating provides a framework for interpreting how these mechanisms can be perturbed by, for example, mutations, pharmacologic modulators, and signaling pathways.

Molecular components of adrenergic stimulation

β-adrenergic stimulation of I_{Ks} plays a critical role in cardiac electrical conduction by shortening action potential duration to accommodate elevated heart rates. There have been considerable efforts to elucidate the molecular pathway for the β-adrenergic regulation of I_{Ks}. In 1988 it was shown that stimulation of protein kinase A (PKA) activity by a cAMP analog can upregulate the delayed rectifier current[21]. Later, it was demonstrated that the scaffolding protein A-kinase anchoring protein 9 (AKAP-9), also known as yotiao, plays a central role in adrenergic regulation of I_{Ks} by compartmentalizing key elements of the PKA signaling pathway and allowing for spatiotemporal control. AKAP-9 binds to the CTD of KCNQ1 and recruits signaling proteins including PKA, protein phosphatase 1 (PP1)[154], adenylyl cyclase 9 (AC9)[155], and the phosphodiesterase PDE4D3[156] (Fig. I4 a). Together these proteins form the I_{Ks} macromolecular complex that can tightly control the phosphorylation state of the channel in response to adrenergic stimulation. PKA phosphorylates KCNQ1 at the S27 residue, adding a negatively charged phosphate group. This modification leads to increased channel activation and slowed deactivation[154,157] (Fig. I4 d). In addition, phosphorylation of AKAP-9 itself contributes to the PKA-mediated upregulation of I_{Ks}[158]. Taken together, these molecular components of mediate I_{Ks} response to β-adrenergic signaling, allowing for control of action potential that is critical to normal physiology and can become aberrant in disease.

I_{Ks} loss-of-function in long QT syndrome

Long QT syndrome (LQTS) is an arrhythmia characterized by a prolonged QT interval on EKG that leads to elevated risks of ventricular fibrillation and sudden cardiac death[159]. In congenital LQTS, genetic mutations predominantly in cardiac ion channels prolong the cardiac

APD, which may trigger EAD's and/or DAD's and cause abnormal electrical activity in the heart as previously discussed. There are 15 subtypes of congenital LQTS, each associated with mutations on a different gene[160]. Among all LQTS subtypes, LQT1 is the most common, representing 30-35% of all congenital LQTS[161]. Insight into the molecular mechanisms of disease mutations have greatly improved our understanding of LQTS pathophysiology and helped provide a first step to the future development of targeted therapies.

Missense mutations in KCNQ1 are responsible for the majority of LQT1 cases and can cause channel loss-of-function through a variety of molecular mechanisms, including defects in ion permeation, channel gating, trafficking, KCNQ1-KCNE1 interaction, PKA-mediated signaling pathway, PIP_2 binding and calmodulin binding[2]. The mechanisms of mutations may bear implications on patient phenotype, severity of arrhythmia, as well as response to therapy. For example, one study showed that mutations in highly conserved KCNQ1 residues, such as those in the P-loop, which contains the selectivity filter, are associated with higher risks of cardiac events[162,163]. These residues are likely conserved because they are critical to channel function. Indeed, three LQT1 mutations near the selectivity filter, T322M, T322A, and G325R have been shown to abolish channel conductance[163,164] and exert dominant negative effects. Another study showed that missense mutations in the cytoplasmic loops between S2-S3 and between S4-S5 are associated with an elevated risk of aborted cardiac arrest and sudden cardiac death[165]. Four mutations in these cytoplasmic loops, G189R, R190Q, R243C, and V254M, all diminish I_{Ks} upregulation in response to forskolin and thus may render patients particularly susceptible to arrhythmic events under stressful conditions. Understanding these mutation-specific mechanisms may lead to improved risk-stratification for LQT1 patients and guide therapeutic options.

While the vast majority of LQTS mutations occur in KCNQ1, a number of disease mutations have also been found in KCNE1 and AKAP-9, which are classified as LQT5 and LQT11, respectively. Co-assembly of KCNQ1 with KCNE1 is key to generating the I_{Ks} current. Thus it follows that KCNE1 mutations can alter the physiologically relevant current of the assembled channel and lead to LQTS. As previously discussed, another protein that associates with KCNQ1 is AKAP-9, an important mediator of adrenergic signaling. That a mutation in AKAP-9 can cause LQTS is a testament to the critical role of PKA signaling in the regulation of the I_{Ks} macromolecular complex[166]. The S1570L mutation, located near the C-terminal binding domain of AKAP-9, disrupts interaction with KCNQ1, reduces cAMP-stimulated phosphorylation of KCNQ1, and abolishes I_{Ks} upregulation in response to cAMP.

I_{Ks} gain-of-function in short QT syndrome and atrial fibrillation

Whereas loss-of-function mutations in I_{Ks} subunits are associated with long QT syndrome, gain-of-function mutations in I_{Ks} are associated with short QT syndrome (SQTS) and/or atrial fibrillation. Atrial fibrillation, the most common arrhythmia in the US, affects more than 3 million adults[167] and is a major cause of morbidity and mortality. In atrial fibrillation, abnormal electrical activity causes excessively rapid atrial contractions that hinder normal cardiac function. Inherited forms of atrial fibrillation are associated with earlier onset of disease compared with typical forms[168]. While they are much rarer, investigating their underlying mechanisms can provide insights on the pathophysiology and management of the much more prevalent forms of disease. In addition, patients with short QT syndrome present with abnormally shortened QT interval on EKG and are at elevated risk of atrial fibrillation and sudden cardiac death[169]. Both short QT syndrome and inherited forms of atrial fibrillation

predominantly result from ion channel mutations, such as in $Na_V1.5$[170], $K_{ir}2.1$[171], $Ca_V1.2$[172], hERG[173] and KCNQ1[174,175].

A number of atrial fibrillation mutations in KCNQ1 significantly slow the kinetics of I_{Ks} deactivation[174-176]. Previous studies showed that deactivation slowing causes significant accumulation of I_{Ks} upon repeated stimulation and underlies β-adrenergic-induced shortening of APD[177]. This pathway has been shown to also induce atrial arrhythmia in transgenic mice expressing I_{Ks}[178], suggesting that while I_{Ks} normally contributes little to atrial action potential, gain-of-function in I_{Ks} can disrupt electrical activity. Accumulation of I_{Ks} excessively shortens action potential duration as well as the refractory period of cardiac tissues, predisposing to re-entry arrhythmia such as atrial fibrillation. Given the central role of I_{Ks} deactivation slowing in arrhythmogenesis, investigating the gating alterations underlying deactivation slowing by KCNQ1 atrial fibrillation mutations can prove critically useful for designing mechanism-based therapies to restore channel function.

Pharmacologic Activation of KCNQ1 and I_{Ks}

Although the most common subtype of LQTS is associated with I_{Ks} loss-of-function, I_{Ks} is not yet a direct target in antiarrhythmic therapy. However, conceptually, I_{Ks} activators could serve useful roles in therapy and provide a mechanism-based approach to rescuing channel loss-of-function. A number of small-molecules that activate I_{Ks} have been identified at the benchside and may guide future development of therapeutic agents. For example, the compounds 4,4-diisothiocyanatostilbene-2,2-disulfonic acid (DIDS) and mefenamic acid both increase I_{Ks} current amplitude[179]. In addition, DIDS has been shown to drastically slow I_{Ks} deactivation. Another KCNQ1 activator, ML277, both increase KCNQ1 amplitude and slow current

deactivation. Interestingly, its effect diminishes with progressive increase in KCNE1:KCNQ1 stoichiometry[180]. While a drug with such properties is not expected to directly serve therapeutic roles, understanding its mechanism of action can provide crucial insight on general mechanisms of channel gain-of-function and guide future efforts to modulate channel function.

Focus of Investigation

For both KCNQ1 atrial fibrillation mutations and molecular activators, slowing of deactivation plays a critical role in increasing channel function. However, the underlying gating mechanism of slowing remains unknown and can shed light on channel function and modulation. Deactivation slowing can potentially result from slowing of voltage sensor movement, slowing of pore opening/closing, alteration of voltage sensor-pore coupling, or a combination of these gating processes in a voltage-dependent ion channel. In this thesis, we examined the gating effects underlying deactivation slowing using voltage clamp fluorometry to assay for voltage sensor movement simultaneously with ionic current through the channel pore. In addition, we utilized kinetic modeling to elucidate gating processes altered by mutations and molecular activators. These studies provide fundamental insights on mechanisms of deactivation slowing and guide future efforts to modulate channel function and develop therapies for arrhythmia.

METHODS

Molecular Biology

RNA was prepared from DNA sequences in the pGEMHE vector after linearization with the restriction enzyme NheI and *in vitro* transcription using the mMESSAGE mMACHINE T7 Transcription Kit from ThermoFisher. For DNA sequences in the pSD64TF vector, the restriction enzyme SacI and mMESSAGE mMACHINE SP6 Transcription Kit were used.

A cysteine site was engineered at residue G219 on the extracellular loop of KCNQ1 between S3 and S4 that can be labelled with the fluorophore Alexa-488 maleimide (Fig. M1 a) to monitor S4 conformational changes. To enhance specificity of labelling, two native cysteine residues (214 and 331) predicted to be accessible to the extracellular environment were mutated to alanine. This construct has been used in multiple VCF studies[83,84,121,181] and is here simply referred to as KCNQ1. The terms

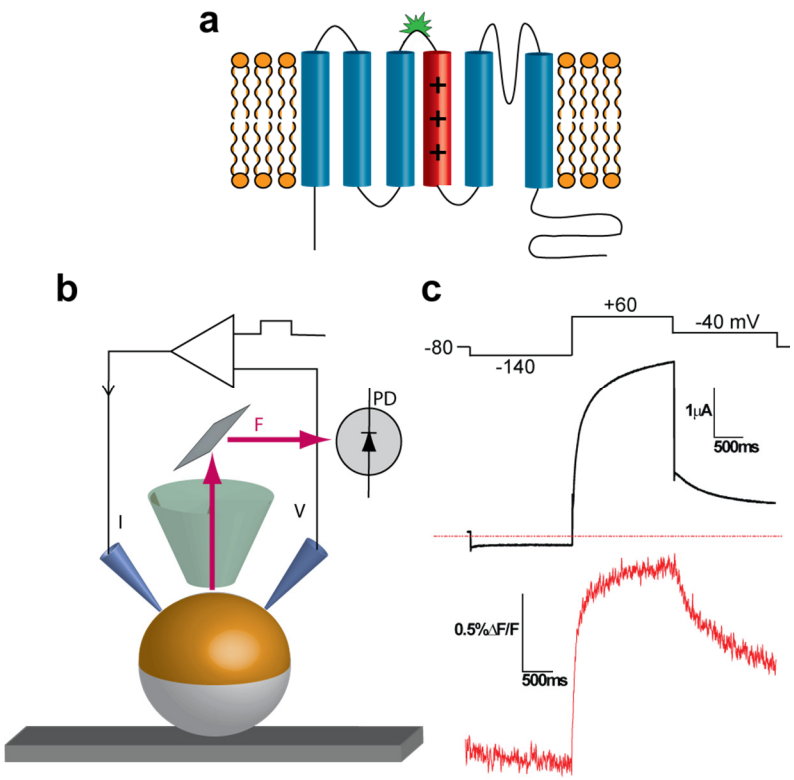

Figure M1. The voltage clamp fluorometry (VCF) technique. (a) In the KCNQ1 VCF construct, a cysteine residue is engineered at the S3-S4 linker, where a fluorophore (shown in green) is covalently attached to monitor conformation changes in the S4 (red cylinder). (b) The schematic of VCF illustrates a *Xenopus laevis* oocyte expressing KCNQ1 labelled with fluorophore. Ionic current is recorded using two-electrode voltage clamp while fluorescence is simultaneously measured by a photodiode. (c) Example VCF recording of KCNQ1 under a single pulse protocol. Current is shown in black while fluorescence is shown in red below. The horizontal dashed line indicates zero current level. Panels (a) and (b) from Jeremiah Osteen.

"KCNQ1^{S140G}" and "KCNQ1^{V141M}" denote KCNQ1 subunits containing mutations. The terms "I_{Ks}^{S140G}" and "I_{Ks}^{V141M}" denote KCNQ1 mutants co-expressed with KCNE1. The term wildtype (WT) refers to the original KCNQ1 construct without engineering for use in VCF.

Oocyte Expression

Defolliculated *Xenopus laevis* oocytes were supplied by Ecocyte Bioscience. For KCNQ1 experiments, 50 ng of KCNQ1 RNA was injected into oocytes. For I_{Ks} experiments, 33 ng KCNQ1 and 10 ng KCNE1 were injected. For KCNE1 experiments with mutant channels, total RNA injected was reduced, but the KCNQ1:KCNE1 RNA ratio was kept the same. For PIP_2 depletion experiments without KCNE1, 33 ng KCNQ1 and 17 ng ciVSP were injected. For PIP_2 depletion experiments with KCNE1, 23.5 ng KCNQ1, 7 ng KCNE1, and 14.7 ng ciVSP were injected, with the same KCNQ1:KCNE1 RNA ratio as previously. In all I_{Ks} injections, the KCNE1:KCNQ1 RNA transcript ratio exceeds 1:1 and is expected to saturate the α-subunit[148]. Injection was performed using Nanoject II from Drummond.

VCF

VCF experiments were performed 2-5 d after injection. Oocytes were labelled with 100 μM Alexa-488 maleimide in ND96 (96 mM NaCl, 2 mM KCl, 1.8 mM $CaCl_2$, 1 mM $MgCl_2$, 5 mM HEPES, pH 7.5 with NaOH) for 30 min at 12 ºC. Following labelling, they were kept on ice to prevent internalization of labelled channels. Oocytes were placed into a recording chamber with animal pole "up" in ND96 solution. 100 μM $LaCl_3$ was used to block endogenous hyperpolarization-activated currents. All recordings were performed at 22-24 ºC using the TC-324B temperature controller from Warner Instrument Co. For UCL2077 experiments, 10 μM

UCL2077 was pipetted into the recording chamber. For ML277 and R-L3 experiments, 10 μM ML277 or R-L3 was applied using the perfusion system. 0.1% DMSO was used in drug control experiments.

Current was recorded using the two-electrode voltage clamp configuration with the Oocyte Clamp OC-725C amplifier (Warner Instrument Corp.). Recording pipettes were pulled to a resistance of 0.7-1.5MΩ using the Model P-97 Flaming/Brown Micropipette puller (Sutter Instrument Co.) and filled with 3 M KCl. Data were digitized with Digidata 1440A low-noise data acquisition system (Axon CNS Molecular Devices) and collected with Clampex 10 software. Fluorescence recordings were made using Olympus BX61WI upright microscope with Oregon Green filter set (41026 – Chroma). Light was focused on the top of oocyte using a 20x water immersion objective. Fluorescence signal was collected by a photodiode and amplified using Axopatch 200A amplifier (Axon Instruments). The signal was subject to a 100Hz lowpass Bessel filter (Frequency Devices Inc.) before being digitized by the Digidata 1440A and collected by Clampex10. See Figure M1 b for a diagram of the VCF setup. By convention, current is represented in black and fluorescence is represented in red (Fig. M1 c). Upward deflection of fluorescence signal represents S4 activation and downward deflection represents S4 deactivation for KCNQ1 and I_{Ks}.

Isochronal activation was measured for KCNQ1 alone using a protocol with holding potential at -80 mV, a 2-s prepulse to -140 mV to more fully deactivate voltage sensors, a 2-s test pulse ranging from +60 mV to -140 mV, a 2-s repolarizing pulse to -40 mV, and a sweep interval of 17 s. For KCNQ1 in the presence of KCNE1, isochronal activation was measured using a protocol with a holding potential at -110 mV, a 3-s prepulse to -140 mV, a 5-s test pulse ranging from +80 mV to -160 mV, a 5-s repolarizing pulse to -40 mV, and a sweep interval of 23 s.

Negative holding potentials and prepulse were used to deactivate channels more fully. To measure the effect of the small-molecule activator ML277 on KCNQ1 isochronal activation, a voltage protocol was used with holding at -80 mV, a 2-s test pulse ranging from -140 mV to +80 mV, a 2-s repolarizing pulse to -120 mV, and a sweep interval of 15 s. For experiments with the activator R-L3, a 2-s prepulse at -120 mV was introduced to close channels more completely.

Rb^+/K^+ Permeability Ratio

Two-electrode voltage clamp experiments were performed 2-5 d after injection. Oocytes were recorded at room temperature (22-24 ºC). Voltage protocol was applied with holding at -110 mV, a 2-s prepulse at -120 mV, a 5-s pulse to +40 mV, followed by repolarization to -60 mV. Currents were recorded under either high external K^+ (100 mM KCl, 1.8 mM $CaCl_2$, 1 mM $MgCl_2$, 5 mM HEPES, pH 7.5 with NaOH) or high external Rb^+ (96 mM RbCl, 4 mM KCl, 1.8 mM $CaCl_2$, 1 mM $MgCl_2$, 5 mM HEPES, pH 7.5 with NaOH). 100 µM $LaCl_3$ was used to block endogenous hyperpolarization-activated currents. Rb^+/K^+ permeability ratios were determined using inward tail current measured at -60 mV following the 5-s activation pulse at +40 mV. Inward tail currents were determined following normalization of outward current to calculate Rb^+/K^+ ratios. These ratios were used to calculate the expected fraction of open channels in the intermediate voltage sensor state at the end of activation or $I_{Ks}{}^{S140G}$ and $I_{Ks}{}^{V141M}$.

Data Analysis

Steady-state voltage-dependence of current was determined from exponential fits of tail currents at -40 mV following the test pulse. Fits were extrapolated to beginning of tails to avoid

"hooks" that result from channel inactivation. GV relationships were fitted with a Boltzmann equation:

$$G(V) = A2 + (A1 - A2)/(1 + \exp((V - V_{1/2})/K))$$

where A1 and A2 are the minimum and maximum, respectively, $V_{1/2}$ is the voltage at half-maximal activation, and K is the slope. Fluorescence was bleach-subtracted and averaged over tens of milliseconds at end of test pulse to reduce errors from signal noise. Voltage-dependence of fluorescence (FV) was also fitted with the Boltzmann equation.

Statistical data analysis was performed using two-tailed student's *t*-test or one-way analysis of variance (ANOVA) with Tukey's post-hoc test. Differences at $P < 0.05$ were considered significant.

Kinetic Modeling

A Markov model of KCNQ1 and I_{Ks} gating was modified from previous studies to reflect more recently published results[83,84]. In this scheme, voltage sensors can exist in resting, intermediate, or fully activated states[84] (Fig. M2). Voltage sensor movement is represented by horizontal transitions in the model

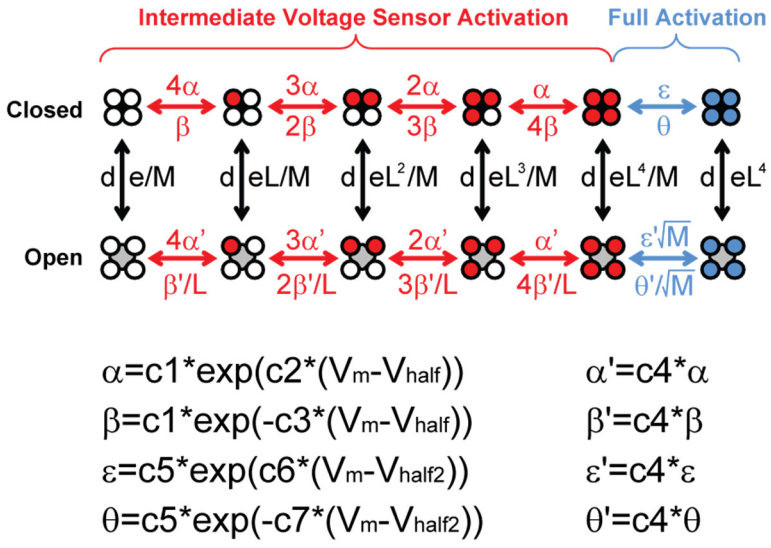

Figure M2. Model schematic with rate parameters. In this scheme, vertical transitions represent pore opening/closing, and horizontal transitions represent voltage sensor movement. Voltage sensor movement proceeds in two steps: first, independent activation of four voltage sensors into the intermediate state (red), followed by a concerted movement to the fully activated state (blue).

and occurs in two steps: first, independent movement of four identical voltage sensors to an intermediate state[121]; second, a concerted movement to a fully activated state[83]. Channel opening/closing is represented by vertical transitions. Channel opening can occur in every voltage sensor configuration but increases in probability with each step of voltage sensor activation. Open states are assumed to have equal conductance.

The total fluorescence signal is calculated with each voltage sensor contributing to ¼ of the fluorescence signal in the first step of activation. The second, "concerted" step of activation accounts for another 14% of total fluorescence, based on our fitting results.

Rate constants that govern voltage sensor transitions are voltage dependent and are formulated based on the Eyring rate theory[182], which describes the rates of transitions as:

$$k = k_{1/2} \exp(\frac{z(V - V_{1/2})F}{RT})$$

where V is the membrane potential, $V_{1/2}$ is the equilibrium potential for the forward-reverse process, F is Faraday's constant (96485 C mol^{-1}), R is the ideal gas constant (8.314 J mol^{-1} K^{-1}), T is the temperature (K), and z and $k_{1/2}$ are parameters for each rate constant. At the equilibrium potential, $k = k_{1/2}$.

Channel pore opening and closing are assumed to be voltage-independent and are governed by the allosteric coupling factor L, which represents the degree of voltage sensor-pore coupling in the first step of voltage sensor activation. Similarly, the coupling factor M represents degree of coupling in the second, concerted step of voltage sensor activation.

The model satisfies microscopic reversibility, a thermodynamic principle that requires forward transition rates to equal reverse rates between any two states at thermodynamic

equilibrium[183]. Microscopic reversibility also ensures that the total number of channels is conserved. In order to satisfy microscopic reversibility, for any loop in the model, the product of rates in the clockwise direction equal the product of rates in the counterclockwise direction.

The wildtype models for KCNQ1 and I_{Ks} contain 14 free parameters. Parameters were fitted using the simulated annealing algorithm to identify a global minimum[184]. The model was constrained using the following data: isochronal activation of conductance and fluorescence, kinetics of fluorescence and current activation and deactivation, and fluorescence deactivation following PIP_2 depletion. The $KCNQ1^{S140G}$ model contains 2 free parameters, while the $I_{Ks}{}^{S140G}$ and $I_{Ks}{}^{V141M}$ models contain 4 free parameters each. Additionally, Rb^+/K^+ permeability ratios were used to constrain $I_{Ks}{}^{S140G}$ and $I_{Ks}{}^{V141M}$ models. Models for drug effects were manually determined.

Chapter 1: Gating mechanisms underlying deactivation slowing by atrial fibrillation mutations in KCNQ1

Summary

KCNQ1 is a voltage-gated potassium channel that is modulated by the β-subunit KCNE1 to generate I_{Ks}, the slow delayed rectifier potassium current, which plays a critical role in repolarizing the cardiac action potential. Two KCNQ1 gain-of-function mutations, S140G and V141M, drastically slow I_{Ks} deactivation and cause a genetic form of atrial fibrillation. However, the underlying gating alterations remain unknown. Voltage clamp fluorometry (VCF) allows simultaneous measurement of voltage sensor movement and ionic current through the channel pore. Here, we use VCF and kinetic modeling to determine the effects of mutations on channel voltage-dependent gating in the absence of KCNE1. We show that S140G directly slows voltage sensor movement, which indirectly slows current deactivation. On the other hand, V141M has minimal effect on channel gating. Our results are consistent with a previous homology model of KCNQ1 and provides the basis for future studies of gating mechanisms underlying I_{Ks} gain-of-function.

Introduction

KCNQ1 is the pore-forming α-subunit of a voltage-gated potassium channel that assembles with the β-subunit KCNE1 in the heart to generate the I_{Ks} current, which is critical for normal repolarization of the cardiac action potential[31,32]. Mutations in I_{Ks} subunits are associated with potentially lethal arrhythmia, including long QT syndrome[85,185], short QT syndrome[186], and atrial fibrillation[174]. Gain-of-function mutations in I_{Ks} subunits that cause atrial fibrillation increase the repolarizing current during repetitive stimulation and shorten the action potential duration[187], which is thought to reduce the refractory period and predispose the heart to electrical re-entry.

Atrial fibrillation is the most common cardiac arrhythmia and affects more than 3 million adults in the United States[167]. Much rarer, genetic forms of atrial fibrillation have been associated with gain-of-function mutations in potassium channel subunits, such as two adjacent mutations in KCNQ1, S140G[174] and V141M[175]. S140G was the first KCNQ1 mutation linked to atrial fibrillation. It is inherited in an autosomal dominant pattern in a Chinese family[174] and causes a gain-of-function I_{Ks} phenotype. Later, a patient with atrial fibrillation and short QT syndrome was found to have a *de novo* missense mutation in KCNQ1. The mutation, V141M, is adjacent to S140G and also causes I_{Ks} gain-of-function[175]. While genetic forms of atrial fibrillation are very rare, they present an opportunity to study underlying mechanisms of I_{Ks} activation and modulation, which may pave the way for developing therapies for more common arrhythmia such as long QT syndrome and typical forms of atrial fibrillation.

KCNQ1, the pore-forming subunit of I_{Ks}, contains a voltage-sensing domain (VSD) and a pore domain. The VSD spans transmembrane helices S1-S4 and contains net positive charges on S4 that allow it to sense changes in membrane potential. The pore domain spans S5-S6 and contains the selectivity filter that allows for K^+ permeation. The VSD is coupled to the pore domain through interactions between the S4-S5 linker and the C-terminus of S6 and requires the lipid molecule phosphatidylinositol 4,5-bisphosphate (PIP_2)[95,97,188]. While KCNQ1 is modulated by KCNE1 to generate the cardiac I_{Ks} current, KCNQ1 by itself is able to form a homotetrameric potassium channel that is capable of voltage-dependent gating.

Both S140G and V141M are located at the extracellular end of the S1 helix of KCNQ1, which is part of the VSD. While initially thought to cause constitutive activation of $I_{Ks,}$ later studies using more negative voltage pulses showed that both mutations drastically slow I_{Ks} deactivation[189,190], which can cause accumulation of open channels under repeated stimulation

and abnormally increase the repolarizing K^+ current. Interestingly, the impact of these mutations on channel deactivation kinetics displays distinct dependence on KCNE1. Whereas S140G slows channel deactivation regardless of the presence of KCNE1, V141M only slows deactivation when KCNE1 is present. This result is supported by a homology model of KCNQ1, in which S140 points toward a salt bridge interaction within the VSD, whereas V141 points away from the α-subunit and toward the putative location of KCNE1[137]. Furthermore, cysteine crosslinking studies have shown that V141 crosslinks with residues on KCNE1, whereas S140 does not[190]. Nonetheless, the gating mechanisms underlying the slow deactivation conferred by these mutations remain unknown. Understanding these gating mechanisms both in the absence and presence of KCNE1 can shed light on KCNQ1 function in addition to its modulation by KCNE1.

In this study, we use VCF to examine the gating effects of these mutations on KCNQ1 in the absence of KCNE1 ($KCNQ1^{S140G}$/ $KCNQ1^{V141M}$). We determine whether any slowing in current deactivation is caused by a slowing in voltage sensor deactivation. We show that $KCNQ1^{S140G}$ slows both current and voltage sensor deactivation, and additionally causes a hyperpolarizing shift in the voltage-dependence of current and voltage sensor activation. On the other hand, $KCNQ1^{V141M}$ has minimal effect on channel gating. In order to dissect the effect of the mutation on channel voltage sensor from the pore, we utilized PIP_2 depletion and UCL2077 inhibition in two separate approaches. Our results show that $KCNQ1^{S140G}$ slows voltage sensor deactivation independently of pore opening. Furthermore, our kinetic models are consistent with $KCNQ1^{S140G}$ directly slowing voltage sensor deactivation, which indirectly slows current deactivation. Simulations of current and fluorescence agree with our VCF data. These findings not only shed light on voltage-dependent gating processes in KCNQ1, but provide an important

stepping stone for studying gating effects of KCNQ1 atrial fibrillation mutations in the presence of KCNE1.

Results

In the absence of KCNE1, S140G, but not V141M, alters voltage sensor movement and channel gating

To study the gating effects of atrial fibrillation mutations using VCF, we employed a KCNQ1 construct containing a cysteine site at the extracellular residue G219 in the S3-S4 linker that can be labelled covalently with a fluorophore. This construct had been used in multiple VCF studies[83,84,121,181] to report S4 movement, and we refer to it here as KCNQ1. We first used a

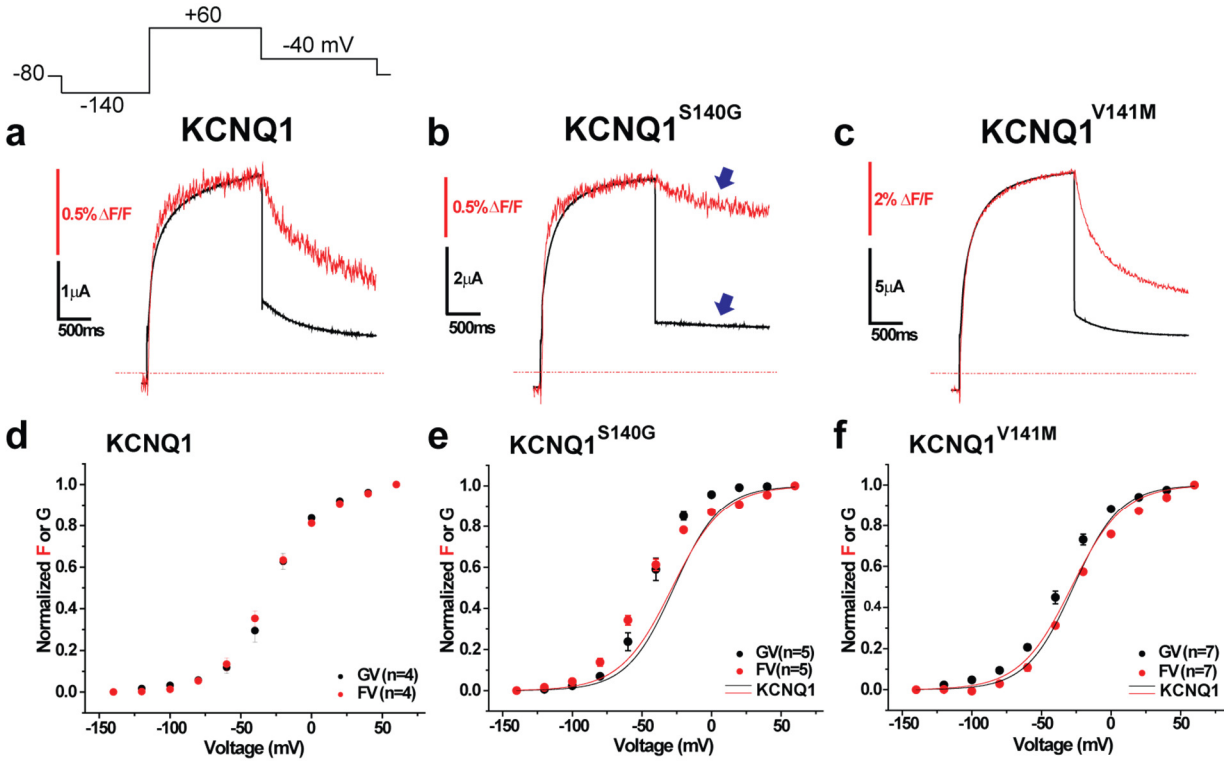

Figure 1.1. S140G, but not V141M, affects voltage sensor deactivation and left-shifts the isochronal activation in the absence of KCNE1. (a-c) Current (black) and fluorescence (red) traces for KCNQ1 (a), KCNQ1^{S140G} (b) , and KCNQ1^{V141M} (c) using the following protocol: from a prepulse of -140 mV, a test pulse was applied at +60 mV, followed by a repolarizing step to -40 mV. Cells were held at -80 mV. (d-f) Normalized isochronal (2 s) activation of fluorescence (red) and conductance (black) for KCNQ1 (d), KCNQ1^{S140G} (e), and KCNQ1^{V141M} (f).

single pulse protocol to determine whether the atrial fibrillation mutations S140G and V141M affect channel current and voltage sensor movement in the absence of KCNE1. From a holding potential of -80 mV, a prepulse to -140 mV was applied to deactivate voltage sensors to the resting position. Then, a single pulse to +60 mV was applied for 2 s followed by repolarization to -40 mV. In comparison to KCNQ1, both $KCNQ1^{S140G}$ and $KCNQ1^{V141M}$ exhibit similar current and fluorescence activation kinetics at +60 mV (Fig. 1.1 a-c). However, $KCNQ1^{S140G}$ appears to slow the deactivation kinetics of both current and fluorescence, whereas $KCNQ1^{V141M}$ does not appear to slow either. To determine the voltage-dependence of activation, we applied the protocol at multiple voltages ranging from -140 mV to +60 mV and plotted the isochronal activation of fluorescence (FV) and conductance (GV) (Fig. 1.1 d-f). Compared with KCNQ1 ($FV_{1/2}$ = -29.3 ± 2.5 mV, $GV_{1/2}$ = -27.2 ± 3.3 mV), $KCNQ1^{S140G}$ ($FV_{1/2}$ = -47.2 ± 2.1 mV, $GV_{1/2}$ = -44.8 ± 2.7 mV) causes a significant hyperpolarizing shift in in both FV and GV, whereas $KCNQ1^{V141M}$ ($FV_{1/2}$ = -23.8 ± 1.3 mV, $GV_{1/2}$ = -36.7 ± 2.0 mV) does not significantly shift either.

In the absence of KCNE1, S140G slows voltage sensor and current deactivation, whereas V141M does not

The primary pathological effect of these atrial fibrillation mutations is a slowing in current deactivation kinetics. Therefore, in addition to previous single pulse measurements, we further examined deactivation by using a voltage protocol that first activates channels at +40 mV, and then repolarizes to -100 mV in order to deactivate channels more completely. Current and fluorescence were measured simultaneously and time to half deactivation during the -100-mV pulse was determined as a marker of deactivation kinetics (Fig. 1.2). Compared with

KCNQ1 ($Ft_{1/2}$ = 232 ± 27 ms, $It_{1/2}$ = 139 ± 17 ms), KCNQ1^{S140G} ($Ft_{1/2}$ = 1214 ± 27 ms, $It_{1/2}$ = 550 ± 51 ms) significantly slows both fluorescence and current deactivation. In contrast, KCNQ1^{V141M} ($Ft_{1/2}$ = 125 ± 11 ms, $It_{1/2}$ = 156 ± 14 ms) slightly speeds fluorescence deactivation without affecting the current deactivation kinetics.

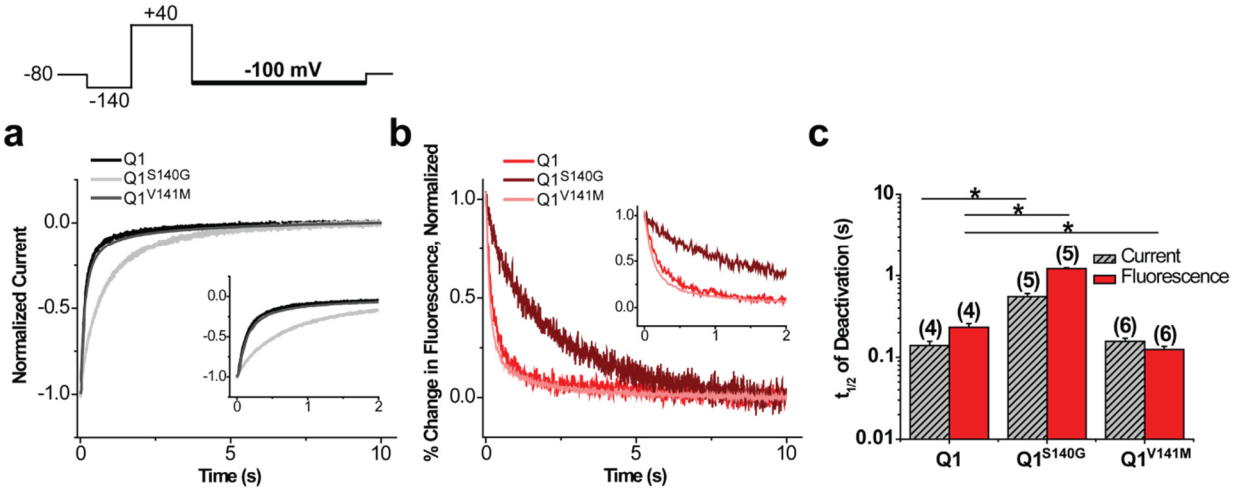

Figure 1.2. In the absence of KCNE1, S140G slows both current and voltage sensor deactivation, whereas V141M slows neither. From a prepulse of -140 mV, an activating pulse was applied at +40 mV, followed by a repolarizing step to -100 mV. Channels were held at -80 mV. (a) Normalized current during deactivation at -100 mV for KCNQ1, KCNQ1^{S140G} and KCNQ1^{V141M}. Inset shows first 2 s of deactivation. (b) Normalized percent change in fluorescence during deactivation at -100 mV. Inset shows first 2 s of deactivation. (c) Time to half deactivation ($t_{1/2}$). Data are shown as mean ± SEM (error bars). *P<0.05; one-way ANOVA with Tukey's test.

S140G slows voltage sensor deactivation independently of channel opening in the absence of KCNE1

Mechanisms other than a direct slowing in voltage sensor movement may result in an apparent slowing in voltage sensor deactivation. For example, voltage sensor deactivation can be slowed indirectly by slowing of pore closing, since the pore is coupled to the voltage sensor. This concept of "retrograde coupling" has been previously illustrated by Zaydman *et al.* who showed that a pore mutation in KCNQ1 that stabilizes the open channel also stabilizes S4s in their activated states. Upon depleting PIP_2, which prevents channel opening (presumably by

uncoupling the pore from the VSD), the effect on the S4s was abolished[95]. As KCNQ1^{S140G} slows voltage sensor movement and current deactivation by a similar order of magnitude, but with a slightly greater effect on the voltage sensor, we explored whether KCNQ1^{S140G} slows voltage sensor movement when channel pore opening is prevented. We focused on KCNQ1^{S140G} over KCNQ1^{V141M}, which has minimal effects on channel gating.

Two approaches were used to test whether pore effects indirectly contribute to slowing of voltage sensor deactivation in KCNQ1^{S140G}. In the first approach, either KCNQ1 or KCNQ1^{S140G} was co-expressed with the voltage-sensing phosphatase from *Ciona intestinalis* (ciVSP). Repeated depolarization activates ciVSP, which leads to depletion of PIP_2 and thus prevents channel opening[191]. When we first co-expressed KCNQ1 with ciVSP and tested for current depletion, we found that repeated depolarizing pulses to +80 mV decrease channel tail current such that by the 12th pulse, only 7.1% ± 4.9% of the initial tail current remains (Fig. 1.3). In contrast, amplitude of fluorescence change remains relatively constant during the time course of current depletion. By the 12th pulse, 94% ± 5% of initial fluorescence remains, indicating intact S4 movement.

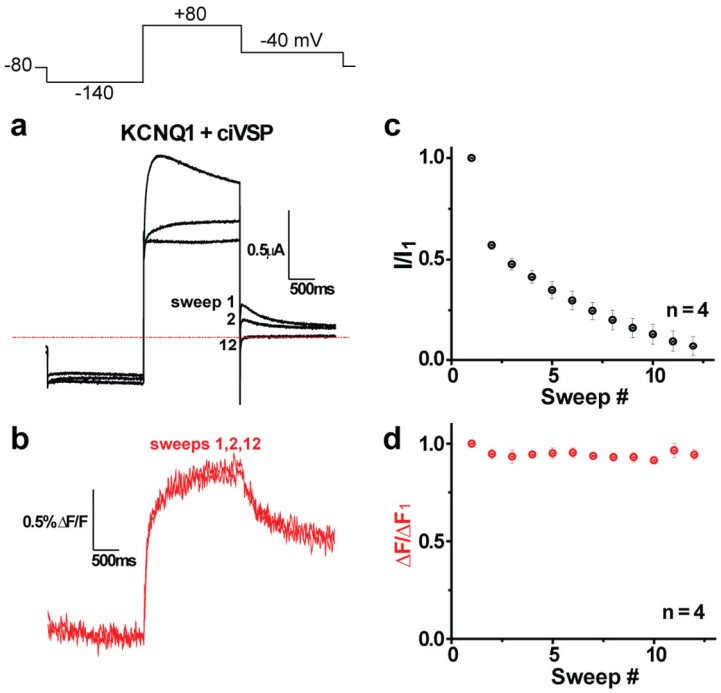

Figure 1.3. PIP_2 depletion diminishes KCNQ1 current amplitude while voltage sensor movement remains intact. The voltage protocol involves depolarization to +80 mV and is repeated for 12 sweeps. (a-b) Traces for sweeps 1, 2, and 12 are shown for current (black) and fluorescence (red). (c-d) Normalized tail current and fluorescence change are plotted against sweep number.

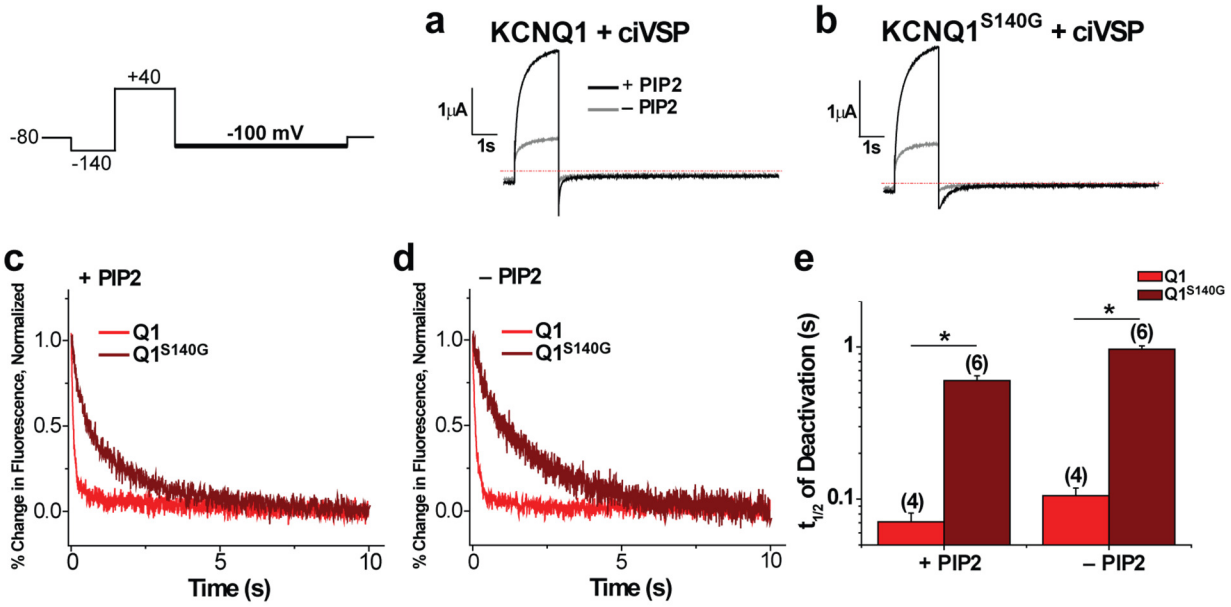

Figure 1.4. In the absence of KCNE1, S140G slowing of voltage sensor deactivation is independent of channel opening based on PIP_2 depletion. The following protocol was used: from a prepulse of -140 mV, an activating pulse was applied at +40 mV, followed by a repolarizing step to -100 mV. Channels were held at -80 mV. This protocol was used before and after PIP_2 depletion by ciVSP, which was activated by repeated depolarization. (a-b) Current before ($+PIP_2$) and after PIP_2 depletion ($-PIP_2$) for KCNQ1 (a) and $KCNQ1^{S140G}$ (b). (c-d) Normalized fluorescence deactivation traces at -100 mV for KCNQ1 (red) and $KCNQ1^{S140G}$ (dark red) before (c) and after (d) PIP_2 depletion. (e) Time to half deactivation ($t_{1/2}$) of fluorescence. Data are shown as mean ± SEM (error bars). *P<0.05; t-test

To determine the effect of S140G on voltage sensor deactivation in the absence of pore effects, we applied a voltage protocol with an activating pulse to +40 mV followed by repolarization to -100 mV both before and after PIP_2 depletion. We observed a drastic decrease in current amplitude following PIP_2 depletion in both KCNQ1 and $KCNQ1^{S140G}$ (Fig. 1.4 a-b), indicating a reduction of PIP_2 levels in the plasma membrane. We then determined the time to half deactivation for fluorescence at -100 mV (Fig. 1.4 c-e). Before PIP_2 depletion, $KCNQ1^{S140G}$ ($Ft_{1/2}$ = 600 ± 46 ms) slows deactivation kinetics compared with KCNQ1 ($Ft_{1/2}$ = 71 ± 10 ms), as expected. Following PIP_2 depletion, $KCNQ1^{S140G}$ ($Ft_{1/2}$ = 966 ± 51 ms) still slows the fluorescence deactivation compared with KCNQ1 ($Ft_{1/2}$ = 105 ± 13 ms).

As a second approach to dissecting the voltage sensor effects of $KCNQ1^{S140G}$ from pore effects, we employed UCL2077, an inhibitor of I_{Ks} previously shown to prevent channel opening

but still allow S4 movement[83]. Application of 10 µM UCL2077 drastically reduces current of both KCNQ1 and KCNQ1^{S140G} (Fig. 1.5 a-b). When we analyzed the fluorescence deactivation, we found that both in the control condition and in the presence of 10 µM UCL2077, KCNQ1^{S140G} significantly slows fluorescence deactivation (Control: $Ft_{1/2}$ = 893 ± 59 ms; UCL2077: $Ft_{1/2}$ = 602 ± 61 ms) compared with KCNQ1 (Control: $Ft_{1/2}$ = 109 ± 23 ms; UCL2077: $Ft_{1/2}$ = 109 ± 7 ms) (Fig. 1.5 c-e). Taken together, the PIP_2 depletion and UCL2007 inhibition experiments show that KCNQ1^{S140G} slows voltage sensor deactivation even in the absence of channel opening.

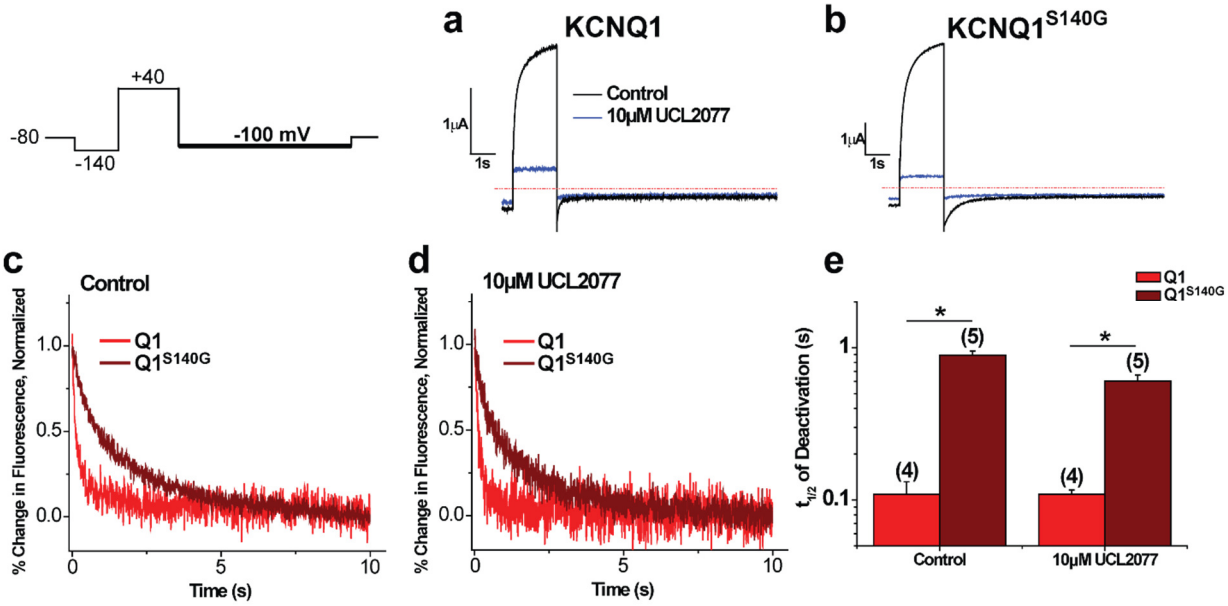

Figure 1.5. UCL2077 inhibition confirms that KCNQ1^{S140G} slows voltage sensor deactivation independently of channel opening. The following protocol was used: from a prepulse of -140 mV, an activating pulse was applied at +40 mV, followed by a repolarizing step to -100 mV. Channels were held at -80 mV. This protocol was used before and after inhibition of current with 10 µM UCL2077. (a-b) Current before and after inhibition with UCL2077 for KCNQ1 (a) and KCNQ1^{S140G} (b). (c-d) Normalized fluorescence deactivation traces at -100 mV for KCNQ1 (red) and KCNQ1^{S140G} (dark red) in drug-free control (c) and in 10 µM UCL2077 (d). (e) Time to half deactivation ($t_{1/2}$) of fluorescence. Data are shown as mean ± SEM (error bars). *P<0.05; t-test

Kinetic modeling informs gating mechanisms for S140G in the absence of KCNE1

To further elucidate the mechanism of S140G on KCNQ1 gating, we simulated current and fluorescence by modifying a previous Markov model of channel gating[121], such that voltage sensors can exist in resting, intermediate, or fully activated states[84] (Fig. 1.6 a). Voltage sensor movement is represented by horizontal transitions in the model and occurs in two steps: first, independent movement of four S4's to an intermediate state; second, a concerted step to a fully

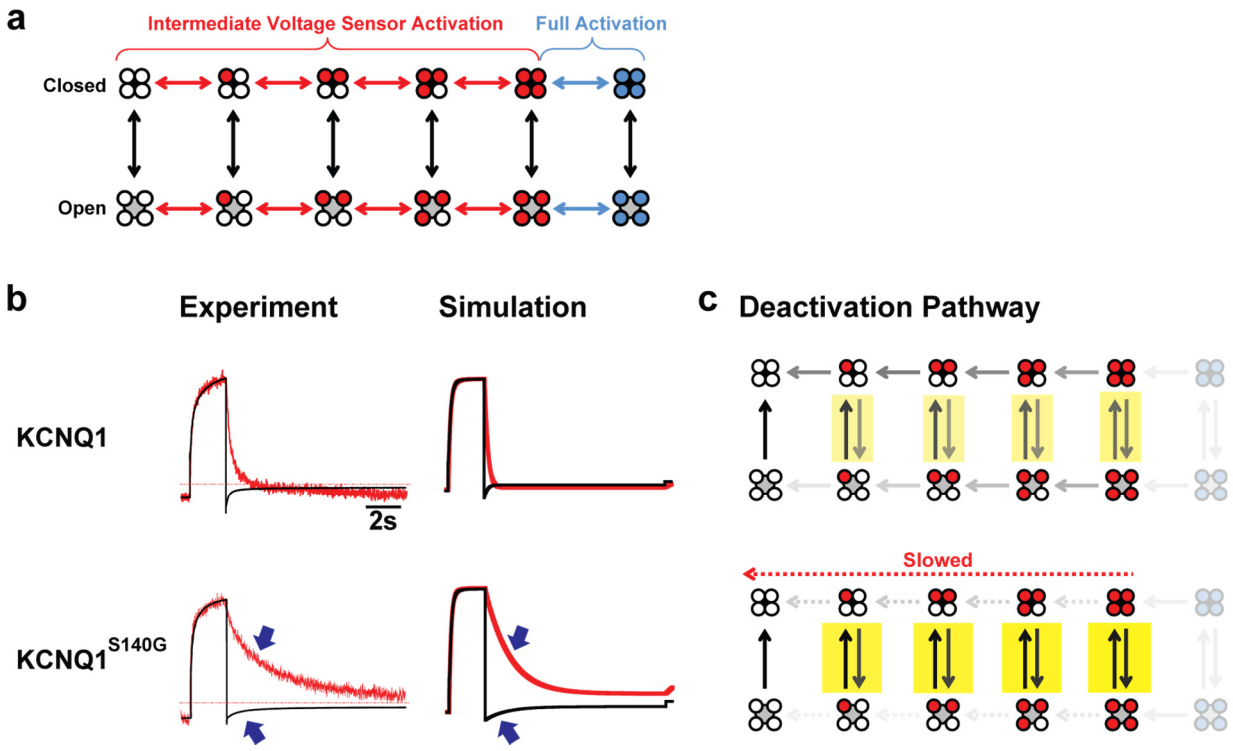

Figure 1.6. Simulating the effects of S140G on KCNQ1 gating in the absence of KCNE1. (a) Model of KCNQ1 gating. In this model, KCNQ1 can exist in distinct channel states. Horizontal transitions represent voltage sensor movement, while vertical transitions represent pore opening/closing. Voltage sensors can exist in the resting (white), intermediate (red), or fully activated state (blue). (b) Comparing experimental with simulated current (black) and fluorescence (red) traces for KCNQ1 and KCNQ1^{S140G}. (c) Descriptions of deactivation pathways at -100 mV for KCNQ1 and KCNQ1^{S140G} based on model rates. Arrows with greater opacity represent higher probability of channels entering the transitions specified. In the absence of KCNE1, the probability of channels existing in fully activated voltage sensor states (transparent) is low. The KCNQ1 channels can open and close in intermediate voltage sensor states during deactivation. KCNQ1^{S140G} slows voltage sensor deactivation, which causes increased channel openings and closings, as indicated by highlighting. KCNQ1^{S140G} thus indirectly slows current deactivation.

activated channel. Channel opening probability increases with each step of voltage sensor activation.

We obtained a model for KCNQ1 alone (Fig. 1.6 b, top) by fitting model parameters to our data for the kinetics and isochronal activation of both fluorescence and current. We also simulated the effect of PIP_2 depletion on fluorescence deactivation by preventing channel opening in the model, and then fitted these parameters to our VCF data. The resulting current and fluorescence simulation under a single pulse protocol closely resembles our VCF data for KCNQ1. Our model suggests that KCNQ1 deactivates through a pathway wherein channels may open and close when some or all voltage sensors are in intermediate states (Fig. 1.6 c, top). As

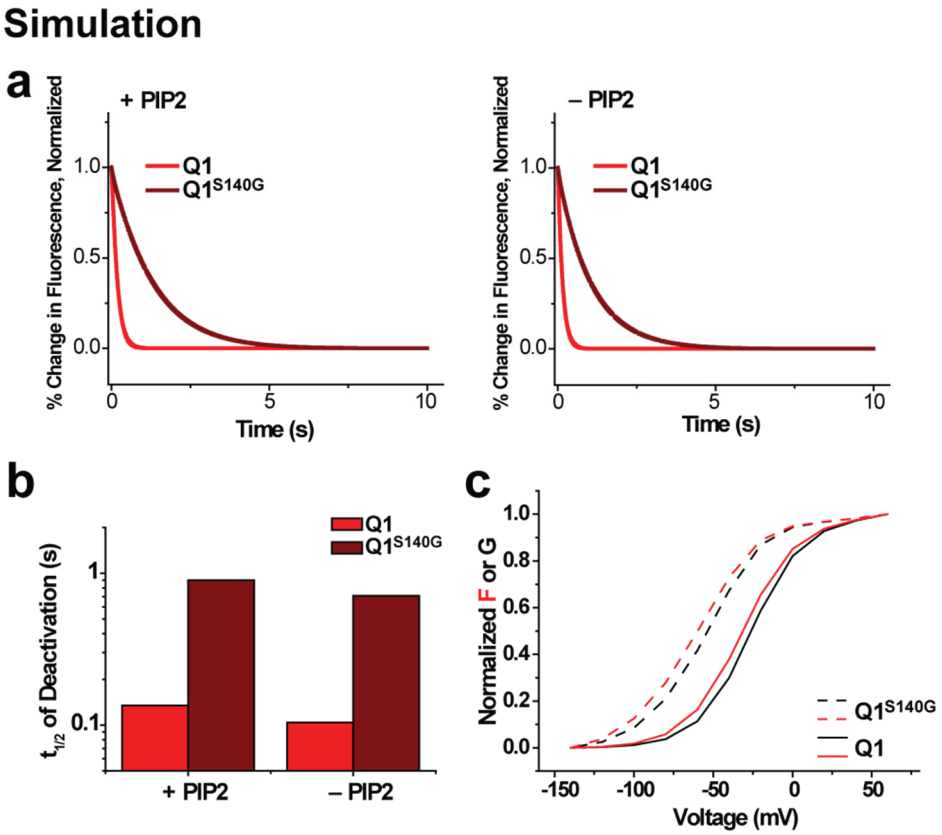

Figure 1.7. Simulation of PIP_2 depletion and isochronal activation for KCNQ1 and KCNQ1^{S140G}. (a) Normalized fluorescence deactivation at -100 mV before (left) and after (right) PIP_2 depletion. (b) Time to half deactivation of fluorescence. PIP_2 depletion was simulated by slowing channel opening 10,000 times, effectively preventing channel opening. (c) Normalized isochronal (2 s) activation for conductance (black) and fluorescence (red) for KCNQ1 and KCNQ1^{S140G}.

voltage sensor deactivation proceeds, channels become less likely to open. This leads to observed channel closure upon repolarization.

After establishing a working KCNQ1 model, we next modeled KCNQ1^{S140G} by altering only the voltage sensor transitions. We found that by only altering two parameters that determine the rate and the midpoint of the first voltage sensor transition (Table S1), all effects of KCNQ1^{S140G} are reproduced: a slowing in current and fluorescence deactivation (Fig. 1.6 b), and a hyperpolarizing shift in isochronal activation of conductance and fluorescence (Fig. 1.7). Furthermore, in our model, the slowing of fluorescence deactivation in KCNQ1^{S140G} is independent of channel opening (Fig. 1.7), consistent with our results from the PIP_2 depletion and UCL2077 inhibition assays. According to the model, directly slowing voltage sensor deactivation increases the number of times channels open when some or all voltage sensors are in intermediate states (Fig. 1.6 c, bottom). The increased number of openings indirectly slows current deactivation. To test whether an alternative gating mechanism might also be consistent with the effects of KCNQ1^{S140G}, we simulated channel current and fluorescence by only slowing pore transitions (Fig. 1.8). This alteration slows current deactivation, but only slightly slows fluorescence deactivation, inconsistent with the VCF data.

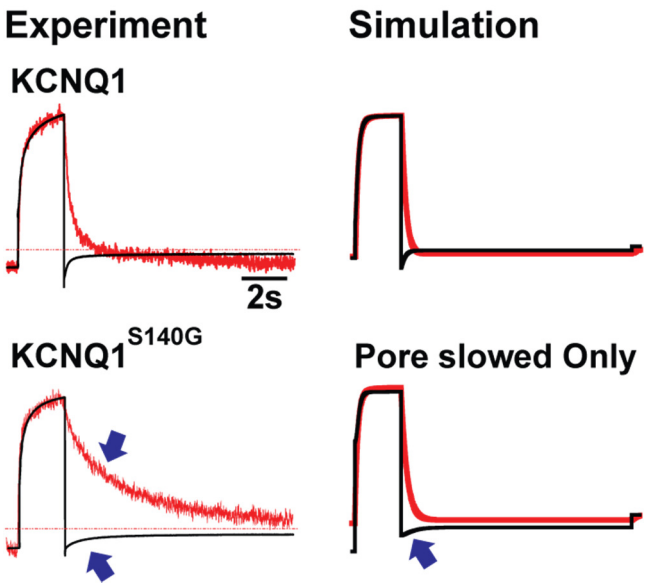

Figure 1.8. Simulation of KCNQ1 pore slowing does not recapitulate the effects of S140G. Fluorescence is shown in red whereas current is shown in black. Experimental and simulated traces are shown side by side for comparison. According to the kinetic model, directly slowing pore slowing slows current deactivation but causes minimal voltage sensor slowing, inconsistent with the effects of KCNQ1^{S140G} (arrows).

Discussion

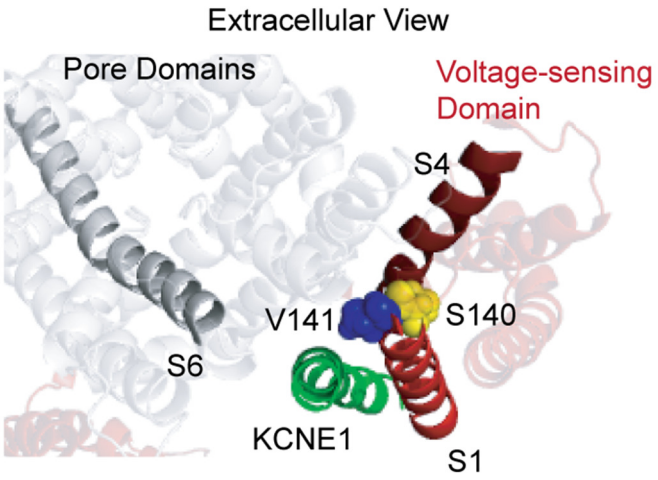

Figure 1.9. Homology model of KCNQ1. This model of open tetrameric KCNQ1 and KCNE1 from Kang *et al.* (2008) shows the atrial fibrillation mutation sites from an extracellular view. On the S1 helix, S140 (yellow) points toward S4, whereas V141 (blue) points away from the channel and toward the putative location of KCNE1.

I_{Ks} deactivation slowing caused by two KCNQ1 atrial fibrillation mutations, S140G and V141M, is thought to play a key role in arrhythmogenesis by excessively increasing the repolarizing current during repetitive stimulation and shortening the action potential duration. Here, we have determined the gating alterations underlying slow deactivation by S140G in the absence KCNE1. Using a combination of VCF and kinetic modeling, we showed that S140G slows current deactivation indirectly by altering voltage sensor movement. Conversely, a neighboring mutation that also causes atrial fibrillation, V141M, has minimal effect on channel gating. These results are consistent with prior studies and a published homology model of KCNQ1, in which S140 faces toward the voltage-sensing S4 (Fig. 1.9) and is in proximity to a salt bridge interaction between R237 on S4 and E160 on S2 in the open state[189,192]. We therefore propose that S140G stabilizes this interaction, thereby explaining the hyperpolarizing shift in the voltage-dependence of voltage sensor activation and slowing of voltage sensor deactivation. In contrast, V141 points towards the lipids and away from the rest of the channel, thereby explaining the lack of effect on channel function by the mutation V141M.

According to our kinetic model, two different gating alterations can slow current deactivation: either a direct slowing of pore transitions, or a direct slowing of voltage sensor

movement which indirectly slows current deactivation. A direct voltage sensor effect in KCNQ1^{S140G} is supported by the good agreement between our simulation and our VCF data. In addition, our PIP_2 depletion and UCL2007 inhibition experiments revealed a direct voltage sensor effect independent of the pore. Furthermore, our simulation of direct pore slowing is does not recapitulate the effects of KCNQ1^{S140G}, further supporting current slowing as the indirect effect of voltage sensor slowing rather than a direct pore effect. Thus, kinetic modeling guided our interpretation of the VCF data and elucidated the underlying gating alterations in KCNQ1^{S140G}.

While our results have elucidated the mechanism of current deactivation slowing for KCNQ^{S140G}, the gating alterations underlying deactivation slowing in the presence of KCNE1 (I_{Ks}^{S140G} and I_{Ks}^{V141M}) remain to be determined. Based on our present findings, one possible explanation is that I_{Ks}^{S140G} and I_{Ks}^{V141M} demonstrate distinct mechanisms of current slowing. On one hand, I_{Ks}^{S140G} may directly slow voltage sensor deactivation similar to KCNQ1^{S140G}, indirectly slowing current deactivation. This assumes that S140G's gating effects are not altered by KCNE1. However, previous measurements of current deactivation kinetics have shown that degree of slowing is greater in I_{Ks}^{S140G} compared with KCNQ1^{S140G}, suggesting that S140G's effect may be partially dependent on KCNE1[190]. Furthermore, the substitution of a serine residue with the much smaller amino acid glycine can cause structural changes beyond the locality of the residue, thereby altering the position of S1 and disrupting interaction with KCNE1. On the other hand, given that V141M has minimal effect on KCNQ1 gating and that V141 crosslinks with residues on KCNE1, I_{Ks}^{V141M} may slow deactivation by perturbing the orientation of KCNE1 relative to KCNQ1. KCNE1 has been previously shown to play a critical role in modulating the coupling between the voltage sensor and the pore[83,84]. It is therefore

possible that perturbing KCNE1 disrupts voltage sensor-pore coupling and contributes to deactivation slowing in I_{Ks}^{V141M}.

In summary, our VCF results and kinetic modeling elucidated the gating alteration underlying deactivation slowing in $KCNQ1^{S140G}$. We showed that $KCNQ1^{S140G}$ directly slows voltage sensor deactivation, which indirectly slows current deactivation. On the other hand, $KCNQ1^{V141M}$ exerts minimal effects on channel gating. These results are consistent with prior functional and structural data and form the basis for studying gating alterations by atrial fibrillation mutations in the physiologic I_{Ks}.

Chapter 2: Gating mechanisms underlying deactivation slowing by atrial fibrillation mutations in I_{Ks}

Summary

I_{Ks}, the slow delayed rectifier potassium current, is formed by the co-assembly of the pore-forming α-subunit KCNQ1 with the β-subunit KCNE1 and plays a critical role in repolarizing the cardiac action potential. In Chapter 1 we studied the effects of two KCNQ1 mutations associated atrial fibrillation, S140G and V141M, on KCNQ1 gating. Here, we elucidate the gating mechanism underlying deactivation slowing in the presence of KCNE1 (I_{Ks}^{S140G} and I_{Ks}^{V141M}), which contributes to the pathophysiology of atrial fibrillation. We tested the hypothesis that I_{Ks}^{S140G}, similar to $KCNQ1^{S140G}$, slows voltage sensor deactivation and indirectly slows current deactivation, whereas I_{Ks}^{V141M} disrupts voltage sensor-pore coupling. Using VCF and kinetic modeling, we found that both I_{Ks}^{S140G} and I_{Ks}^{V141M} alter voltage sensor-pore coupling and slow pore closing, leading to slowing of I_{Ks} deactivation. Our finding that the β-subunit modifies the gating effects of both mutations implicates novel molecular mechanisms through which KCNE1 modulates voltage sensor-pore coupling and pore motions.

Introduction

The pore-forming subunit KCNQ1 is modulated by the β-subunit KCNE1 to generate I_{Ks}, which plays a critical role in repolarizing the cardiac action potential. Mutations in both subunits have been associated with potentially lethal arrhythmia including long QT syndrome, short QT syndrome, and atrial fibrillation. Four subunits of KCNQ1 assemble to generate a voltage-dependent ion channel with four voltage-sensing domains (VSDs) and a central pore. Each voltage-sensing domain is composed of transmembrane helices S1-S4 and contains the positively charged S4 helix that responds to changes in membrane potential. The channel pore is formed

by the pore domains (S5-P-loop-S6) of four KCNQ1 subunits. Movement of the S4 is coupled to the pore through the S4-S5 linker and requires the presence of the lipid molecule PIP_2.

While KCNQ1 by itself can generate a voltage-dependent current, it is modulated by KCNE1 to generate I_{Ks}, characterized by a sigmoidal activation kinetics. KCNE1 consists of a single transmembrane helix and is thought to have multiple and extensive points of contact with KCNQ1 that reside within both the VSD and the pore domain[135-137,139-141]. The effects of KCNE1 on KCNQ1 function include a delay in the onset of activation, an increase in current amplitude, and a depolarizing shift in the current-voltage relationship[31,32]. Voltage clamp fluorometry (VCF) experiments, which simultaneously measure voltage sensor movement and ionic current through the channel pore, have shown that KCNE1 alters the VSD-pore coupling in KCNQ1, delays the opening of the activation gate, and causes a hyperpolarizing shift in the voltage-dependence of the main voltage sensor activation and a depolarizing shift in the voltage-dependence of current activation[83,193]. The ratio of KCNE1 to KCNQ1 subunits in I_{Ks} remains controversial, with some evidence suggesting a fixed 2:4 ratio while others suggesting a flexibility in ratio that serves as a mechanism of channel regulation[145-149].

Deactivation slowing is thought to be the key pathophysiological mechanism by which two KCNQ1 mutations, S140G and V141M, cause a genetic form atrial fibrillation. I_{Ks} deactivation slowing causes accumulation of open channels under repeated stimulation, which increases the repolarizing current in cardiomyocytes, shortens the action potential duration, and predisposes the heart to re-entry arrhythmia. We have shown that in the absence of KCNE1, S140G slows voltage sensor deactivation, which indirectly slows current deactivation, whereas V141M has minimal effect on channel gating. Based on these results, we hypothesized that deactivation slowing in the presence of KCNE1 may be due to different mechanisms between

S140G and V141M: I_{Ks}^{S140G} may slow voltage sensor movement to indirectly slow current deactivation, whereas I_{Ks}^{V141M} may perturb the orientation of KCNE1 relative to KCNQ1 to disrupt voltage sensor–pore coupling and slow deactivation. However, without measurement of voltage sensor movement, the gating alterations underlying deactivation slowing in I_{Ks}^{S140G} and I_{Ks}^{V141M} remain unknown.

Here, we use VCF and kinetic modeling to determine the gating effects of I_{Ks}^{S140G} and I_{Ks}^{V141M}. We show that I_{Ks}^{S140G} slows both current and voltage sensor deactivation, whereas I_{Ks}^{V141M} slows current deactivation without slowing voltage sensor deactivation. In contrast to $KCNQ1^{S140G}$, voltage sensor slowing in I_{Ks}^{S140G} is dependent on pore opening, suggesting that an alternative mechanism of slowing is present. Interestingly, our kinetic models inform that both I_{Ks}^{S140G} and I_{Ks}^{V141M} alter VSD-pore coupling and slow pore closing, changing the pathway of deactivation such that channels in intermediate voltage sensor states can either reopen or stay open. These findings provide key insights that aid the development of mechanism-based pharmacologic therapies for arrhythmias associated with I_{Ks} dysfunction.

Results

In the presence of KCNE1, S140G and V141M cause similar dysfunction in channel currents, but distinct effects on voltage sensor movement

To understand the mechanisms underlying the effects of the atrial fibrillation mutations on the physiologic I_{Ks} current, we co-expressed KCNQ1 or KCNQ1 mutants with KCNE1 and used VCF to measure voltage sensor movement simultaneously with current. As in previous studies, we utilized a KCNQ1 construct containing a G219C site in the S3-S4 linker that can be labelled covalently with a fluorophore to report voltage sensor movement. Figure 2.1 a-c shows

currents and fluorescence changes measured in I_{Ks} and mutant channels in response to voltage pulses to +80 mV for 5 s followed by repolarization to -40 mV. For I_{Ks}, fluorescence activation precedes current activation, as previously reported[83]. Neither mutant channel appreciably affects the kinetics of current activation. However, whereas I_{Ks} deactivates completely at -40 mV, neither I_{Ks}^{S140G} nor I_{Ks}^{V141M} deactivates appreciably. Interestingly, I_{Ks}^{S140G} and I_{Ks}^{V141M} exert

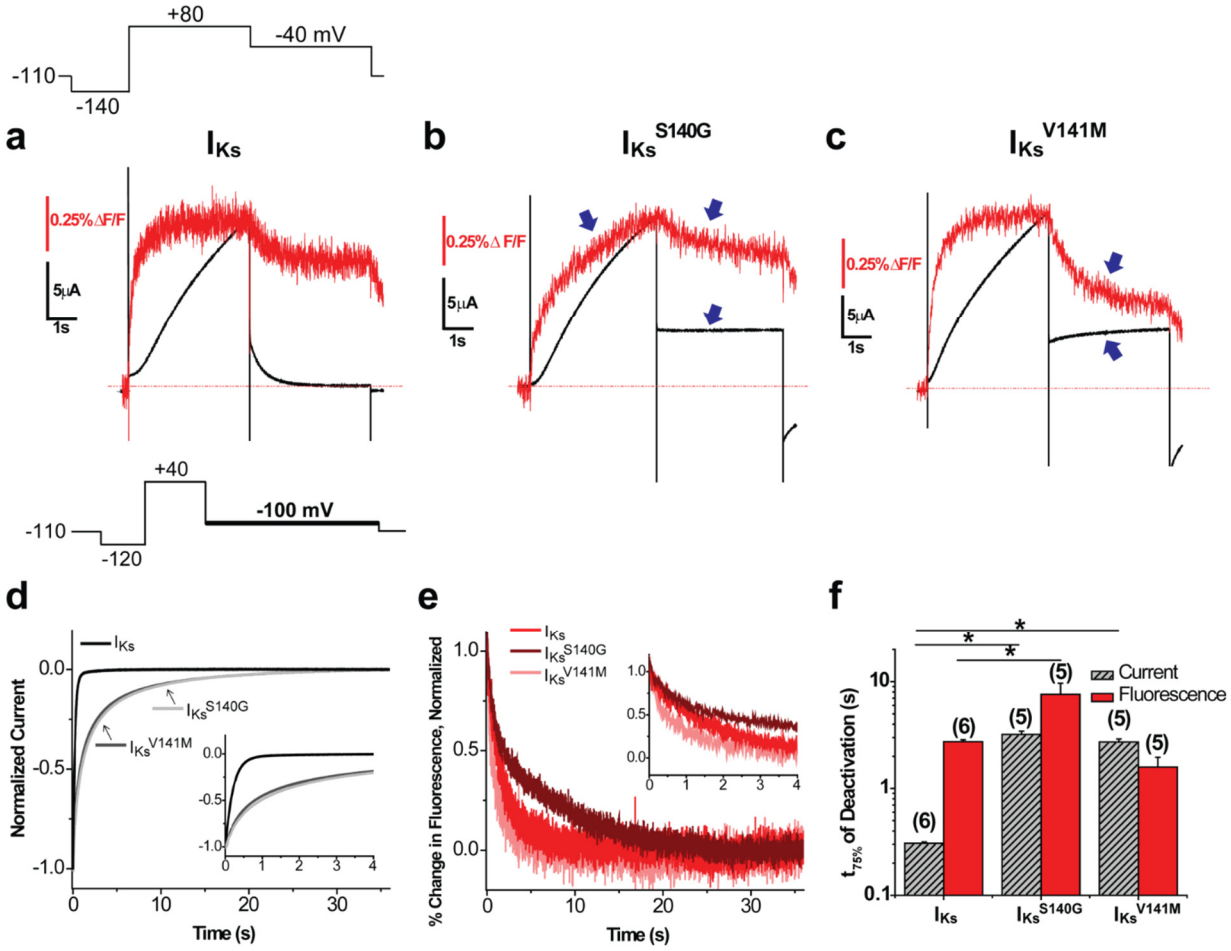

Figure 2.1. In the presence of KCNE1, S140G slows current deactivation and voltage sensor movement whereas V141M slows current deactivation without slowing voltage sensor movement. (a-c) Current and fluorescence traces for I_{Ks} (a), I_{Ks}^{S140G} (b), and I_{Ks}^{V141M} (c) in the presence of KCNE1 using a single pulse protocol. From a prepulse of -140 mV, a test pulse was applied at +80 mV followed by a repolarizing step to -40 mV. Cells were held at -110 mV. Arrows indicate effect of mutations on current or fluorescence. (d) Normalized current during deactivation at -100 mV for I_{Ks}, I_{Ks}^{S140G}, and I_{Ks}^{V141M}. Inset shows the first 4 s of deactivation. Deactivation was examined using the following voltage protocol: from a prepulse of -120 mV, an activating pulse was applied at +40 mV, followed by a repolarizing step to -100 mV. Channels are held at -110 mV. (e) Normalized percent change in fluorescence during deactivation at -100 mV. Inset shows first 4 s of deactivation. (f) Time to 75% deactivation ($t_{75\%}$). Data are shown as mean ± SEM (error bars). *P<0.05; one-way ANOVA with Tukey's test.

distinct effects on voltage sensor movement. I_{Ks}^{S140G} apparently slows both the activation and deactivation kinetics of voltage sensor movement. On the other hand, I_{Ks}^{V141M} does not apparently alter voltage sensor kinetics, but leads to a different steady state level at -40 mV. Additional control experiments demonstrate that measured current for I_{Ks}, I_{Ks}^{S140G} and I_{Ks}^{V141M} are inhibited by 100 μM Chromanol 293B (Supplementary Fig. S1).

As deactivation of mutant I_{Ks} is incomplete at -40 mV, we applied another voltage protocol in which we activated channels at +40 mV and then deactivated at -100 mV to close channels more fully. We determined the time to 75% deactivation as a marker for deactivation kinetics (Fig. 2.1 d-f). Compared with I_{Ks} ($Ft_{75\%}$ = 2.74 ± 0.12 s, $It_{75\%}$ = 0.307 ± 0.009 s), I_{Ks}^{S140G} ($Ft_{75\%}$ = 7.59 ± 2.06 s, $It_{75\%}$ = 3.20 ± 0.23 s) significantly slows both voltage sensor and current deactivation by 2.8- and 10.4-fold, respectively. I_{Ks}^{V141M} ($Ft_{75\%}$ = 1.59 ± 0.37 s, $It_{75\%}$ = 2.73 ± 0.18 s) also drastically slows current deactivation kinetics (8.9-fold), but does not slow voltage sensor deactivation. The differing effects of the two mutations on voltage sensor movement suggest that they may slow current deactivation through distinct mechanisms in the presence of KCNE1.

In the presence of KCNE1, both S140G and V141M alter isochronal activation of conductance and fluorescence

Voltage-dependent activation curves illustrate the relationship between voltage sensor movement and pore opening and thus provide insight on voltage sensor-pore coupling. Steady-state measurement for I_{Ks} is difficult due to its very slow activation kinetics, and requires very long activating pulses that are not ideal for VCF experiments. We therefore measured isochronal activation curves using 5-s pulses to study voltage-dependent activation of voltage sensors and

the pore. When we plotted isochronal activation of fluorescence (FV) and conductance (GV) for I_{Ks}, we found that, as previously shown, KCNE1 divides voltage sensor activation into two components: a main component at hyperpolarized potentials where the channel remains closed, and a second component at depolarized potentials associated with channel opening (Fig. 2.2). For both I_{Ks}^{S140G} and I_{Ks}^{V141M}, there is a depolarizing shift in the main FV and a hyperpolarizing shift in the GV, leading to decreased separation between FV and GV. The second component in the FV associated with channel opening is not discernable in both mutants and may overlap with the main component. These results suggest that both I_{Ks}^{S140G} and I_{Ks}^{V141M} alter the relationship between voltage sensor and pore.

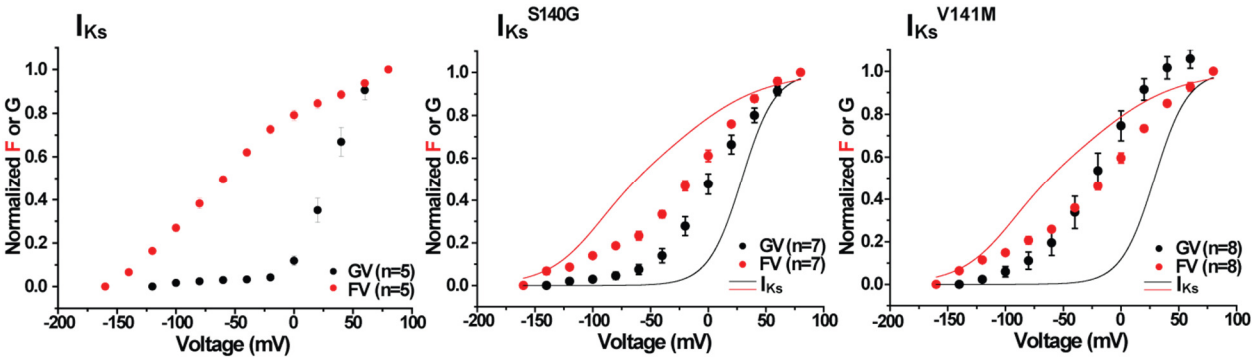

Figure 2.2. Normalized isochronal (5 s) activation for fluorescence and conductance for I_{Ks}, I_{Ks}^{S140G}, and I_{Ks}^{V141M}. Lines represent I_{Ks} for comparison. Cells were held at -110 mV, prepulsed to -140 mV to deactivate channels, followed by test pulses between +80 mV and -160 mV in intervals of 20 mV. Fluorescence is shown in red whereas conductance is shown in black.

In the presence of KCNE1, S140G slowing of voltage sensor deactivation is dependent on channel opening

As previously discussed, direct effects on the channel pore may indirectly slow voltage sensor deactivation as the result of retrograde coupling. We previously utilized PIP_2 depletion and UCL2077 to prevent channel pore opening and dissect the voltage sensor effects of a mutation. We showed in Chapter 1 that in the absence of KCNE1, S140G slows voltage sensor

deactivation independently of channel opening. To investigate whether the same holds in the presence of KCNE1, we again used these two different approaches to prevent channel opening. To first demonstrate the effect of PIP_2 depletion on current amplitude and voltage sensor activation in I_{Ks}, we co-expressed I_{Ks} with ciVSP and repeatedly depolarized the cell to +80 mV to activate the phosphatase. Repeated depolarization reduces tail current amplitude, as shown in Figure 2.3. However, the simultaneously measured fluorescence signal remains intact, indicating that voltage sensor movement is preserved as PIP_2 is depleted. Furthermore, to verify the effect of UCL2077 on I_{Ks} gating, isochronal activation of I_{Ks} was recorded before and after application of 10 µM UCL2077. As previously published, 10 µM UCL2077 effectively inhibits the I_{Ks} current (Supplementary Fig. S2), and at the same time reduces the second component of fluorescence that correlates with channel opening. This is consistent with previous findings and suggest that UCL2077 does not simply block the channel pore, but stabilize the closed conformation of the channel.

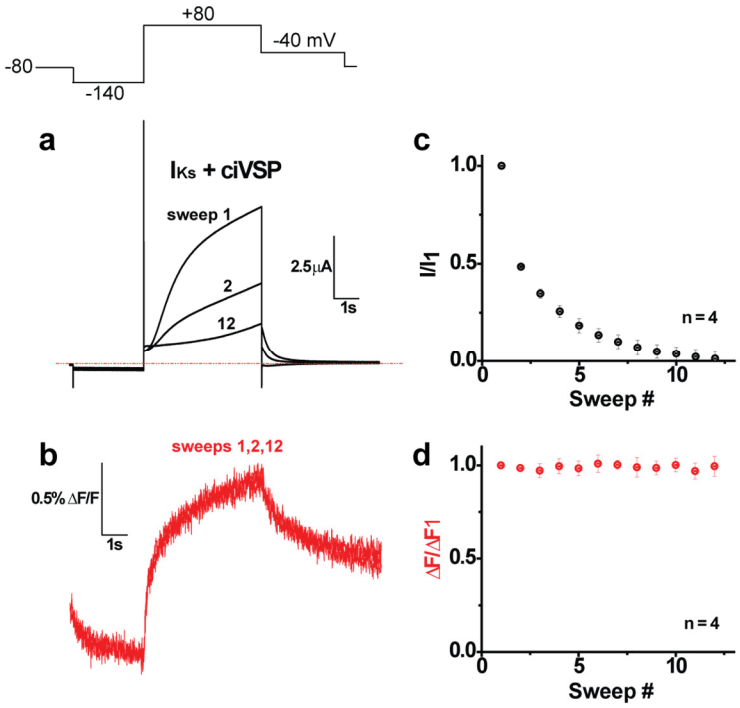

Figure 2.3. PIP_2 depletion diminishes I_{Ks} current amplitude while voltage sensor movement remains intact. The voltage protocol involves depolarization to +80 mV and is repeated for 12 sweeps. (a-b) Traces for sweeps 1, 2, and 12 are shown for current (black) and fluorescence (red). (c-d) Normalized tail current and fluorescence change are plotted against sweep number.

Given that I_{Ks}^{S140G}, not I_{Ks}^{V141M}, slows fluorescence deactivation, we focused our PIP_2 depletion and UCL2077 inhibition experiments on I_{Ks}^{S140G}. When I_{Ks} or I_{Ks}^{S140G} was co-expressed with ciVSP, activating ciVSP by repeated membrane depolarization resulted in a reduction of current amplitude in both channels, indicating a reduction in PIP_2 (Fig. 2.4 a-b).

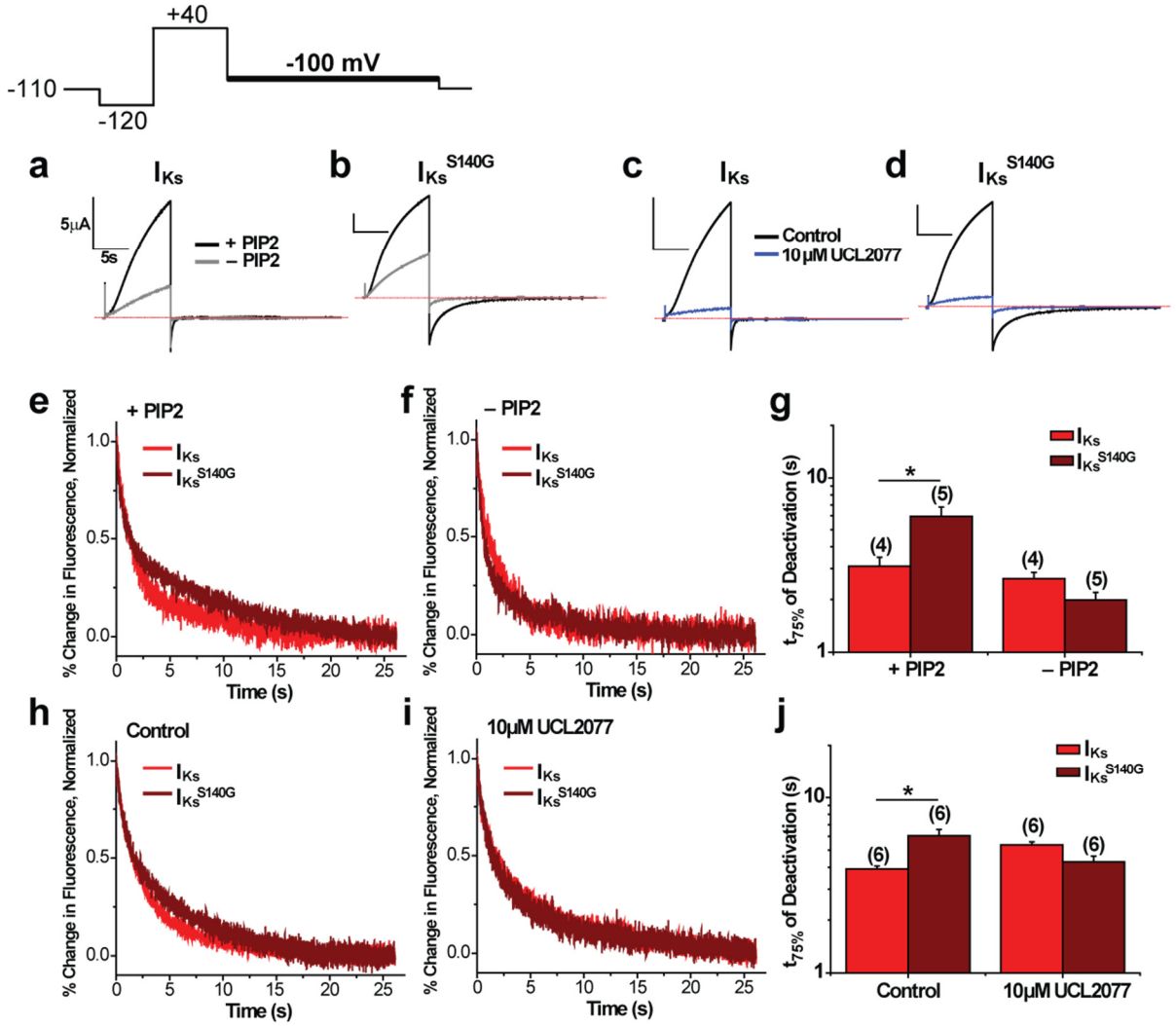

Figure 2.4. In the presence of KCNE1, S140G slowing of voltage sensor deactivation is dependent on channel opening. The following protocol was used: from a prepulse of -140 mV, an activating pulse was applied at +40 mV, followed by a repolarizing step to -100 mV. Channels were held at -110 mV. (a-b) Current measured before (+PIP_2) and after PIP_2 depletion (-PIP_2) for I_{Ks} (a) and I_{Ks}^{S140G} (b). (c-d) Current measured in drug-free control and in 10 μM UCL2077 for I_{Ks} (c) and I_{Ks}^{S140G} (d). (e-f) Normalized fluorescence deactivation traces at -100 mV before (e) and after PIP_2 depletion (f) for I_{Ks} (red) and I_{Ks}^{S140G} (dark red). (g) Time to 75% deactivation ($t_{75\%}$) of fluorescence before and after PIP_2 depletion. (h-i) Normalized fluorescence deactivation traces at -100 mV in drug-free control (h) and in 10 μM UCL2077 (i) for I_{Ks} (red) and I_{Ks}^{S140G} (dark red). (j) Time to 75% deactivation ($t_{75\%}$) of fluorescence in control and in 10 μM UCL2077. Data are shown as mean ± SEM (error bars). *P<0.05; one-way ANOVA with Tukey's test (including I_{Ks}^{V141M}).

Application of 10 μM UCL2077 also reduces current amplitude in both channels (Fig. 2.4 c-d). Fluorescence deactivation (Fig. 2.4 e-g) was simultaneously measured with current to show that, prior to PIP_2 depletion, I_{Ks}^{S140G} ($Ft_{75\%}$ = 5.95 ± 0.88 s) significantly slows fluorescence deactivation compared with I_{Ks} ($Ft_{75\%}$ = 3.10 ± 0.38 s). However, surprisingly, following PIP_2 depletion, I_{Ks}^{S140G} ($Ft_{75\%}$ = 1.99 ± 0.21 s) no longer slows deactivation compared with I_{Ks} ($Ft_{75\%}$ = 2.64 ± 0.22 s), contrary to what we observed in $KCNQ1^{S140G}$. Similarly, in drug-free conditions, I_{Ks}^{S140G} ($Ft_{75\%}$ = 6.06 ± 0.52 s) slows fluorescence deactivation compared with I_{Ks} ($Ft_{75\%}$ = 3.90 ± 0.17 s); however, following current inhibition with 10 μM UCL2077, I_{Ks}^{S140G} ($Ft_{75\%}$ = 4.30 ± 0.34 s) no longer slows fluorescence deactivation ($Ft_{75\%}$ = 5.36 ± 0.22 s) (Fig. 2.4 h-j). These results show that in the presence of KCNE1, S140G slowing of voltage sensor movement is dependent on channel opening.

Although I_{Ks}^{V141M} does not slow voltage sensor deactivation, we examined the effect of PIP_2 depletion and UCL2077 inhibition on I_{Ks}^{V141M} fluorescence deactivation as a control experiment. Both activation of ciVSP as well as application of 10 μM UCL2077 reduced current amplitude (Fig. 2.5). I_{Ks}^{V141M} does not significantly alter fluorescence deactivation both before ($Ft_{75\%}$ = 1.79 ± 0.17 s) and after PIP_2 depletion ($Ft_{75\%}$ = 2.26 ± 0.39 s). Furthermore, I_{Ks}^{V141M} does not significantly alter fluorescence deactivation kinetics in control conditions prior to application of 10 μM UCL2077 ($Ft_{75\%}$ = 3.58 ± 0.39 s). Following application of 10 μM UCL2077, I_{Ks}^{V141M} speeds fluorescence deactivation 1.8 fold ($Ft_{75\%}$ = 2.99 ± 0.31 s) compared with I_{Ks}. However, this result was not observed in the PIP_2 depletion experiment and thus may be unrelated to the pore-closing effect of UCL2077.

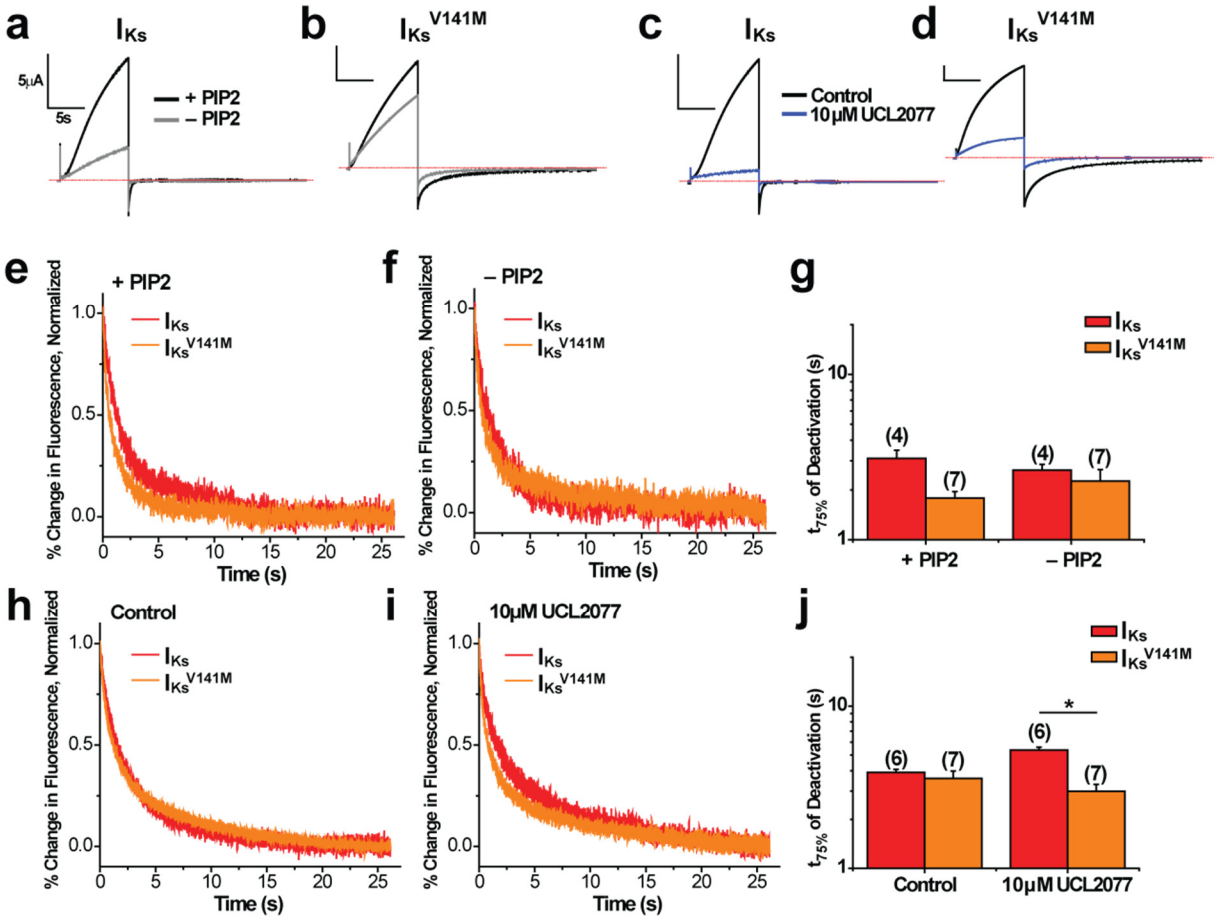

Figure 2.5. Effect of I_{Ks}^{V141M} on voltage sensor movement either under PIP_2 depletion or UCL2077 inhibition. The following protocol was used: from a prepulse of -140 mV, an activating pulse was applied at +40 mV, followed by a repolarizing step to -100 mV. Channels were held at -110 mV. (a-b) Current measured before ($+PIP_2$) and after PIP_2 depletion ($-PIP_2$) for I_{Ks} (a) and I_{Ks}^{V141M} (b). (c-d) Current measured in drug-free control and in 10 μM UCL2077 for I_{Ks} (c) and I_{Ks}^{V141M} (d). (e-f) Normalized fluorescence deactivation traces at -100 mV before (e) and after PIP_2 depletion (f) for I_{Ks} (red) and I_{Ks}^{V141M} (orange). (g) Time to 75% deactivation of fluorescence. (h-i) Normalized fluorescence deactivation traces at -100 mV in drug-free control (h) and 10 μM UCL2077 (i) for I_{Ks} (red) and I_{Ks}^{V141M} (orange). (j) Time to 75% deactivation of fluorescence (right). Data are shown as mean ± SEM (error bars). *P<0.05; one-way ANOVA with Tukey's test.

Kinetic modeling informs gating mechanisms for S140G and V141M in the presence of KCNE1

We modeled the effects of S140G and V141M in the presence of KCNE1 using the same gating scheme as described previously (Fig. 2.6 a). This scheme describes three possible states for voltage sensors: resting, intermediate, and activated. Horizontal transitions represent voltage sensor movement while vertical transitions represent pore opening/closing. We first modeled I_{Ks} by fitting parameters to our VCF data, including isochronal activation, activation kinetics, as well as deactivation kinetics for both current and fluorescence (Fig. 2.6 b top). Our model simulations of I_{Ks} show good agreement with previous VCF recordings by Barro-Soria *et al.* (Supplementary Fig. S3).

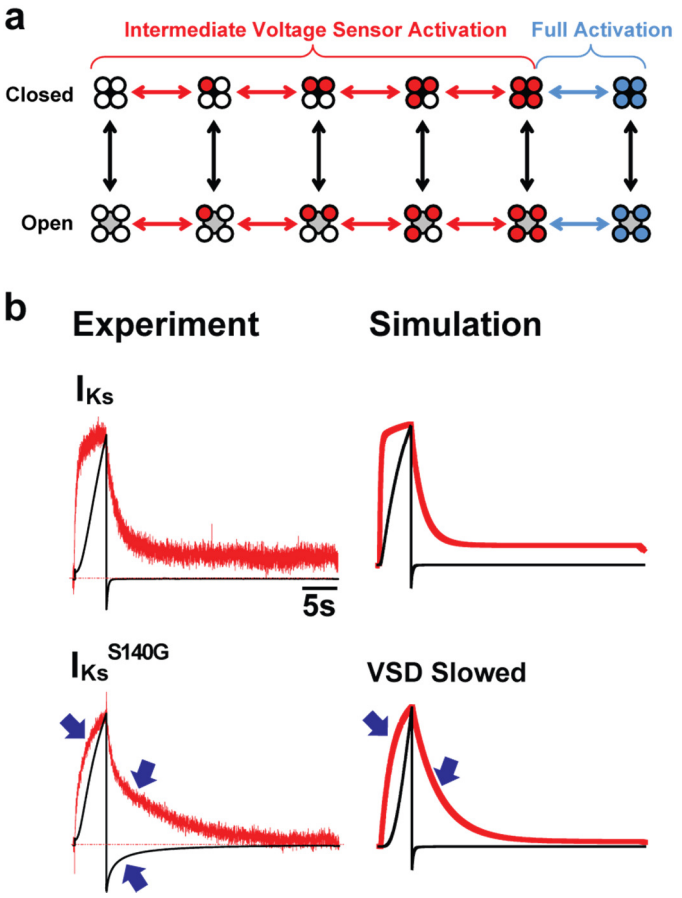

Figure 2.6. Simulation of I_{Ks} voltage sensor movement slowing does not recapitulate the effects of S140G. (a) Model of KCNQ1 gating. In this model, horizontal transitions represent voltage sensor movement, while vertical transitions represent pore opening/closing. Voltage sensors can exist in the resting (white), intermediate (red), or fully activated state (blue). (b) According to the kinetic model, slowing only voltage sensor movement causes minimal slowing in current deactivation, inconsistent with the observed effects of I_{Ks}^{S140G} (arrows). Fluorescence is shown in red and current is shown in black. Experimental and simulated traces are shown side by side for comparison.

Given that $KCNQ1^{S140G}$ directly slows voltage sensor movement, we first explored whether a direct voltage sensor slowing can also account for the effects of I_{Ks}^{S140G} on fluorescence and current deactivation. When we only slowed voltage sensor transitions in our

kinetic model of I_{Ks}, we found that, as expected, fluorescence deactivation slowed (Fig. 2.6 b bottom). However, there was minimal slowing of current deactivation in our model, inconsistent with the observed effects of I_{Ks}^{S140G}. This result suggests that, unlike $KCNQ1^{S140G}$, the slowing of current deactivation in I_{Ks}^{S140G} cannot be explained by a direct voltage sensor slowing.

Next, we modeled the effects of I_{Ks}^{S140G} and I_{Ks}^{V141M} by varying 4 parameters in the I_{Ks} model, with most changes occurring in the rate of the pore closing transition and a factor that controls voltage sensor-pore coupling (Table S2). As before, model parameters were fitted to our experimental data on activation/deactivation kinetics, isochronal activation, and PIP_2 depletion. To further constrain the model, we determined the Rb^+/K^+ permeability ratios of I_{Ks} and mutant channels. It has been previously shown that the Rb^+/K^+ permeability ratio in KCNQ1 and I_{Ks} depends on the degree of voltage sensor activation[84]. Specifically, channels in the intermediate voltage sensor state have a higher Rb^+/K^+ permeability ratio than channels in the fully activated voltage sensor state. This allows us to estimate the fraction of ion channels in the

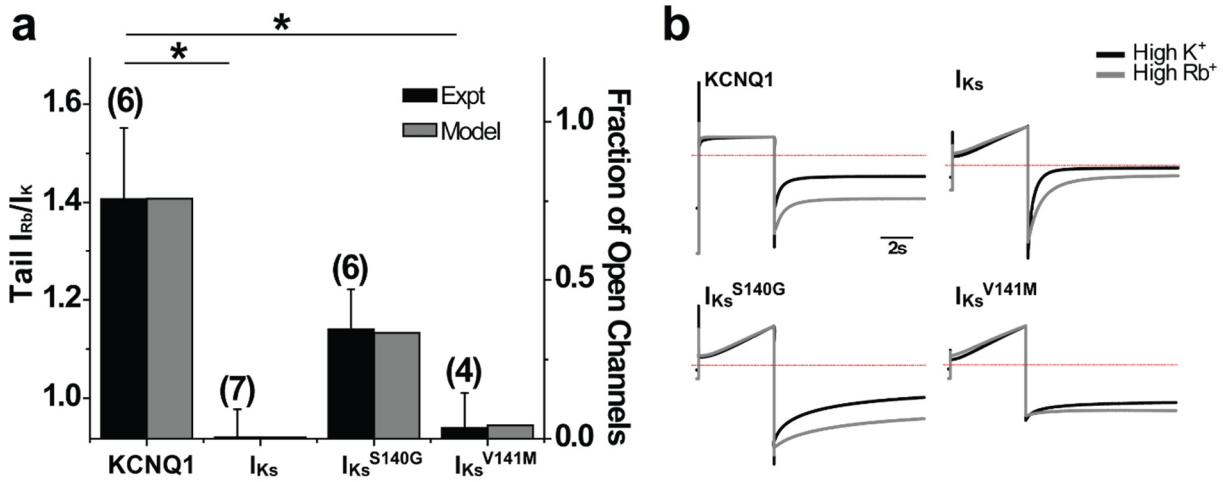

Figure 2.7. Using Rb^+/K^+ permeability ratios to constrain kinetic models of I_{Ks} mutants. (a) Comparison of measured tail Rb^+/K^+ ratio with fraction of open channels in the intermediate VSD state following activation, as calculated from model after constraining. Rb^+/K^+ permeability ratio was determined from inward tail current measured either under high external K^+ or Rb^+ concentration. The ratios were converted to expected fraction of open channels in the intermediate VSD state and then used to constrain the model. Results for KCNQ1 and I_{Ks} were used for normalization. Data are shown as mean ± SEM (error bars). *P<0.05; one-way ANOVA with Tukey's test. (b) Averaged current recordings under high external K^+ or Rb^+ concentration.

intermediate voltage sensors state, which helps further constrain the model. We determined the Rb^+/K^+ permeability ratios using inward tail current measured at -60 mV following a 5-s activation pulse to +40 mV. The Rb^+/K^+ ratio of KCNQ1 (1.41 ± 0.14) is significantly greater than that of I_{Ks} (0.92 ± 0.06), suggesting that a greater fraction of open channels exists in the intermediate voltage sensor state for KCNQ1 compared with I_{Ks} (Fig. 2.7). This is supported by a control experiment using the true wildtype KCNQ1 (Supplementary Fig. S4). As for the I_{Ks} mutations, the Rb^+/K^+ ratio of I_{Ks}^{S140G} (1.14 ± 0.08) is between that of KCNQ1 and I_{Ks}, whereas the ratio of I_{Ks}^{V141M} (0.94 ± 0.07) is similar to I_{Ks} (Fig. 2.7). Using these ratios, we calculated the expected fraction of open channels in the intermediate voltage sensor state following the activation pulse, and fitted our model of I_{Ks}^{S140G} and I_{Ks}^{V141M} to these results.

Our resulting model simulates the distinct effects of S140G and V141M on current and fluorescence kinetics in the presence of KCNE1. In our model, I_{Ks}^{S140G} slows fluorescence and current deactivation, whereas I_{Ks}^{V141M} slows current deactivation without slowing fluorescence deactivation (Fig. 2.9 a). These effects are consistent with our experimental data. Furthermore, the model is in agreement with our data on the effects of the two mutations on isochronal activation and fluorescence deactivation under PIP_2 depletion (Fig. 2.8). Specifically, I_{Ks}^{S140G} slowing of fluorescence deactivation is dependent on pore opening, whereas I_{Ks}^{V141M} has minimal effects on fluorescence deactivation regardless of whether pore opening is allowed.

We calculated transition rates in our kinetic models at -100 mV for I_{Ks}, I_{Ks}^{S140G} and I_{Ks}^{V141M} to determine the pathway of channel deactivation (Fig. 2.9 b). Our model of I_{Ks} shows that, as previously established, KCNE1 alters the coupling between the VSD and the pore in KCNQ1, preventing channel opening when voltage sensors are in the intermediate state[84]. As a result, I_{Ks} follows a deactivation pathway in which pore closing precedes voltage sensor

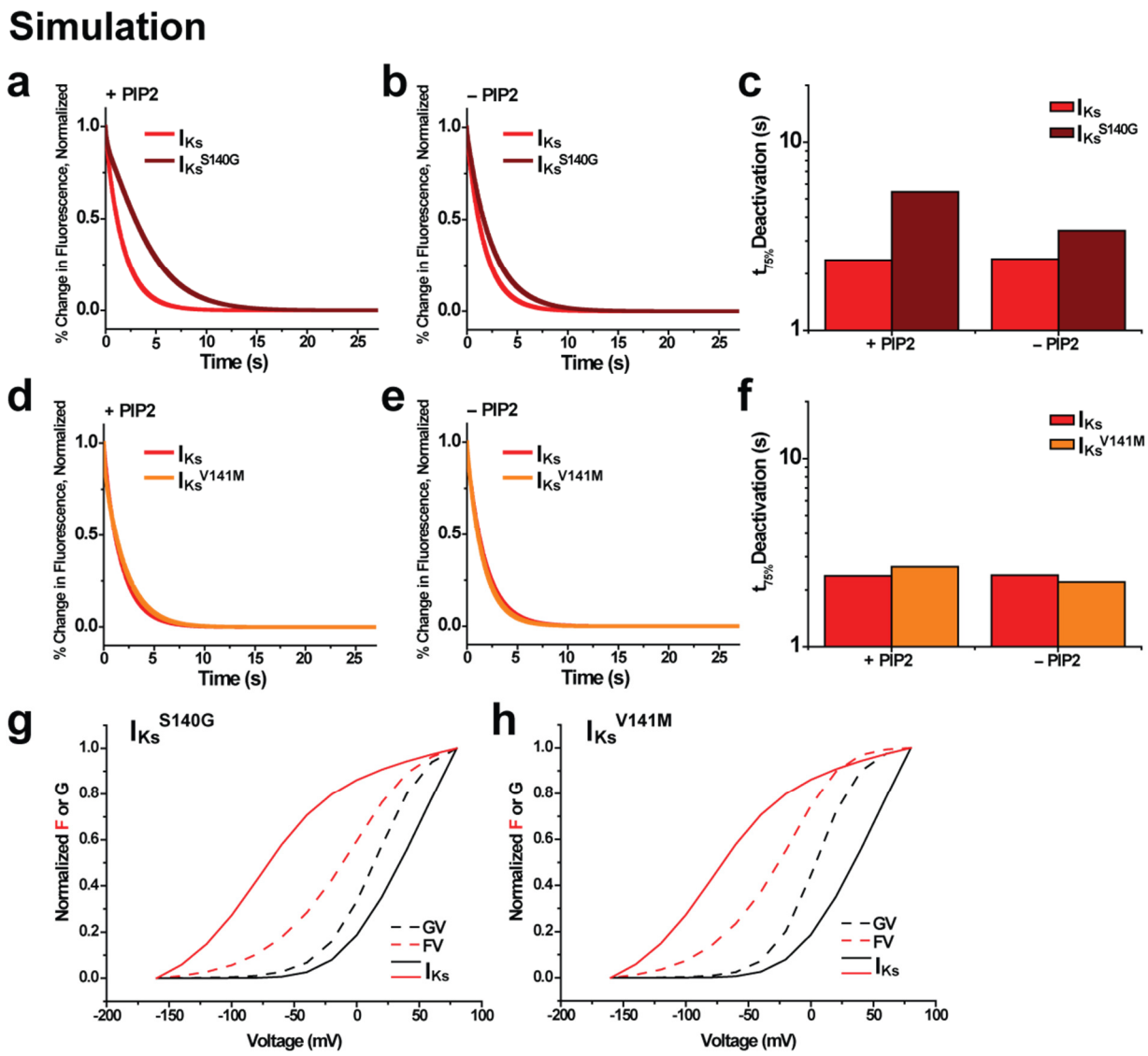

Figure 2.8. Simulating PIP_2 depletion and isochronal activation for I_{Ks} and mutants. (a-f) Simulated normalized fluorescence deactivation traces before (a,d) and after PIP_2 depletion (b,e), and time to 75% deactivation of fluorescence for I_{Ks}^{S140G} (c) and I_{Ks}^{V141M} (f). PIP_2 depletion was simulated by slowing channel opening 10,000 times, effectively preventing channel opening. (g-h) Normalized isochronal (5 s) activation for conductance (black) and fluorescence (red) for I_{Ks}^{S140G} (g) and I_{Ks}^{V141M} (h). Lines represent I_{Ks} for comparison.

deactivation. I_{Ks}^{S140G} alters the pathway of deactivation, such that channels are allowed to reopen in the intermediate voltage sensor states. Interestingly, reopenings delay voltage sensor transitions to indirectly slow voltage sensor deactivation. This is the opposite result from $KCNQ1^{S140G}$, where voltage sensor slowing indirectly slows current deactivation. Our model shows that I_{Ks}^{V141M} deactivates through yet a different pathway, where most voltage sensor deactivation occurs prior to pore closing. Despite their contrasting deactivation pathways, I_{Ks}^{S140G} and I_{Ks}^{V141M} share similarities in their gating effects as recapitulated in our models. Both I_{Ks}^{S140G} and I_{Ks}^{V141M} alter VSD-pore coupling, such that channels in intermediate voltage sensor states are allowed to reopen or remain open. In addition, our models are consistent with both I_{Ks}^{S140G} and I_{Ks}^{V141M} slowing the pore closing transition.

Discussion

KCNE1 modulates multiple biophysical properties of KCNQ1, including voltage-dependent gating, to generate the cardiac I_{Ks} current. Our findings show that in the presence of KCNE1, the two atrial fibrillation mutations slow current deactivation by altering the gating pathway of deactivation. I_{Ks}^{S140G} slows current deactivation by causing channels to reopen during early steps of voltage sensor deactivation. These reopenings delay voltage sensor transitions and indirectly slows voltage sensor deactivation. This is consistent with PIP_2-dependent slowing of fluorescence deactivation, because PIP_2 depletion prevents channel opening and therefore removes the reopenings that delay deactivation. I_{Ks}^{V141M} alters the pathway of deactivation yet differently, such that the pore closes after most or all voltage sensors have deactivated. These two distinct pathways of channel deactivation are consistent with our VCF results and contribute to slowing of current deactivation in the presence of KCNE1.

While I_{Ks}^{S140G} and I_{Ks}^{V141M} lead to different pathways of deactivation, they share two important similarities in their effects on channel gating. First, both mutations alter VSD-pore coupling. It has been previously shown that KCNQ1 alone is able to open with intermediate voltage sensor activation[121] and that the addition of the β-subunit KCNE1 results in a channel that mostly opens after full voltage sensor activation. Our experiments and models show that both I_{Ks}^{S140G} and I_{Ks}^{V141M} increase the open probability of channels in the intermediate voltage

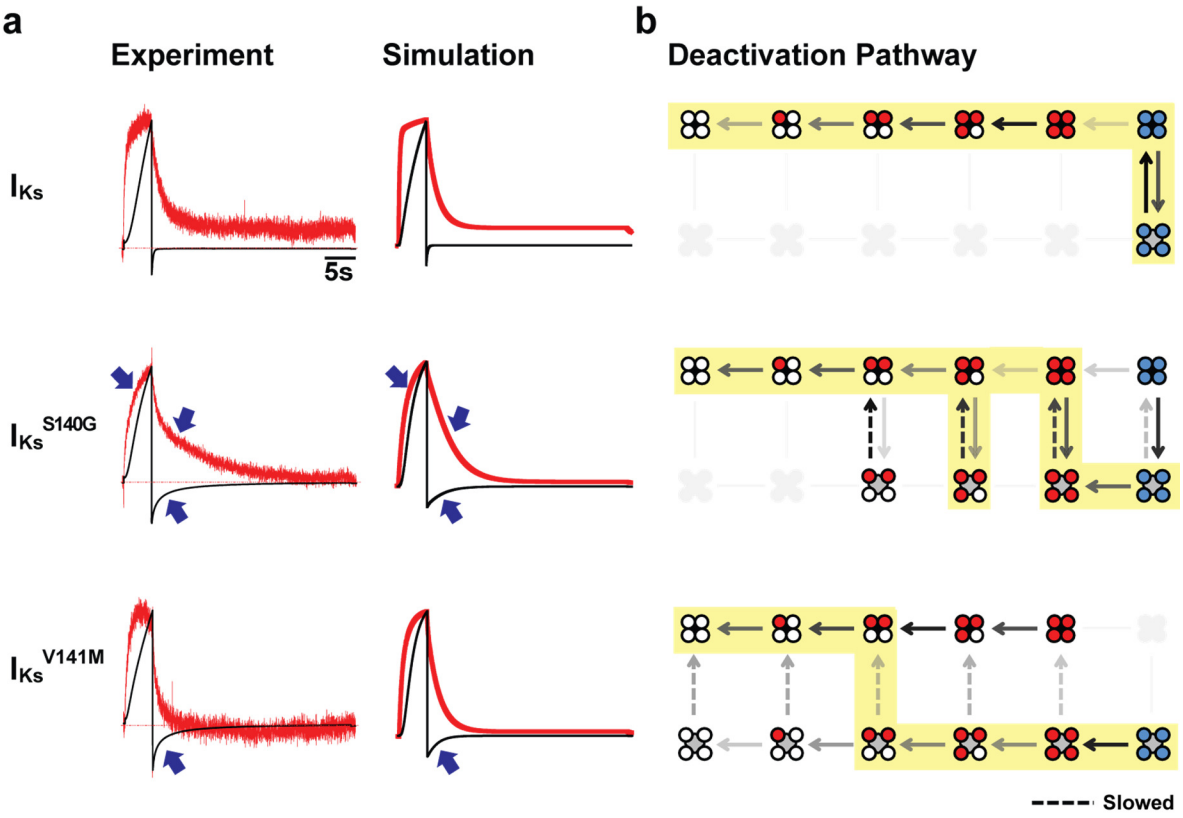

Figure 2.9. Simulating the gating effects of S140G and V141M in the presence of KCNE1. (a) Comparing experimental with simulated current (black) and fluorescence (red) traces for I_{Ks} (top), I_{Ks}^{S140G} (middle), and I_{Ks}^{V141M} (bottom). (b) Description of deactivation pathways at -100 mV based on model rates. Arrows with greater opacity represent higher probability of channels entering the transitions specified. States that channels rarely or never enter are grayed out. Highlighting illustrates the most probable pathway of channel deactivation based on rates at -100 mV, starting from the fully activated open state. I_{Ks} channels opens and closes only when voltage sensors are fully activated (top). I_{Ks}^{S140G} alters VSD-pore coupling and slows pore closing, altering the deactivation pathway such that during early steps of voltage sensor deactivation, channels may repeatedly open and close several times (middle). Like I_{Ks}^{S140G}, I_{Ks}^{V141M} also alters VSD-pore coupling to allow channel opening in intermediate VSD states (bottom). In addition, I_{Ks}^{V141M} slows pore closing. However, the deactivation pathway is different from I_{Ks}^{S140G} in that voltage sensors deactivate to a greater extent prior to pore closing.

sensor states. We propose that the mutations S140G and V141M partially reverse the KCNE1-induced change in VSD-pore coupling, thereby allowing channels to open when the voltage sensors are in intermediate states such as in the case of KCNQ1 alone. A second similarity between I_{Ks}^{S140G} and I_{Ks}^{V141M} is a slowing of the pore closing transition. This may be surprising because both S140G and V141M are located near the extracellular end of the S1 helix, which is part of the VSD. However, prior crosslinking studies have shown that the extracellular end of the KCNE1 transmembrane helix is in close proximity to both S1 and S6 of KCNQ1[135,139]. Furthermore, the homology model of the KCNQ1-KCNE1 complex from Kang *et al.* shows KCNE1 at a position between the S1 and the S6 of two different KCNQ1 subunits[137] (Fig. 2.10, a). Functional studies have shown that crosslinking K41 on KCNE1 with I145 on KCNQ1, roughly one turn above V141 on the S1 helix, slows current deactivation ~5-fold at -40 mV[135]. Crosslinking L42 on KCNE1 with V324 on the S6 of KCNQ1 results in extremely slow deactivation[135]. These results suggest that the extracellular end of the S1 helix may interact with KCNE1 to indirectly modulate the S6 helix and influence gate motions. We propose that in the presence of KCNE1, both S140G and V141M slow pore closing through these molecular interactions (Fig. 2.10, b). Mutation at V141, a position which also has been shown to crosslink with KCNE1[190], may directly disrupt the orientation of KCNE1 relative to the S6, restricting molecular motions involved in pore closing. Mutation at S140, which faces toward the VSD of KCNQ1 and does not crosslink with KCNE1[190], may perturb KCNE1 indirectly through its neighboring residue V141. Although the homology model suggests that S140G should still directly slow voltage sensor deactivation in the presence of KCNE1, it is important to note that KCNE1 itself slows voltage sensor deactivation in our data. If KCNE1 and S140G slow voltage sensor deactivation through a common molecular pathway, no additional effect on VSD

deactivation by S140G would be observed in the presence of KCNE1. The possibility of KCNE1 mediating an indirect interaction between S1 and S6, which are part of the VSD and

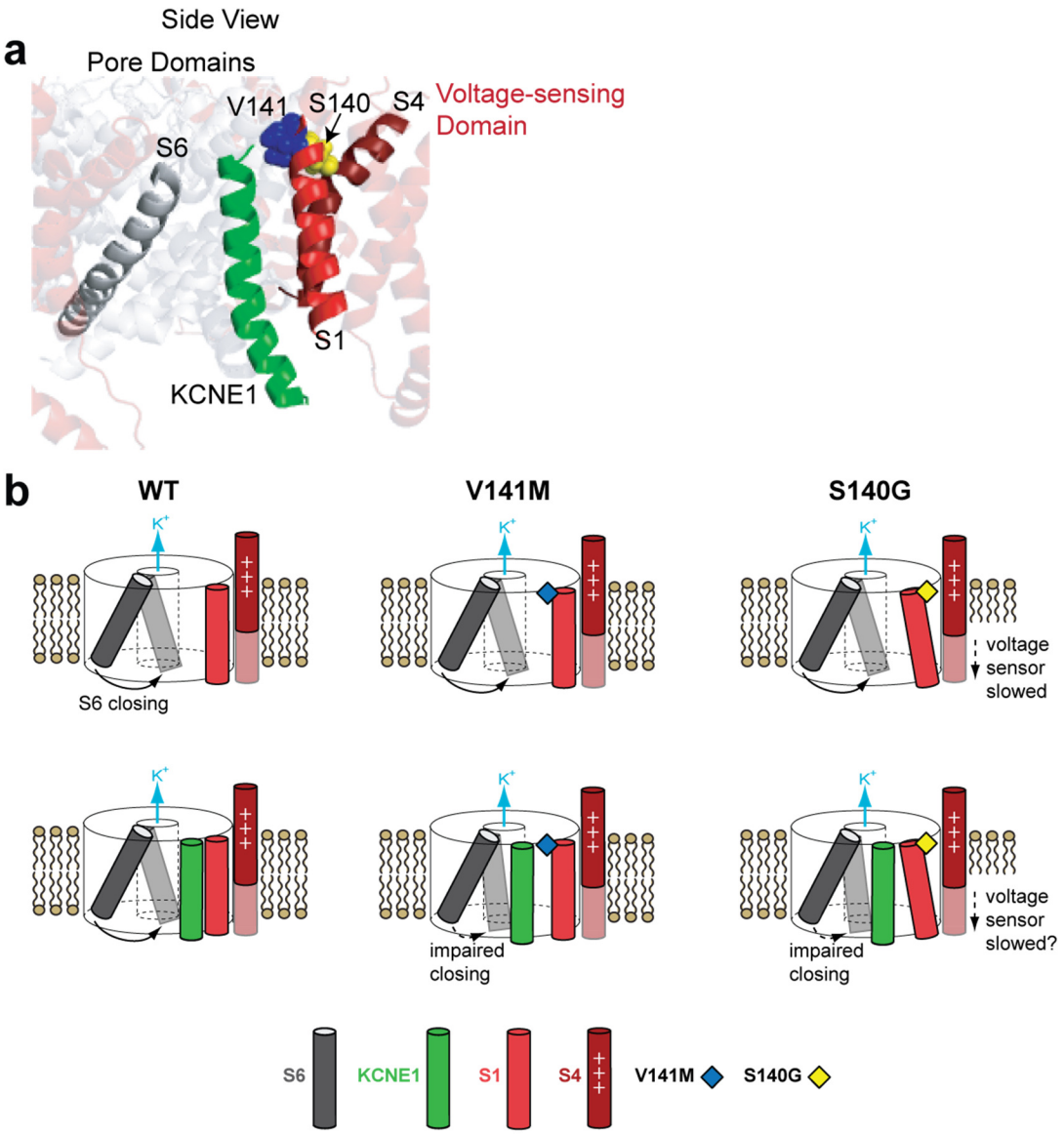

Figure 2.10. Proposed molecular mechanisms underlying the effects of S140G and V141M on channel gating. (a) Homology model of open tetrameric KCNQ1 and KCNE1 from Kang *et al.* (2008) from a side view (a). On the S1 helix, S140 (yellow) points toward S4, whereas V141 (blue) points toward KCNE1. The extracellular end of the S6 helix is in proximity to KCNE1. (b) Cartoon representation of proposed molecular mechanisms of S140G and V141M. The channel pore is represented by a cylinder with the K^+ permeation pathway at its center. For KCNQ1 alone (top row), V141M has minimal effect on channel gating, whereas S140G disrupts S4 and slows its movement. In the presence of KCNE1 (bottom row), both V141M and S140G alter VSD-pore coupling and slow pore closing. V141M may directly disrupt the orientation of KCNE1, impairing motion of the S6 during channel closing. S140G may cause a similar disruption of KCNE1 indirectly through other residues on S1 that face KCNE1.

pore domain respectively, may explain how S140G and V141M alter VSD-pore coupling only in the presence of KCNE1. In addition, there are pharmacologic activators of I_{Ks} whose functions depend on the presence of KCNE1[194]. This together with our findings are consistent with the central role of KCNE1 in modulating KCNQ1 gating.

In modeling the gating effects of I_{Ks}^{S140G} and I_{Ks}^{V141M} we attempted varying different permutations of parameters that might alternatively explain our VCF data, but they produced worse fit of the data compared to our final model. For example, we found that a simpler model where pore deactivation is slowed without altering voltage sensor-pore coupling pore gave very poor fits of isochronal activation for both mutants. Another simple model where coupling is altered without slowing pore deactivation does not fit the constraints imposed by Rb^+/K^+ permeability ratios. These attempts suggest that both pore slowing and coupling alterations are required to explain the effects of the I_{Ks} mutants.

One limitation in our study is that, because I_{Ks}^{S140G} and I_{Ks}^{V141M} deactivate very slowly, current accumulation occurred between sweeps of the isochronal activation experiment. This accumulation likely caused an artefactual left-shift in the GV. However, we found that recordings of I_{Ks}^{S140G} and I_{Ks}^{V141M} with minimal accumulation still showed a left-shifted GV compared with I_{Ks}. In addition, in simulating the GV curve, our kinetic model takes into account possible current accumulation by utilizing the same isochronal activation protocol (including sweep duration) as our experiment. A left-shifted GV curve is also seen in our model, although not to the extent seen experimentally. A second limitation is that our oocyte experiments were performed at 22-24°C, where channel kinetics are slower than in the human heart (37°C). Nonetheless, when corrected for temperature-dependence based on prior measurements of Q_{10} (2.58)[195], the slowly deactivating mutant I_{Ks} is expected to also accumulate at physiological

temperatures. Thus, the gating mechanisms underlying slow deactivation in our study hold physiological significance.

In conclusion, the VCF studies presented here provide insight on the gating mechanisms involved in the slowing of current deactivation by two atrial fibrillation mutations, S140G and V141M. The slow current deactivation in both I_{Ks}^{S140G} and I_{Ks}^{V141M} is mainly due to their effects on the voltage sensor-pore coupling and the pore closing transition. This finding is particularly novel, because I_{Ks}^{S140G} was previously assumed to slow current deactivation primarily by affecting the voltage sensor, similar to $KCNQ1^{S140G}$. In addition, our study suggests that KCNE1 plays a central role in mediating the slow deactivation by both mutations. As such, future efforts to identify molecular activators and inhibitors of I_{Ks} can benefit from targeting the β-subunit and inter-subunit interactions to alter physiologically relevant channel function. These modulators may lead to mechanism-based pharmacologic agents and optimize therapy for arrhythmia associated with mutations in KCNQ1, such as long QT syndrome type 1 and atrial fibrillation.

Chapter 3: Gating alterations by small-molecule activators leading to deactivation slowing in KCNQ1

Summary

I_{Ks} is generated by the co-assembly of the pore-forming α-subunit KCNQ1 with the accessory β-subunit KCNE1 and plays a critical role in cardiac impulse conduction by repolarizing the cardiac action potential. In Chapter 1 and Chapter 2 we explored the gating effects of two KCNQ1 atrial fibrillation mutations, S140G and V141M, both of which drastically slow I_{Ks} deactivation. Many molecular activators of KCNQ1 and I_{Ks} both increase current amplitude and slow deactivation as well. Two KCNQ1 activators, ML277 and R-L3, have been previously shown to slow current deactivation, but the underlying gating alterations remain known. We utilized VCF and kinetic modeling to show that ML277 and R-L3 have distinct mechanisms of effect on KCNQ1 gating. Whereas ML277 slows current deactivation with small effects on voltage sensor deactivation, R-L3 slows voltage sensor deactivation with smaller effects on current deactivation. Kinetic modeling can account for the effects of ML277 by directly slowing channel pore transitions, while R-L3's effects are recapitulated with a slowing of voltage sensor deactivation, which indirectly slows current deactivation. These results demonstrate that different molecular activators achieve channel gain-of-function through distinct mechanisms, thereby providing a key step toward developing mechanism-specific modulators of channel function as therapy for arrhythmia.

Introduction

KCNQ1 is the pore-forming α-subunit that co-assembles with the β-subunit KCNE1 to generate I_{Ks}, which repolarizes the cardiac action potential and is critically important to normal cardiac impulse conduction. Loss-of-function mutations in I_{Ks} may excessively prolong the action potential duration and cause long QT syndrome type 1, which predisposes patients to life-

threatening arrhythmia such as *torsades de pointes*. An existing problem in the clinical management of arrhythmia is that most antiarrhythmic medications do not target specific ion channels or gating mechanisms and cause undesired side effects such as additional arrhythmia[196,197]. There is a need to develop mechanism-based therapies to optimize treatment and reduce side effects. Understanding how I_{Ks} loss-of-function can be rescued by I_{Ks} activators in LQTS may offer a paradigm for future drug design.

Although I_{Ks} activators are not currently used in clinical treatment of long QT syndrome, a number of molecular activators of I_{Ks} have been discovered[34] and may guide the development of mechanism-specific therapeutics. In addition, a number of activators increase KCNQ1 function but not the physiologically relevant channel formed in association with KCNE1. Although these modulators are unlikely to be clinically useful, investigating the mechanisms underlying their effects may provide fundamental insights on how channel function can be increased. Furthermore, different KCNQ1 activators may target distinct gating components of I_{Ks}, providing a basis for developing mechanism-based therapies.

While the cardiac I_{Ks} current is generated by the co-assembly of KCNQ1 with KCNE1, four subunits of KCNQ1 can come together in the absence of KCNE1 to form an ion channel capable of voltage-dependent gating. The channel consists of four voltage-sensing domains (VSD) and a central pore. The S4 transmembrane helix of each VSD contains positive charges that allow the S4 to move in response to changes in membrane potential. S4 movement is, in turn, coupled to the channel pore through the S4-S5 linker in the presence of PIP_2, leading to opening/closing of the pore. Each of these individual channel components can potentially be modulated by small molecules to alter channel function.

ML277 has been previously identified as a specific and potent activator of KCNQ1 (EC_{50} = 0.26 μM in CHO cells)[198]. It is selective against $Na_V1.5$, $Ca_V1.2$, hERG, as well as other isoforms of KCNQ, including KCNQ2 and KCNQ4[180,198]. ML277 not only increases KCNQ1 current amplitude, but also slows current activation and deactivation. Deactivation slowing has been previously shown to be a critical mechanism by which atrial fibrillation mutations as well as adrenergic stimulation cause accumulation of I_{Ks} in the context of repeated stimulation in the heart, thereby shortening the action potential. Nonetheless, gating mechanisms underlying ML277's slowing of deactivation remains unknown. An additional property of ML277 is that progressive increase in KCNE1:KCNQ1 stoichiometry reduces the effect of ML277[2]. According to molecular dynamic simulations, ML277 binds to a pocket in KCNQ1 that's adjacent to the VSD, the pore domain, and the S4-S5 linker[199]. Previous mutagenesis experiments further suggest that ML277 binds to the S4-S5 linker and the pore domain (Fig. 3.1). It is possible that the presence of KCNE1 occludes the binding site of ML277.

Similar to ML277, the benzodiazepine derivative R-L3 both increases current amplitude and slows current deactivation of KCNQ1[200]. R-L3 selectively activates KCNQ1 over other currents, including the L-type Ca^{2+} current as well as I_{Kr}[200]. However, R-L3 does not activate I_{Ks} at a saturating KCNE1:KCNQ1 ratio[200]. Mutations of channel pore residues can drastically reduce R-L3's

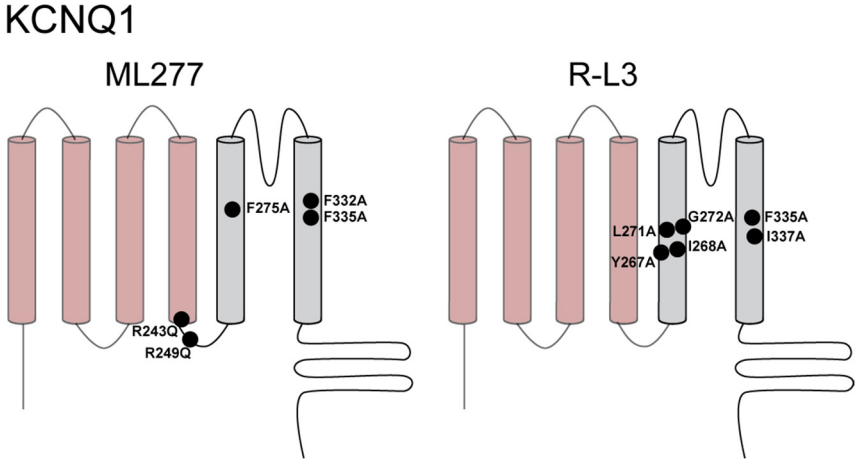

Figure 3.1. Potential binding sites for ML277 and R-L3 in KCNQ1 based on previous mutagenesis studies. The locations of mutations that drastically reduce drug effects on current amplitude are shown. Transmembrane helices that are part of the voltage sensing domain and the pore domain are shown in red and grey, respectively.

effect, suggesting that R-L3 binds to the pore (Fig. 3.1). However, R-L3's effect on the VSD has not been tested. Furthermore, without functional data, gating mechanisms underlying R-L3's effects, in particular it's slowing of deactivation, remain unknown.

Here, we use mutagenesis, VCF, and kinetic modeling to show that ML277 and R-L3 cause distinct alterations of KCNQ1 gating. Our chimera study shows that the pore domain of KCNQ1 endows channel activation by ML277. VCF results show that ML277 slows current deactivation with a smaller slowing of fluorescence deactivation. In addition, ML277 does not shift the voltage-dependence of activation for both conductance (GV) and fluorescence (FV). In contrast, R-L3 drastically slows fluorescence deactivation with a smaller slowing in current deactivation, and it causes a hyperpolarizing shift in both the FV and GV. Kinetic modeling suggests that ML277 directly slows pore opening and closing, whereas R-L3 slows voltage sensor deactivation, which indirectly slows current deactivation. These results shed light on different mechanisms leading to slowing of deactivation by molecular activators, thus providing a key step toward future investigation of mechanism-based rescue of channel mutations.

Results

The KCNQ1 pore domain endows channel activation by ML277

To determine whether ML277 activates KCNQ1 by acting on the pore domain, we take advantage of the fact that ML277 activates KCNQ1 but has minimal effect on the closely related KCNQ2. To measure current, we used a single pulse voltage protocol consisting of a holding potential at -80 mV, a 2-s test pulse to +60 mV, followed by a repolarizing pulse to -120 mV. For WT KCNQ1, application of 10 μM significantly increases amplitude (194 ± 19%) and slowed the time constant of current deactivation (367 ± 64%) (Fig. 3.2). However, for WT

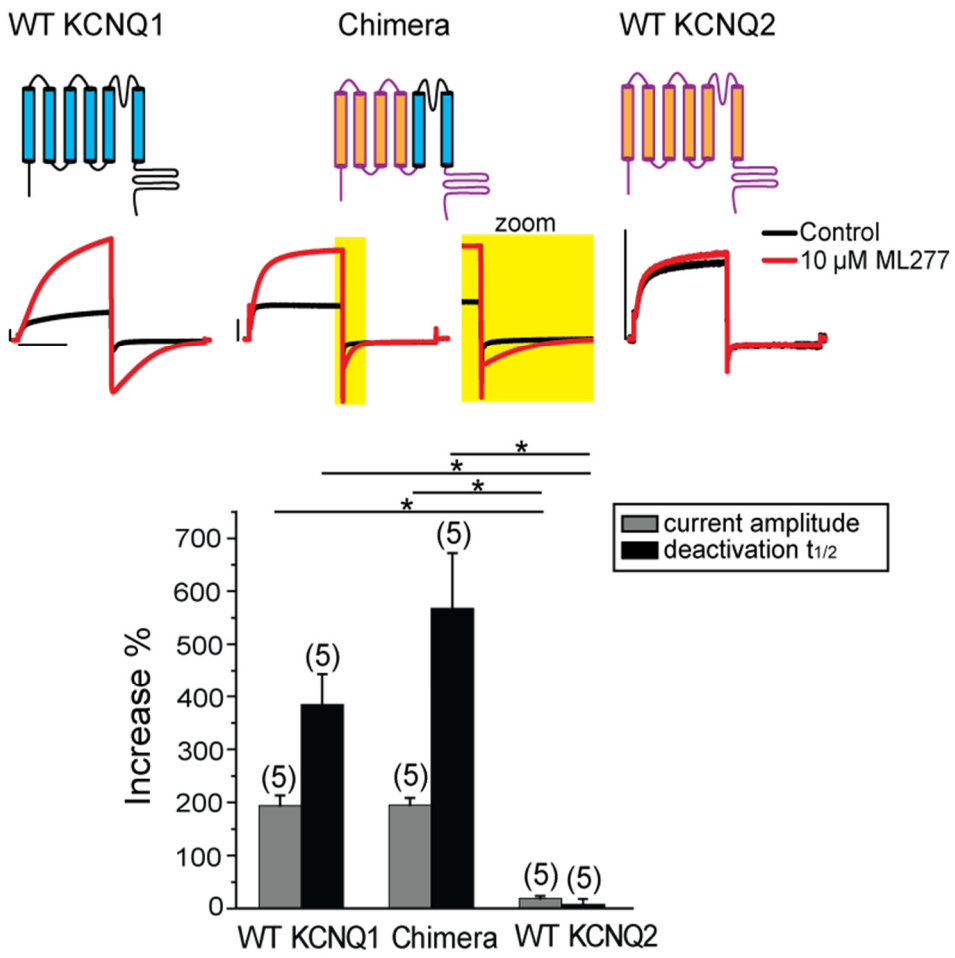

Figure 3.2. The pore domain endows KCNQ1 response to ML277. The effect of ML277 was tested in WT KCNQ1, WT KCNQ2, and a chimera that is KCNQ2 except for its pore domain (S5-P-S6), which is from WT KCNQ1. Cells were held at -80 mV, depolarized to +20 mV for 2 s, and repolarized to -120 mV. Current was recorded in control condition (black) and following addition of 10 µM ML277 (red). Horizontal scale bar represents 1s, and vertical scale bars represent 1µA. The percent increase in current amplitude and in time of half deactivation are summarized at the bottom. Data are shown as mean ± SEM (error bars). *P<0.05; one-way ANOVA with Tukey's test. Figure adapted from Lei Chen.

KCNQ2, ML277 only increases amplitude by 19 ± 4% and slows deactivation by 10 ± 11%. We then tested the ability of ML277 to activate a KCNQ1-KCNQ2 chimera. The chimera is KCNQ2 except for the pore domain (S5, S6, and P-loop between S5 and S6), which is from WT KCNQ1. We observed that 10 µM ML277 both increases the current amplitude by 195 ± 14% and slows current deactivation by 567 ± 105% for the chimera. The degree of activation and slowing is similar to wildtype, demonstrating that the pore domain of KCNQ1 endows response to ML277.

ML277 slows current deactivation with smaller effects on voltage sensor deactivation

To determine the effects of ML277 on channel gating, we utilized VCF to simultaneously measure current and fluorescence. As in our previous studies, we used a KCNQ1 construct containing a cysteine site at the residue G219 in the S3-S4 linker that can be labelled with a fluorophore to report S4 movement. We refer to the construct here as KCNQ1. Using the same single pulse protocol as previously, we found that application of 10 μM ML277 significantly

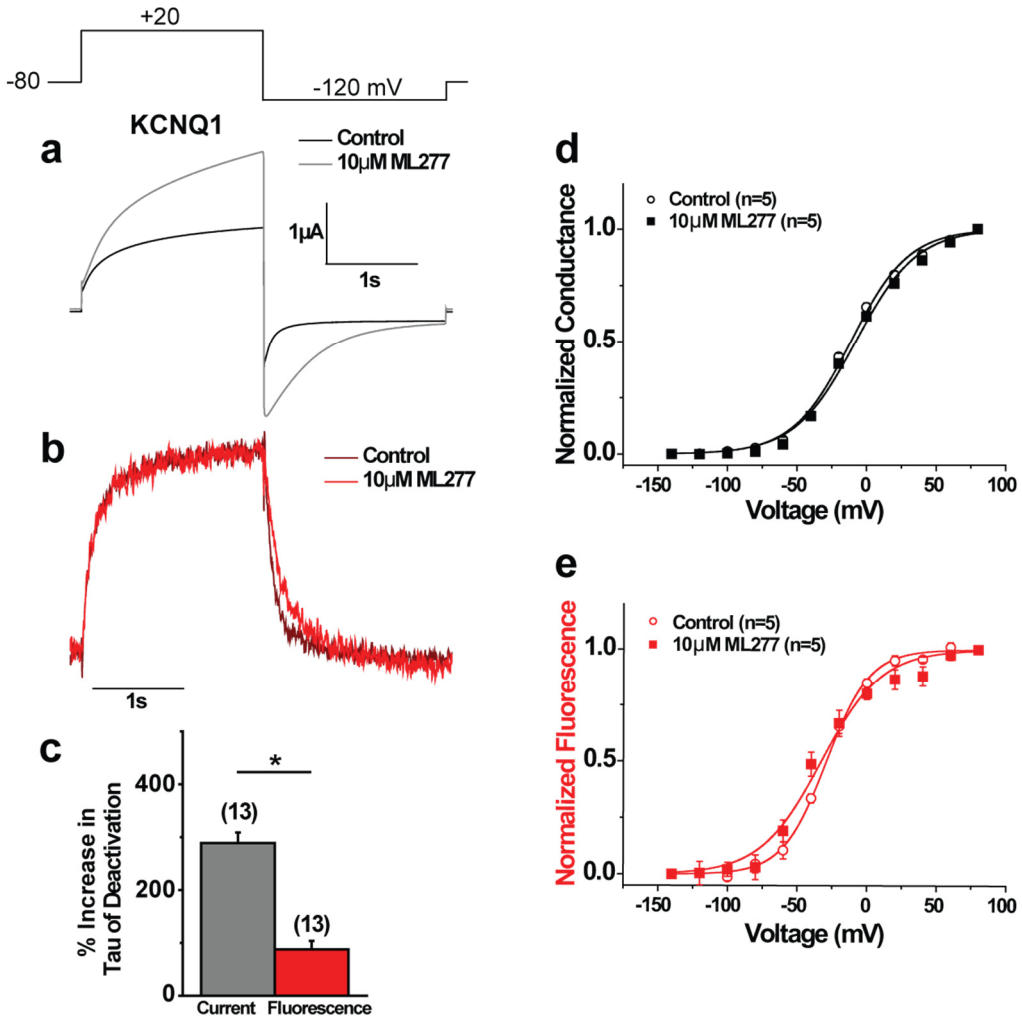

Figure 3.3. ML277 has minimal effect on the voltage sensor movement of KCNQ1. (a-b) Current (a) and normalized fluorescence (b) traces of KCNQ1. Cells were held at -80 mV, depolarized to +20 mV for 2 s, and repolarized to -120 mV for 2 s to record tail currents. (c) Comparing effect of ML277 on current and fluorescence deactivation kinetics time constant (tau) at -120 mV. Data are shown as mean ± SEM (error bars). *P<0.05; paired t-test. (d-e) Normalized isochronal activation curves for conductance (d) and fluorescence (e). Lines represent fits of data. Error bars represent SEM. In the isochronal activation protocol, cells were held at -80 mV, stepped between -140 mV and +80 mV for 2 s, followed by a pulse to -120 mV for 2 s.

increases the current amplitude of KCNQ1 by 95 ± 8% (Fig. 3.3). ML277 also increases the current deactivation time constant by 289 ± 20%. On the other hand, ML277 only mildly slows fluorescence deactivation, with an 88 ± 16% increase in time constant. This effect is significantly smaller than that of the current deactivation. We additionally measured the voltage-dependence of fluorescence (FV) and conductance (GV) activation and found that ML277 does not significantly shift the GV nor FV.

R-L3 slows voltage sensor deactivation with smaller effects on current deactivation

To determine the gating effects of R-L3, we applied the same single pulse protocol, with the exception of introducing a prepulse at -120 mV to close channels more completely, and measured voltage sensor movement with ionic current. We used 10 μM R-L3 in our experiments, which led to greater effects on deactivation and current amplitude than at lower concentrations. We found that R-L3 significantly increased the current amplitude by 28 ± 4% and the time constant of current deactivation by 199 ± 22% (Fig. 3.4). In contrast with ML277, R-L3 slows fluorescence deactivation more prominently, with a 335 ± 22% increase in the fluorescence deactivation time constant. The percent change in fluorescence deactivation time constant is significantly greater than that of current deactivation. In addition, R-L3 causes a significant hyperpolarizing shift in the GV by -6.0 ± 2.0 mV and in the FV by -13.8 ± 2.1 mV.

Kinetic modeling informs distinct mechanisms of effect of ML277 and R-L3

We modeled the effects of ML277 and R-L3 on channel gating using the same gating scheme described in previous chapters. In this scheme, voltage sensor movement is represented by horizontal transitions and occurs in two steps: first, independent movement of four S4's to an

intermediate state; second, a concerted step to the fully activated state (Fig. 3.5 a). Our previously derived model of KCNQ1 shows that channel opening occurs mainly when some or all voltage sensors are in the intermediate state. Each step in voltage sensor activation increases probability of channel opening in an allosteric manner.

To simulate the gating effect of ML277, we slowed the pore opening and closing transitions in addition to increasing the current amplitude from our KCNQ1 model (Table S3).

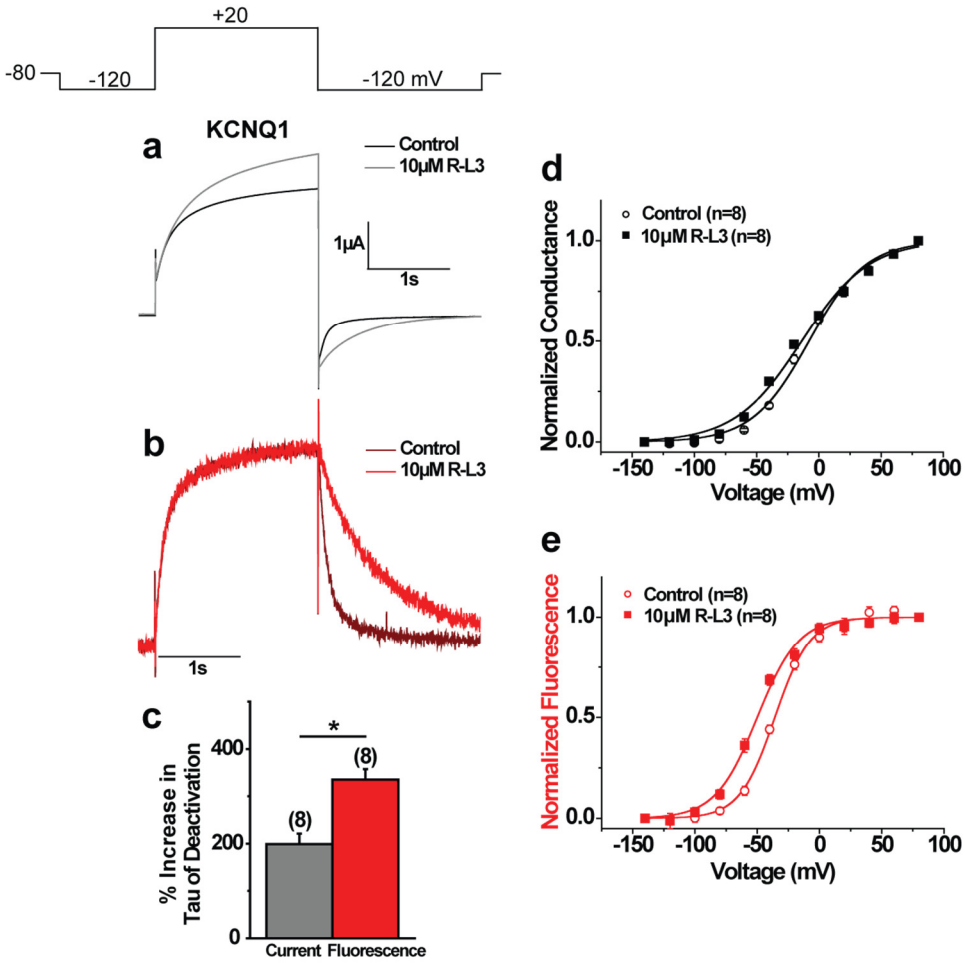

Figure 3.4. R-L3 alters voltage sensor movement of KCNQ1. (a-b) Current (a) and normalized fluorescence (b) traces of KCNQ1. Cells were held at -80 mV, prepulsed to -120 mV for 2 s, depolarized to +20 mV for 2 s, and repolarized to -120 mV for 2 s to record tail currents. (c) Comparing effect of R-L3 on current and fluorescence deactivation kinetics time constant (tau) at -120 mV. Data are shown as mean ± SEM (error bars). *P<0.05; paired t-test. (d-e) Normalized isochronal activation curves for conductance (d) and fluorescence (e). Lines represent fits of data. Error bars represent SEM. In the isochronal activation protocol, cells were held at -80 mV, prepulsed to -120 mV for 2 s, stepped between -140 mV and +80 mV for 2 s, followed by a pulse to -120 mV for 2 s.

We simulated current and fluorescence using same single pulse voltage protocol as our experiments. In addition, we simulated FV and GV curves. Our simulation shows slowing in both current activation and deactivation (Figure 3.5), similar to the effects of ML277. The time constant of current deactivation slowing is increased by 363% and accompanied by a small (14%) increase in the time constant of fluorescence deactivation. Furthermore, there is no change in the activation kinetics of fluorescence, similar to the VCF data. In addition, there is no

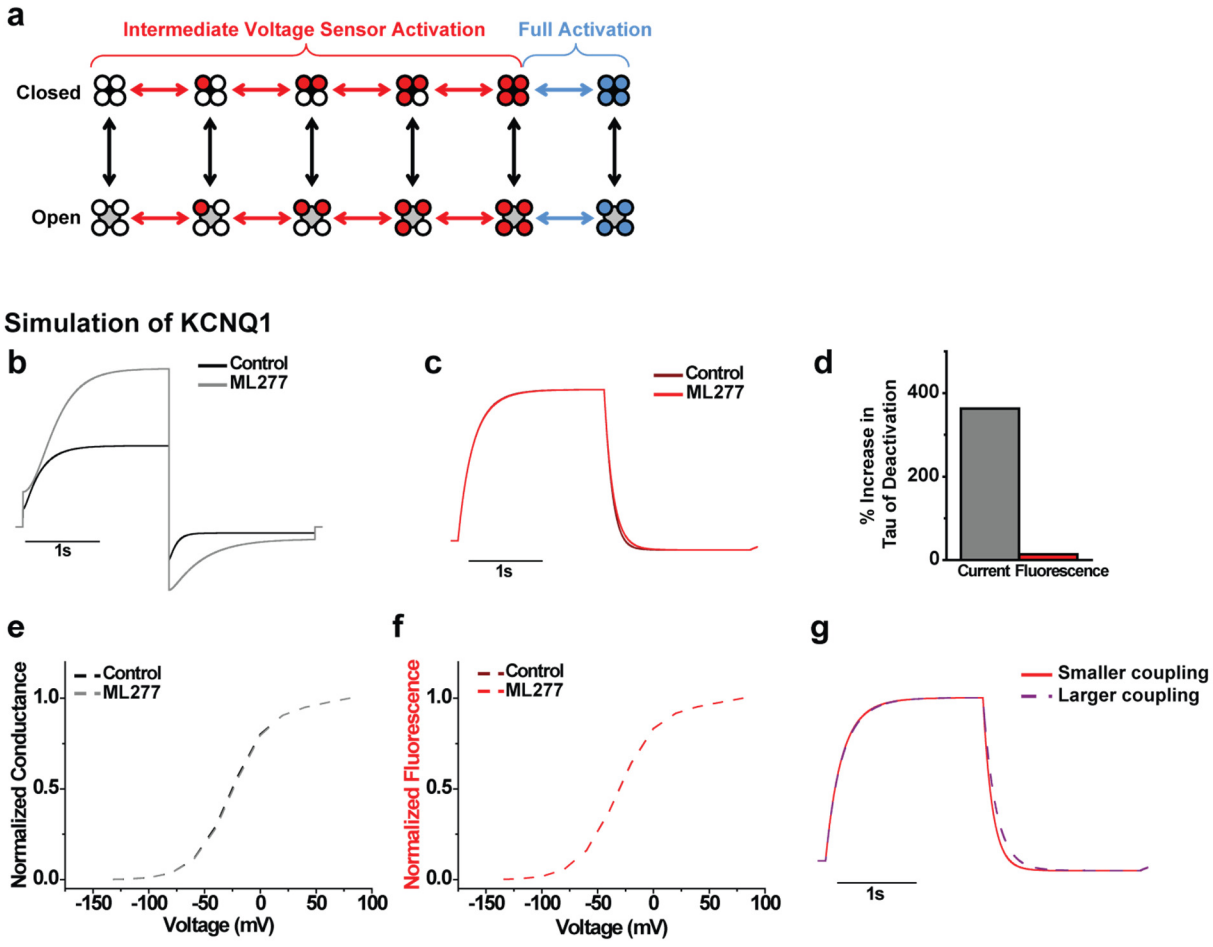

Figure 3.5. Simulating the effects of ML277 using a kinetic model of KCNQ1. (a) Model of KCNQ1 gating. In this model, horizontal transitions represent voltage sensor movement, while vertical transitions represent pore opening/closing. Voltage sensors can exist in the resting (white), intermediate (red), or fully activated state (blue). To simulate the effect of ML277, the pore opening/closing transition was slowed and current amplitude was increased. Voltage sensor transitions were not altered. (b-c) Simulated current (b) and fluorescence (c) using the same single pulse protocol as in VCF experiments. (d) Percent increase in time constant of deactivation (tau) at -120 mV. (e-f) Simulated isochronal activation for conductance (e) and fluorescence (f), using the same protocol as in VCF experiments. (g) Simulating the effect of increased voltage sensor-pore coupling on fluorescence deactivation after pore transitions have been slowed.

shift in the GV nor FV curves. Thus, merely slowing pore transitions recapitulates most observed effects of ML277.

We simulated the effects of R-L3 by altering a different gating mechanism from that of ML277. Instead of slowing pore opening/closing, we decreased the deactivation rate of the main voltage sensor transition by 240% in our model. This increases the time constant of fluorescence deactivation by 224% and the time constant of current deactivation by 187% (Figure 3.6). In addition, there is a small (2.9%) increase in current amplitude. Furthermore, we found a hyperpolarizing shift in both the FV and GV by 18.5 mV and 18.1 mV, respectively. These simulations recapitulate most of R-L3's effects from our VCF data.

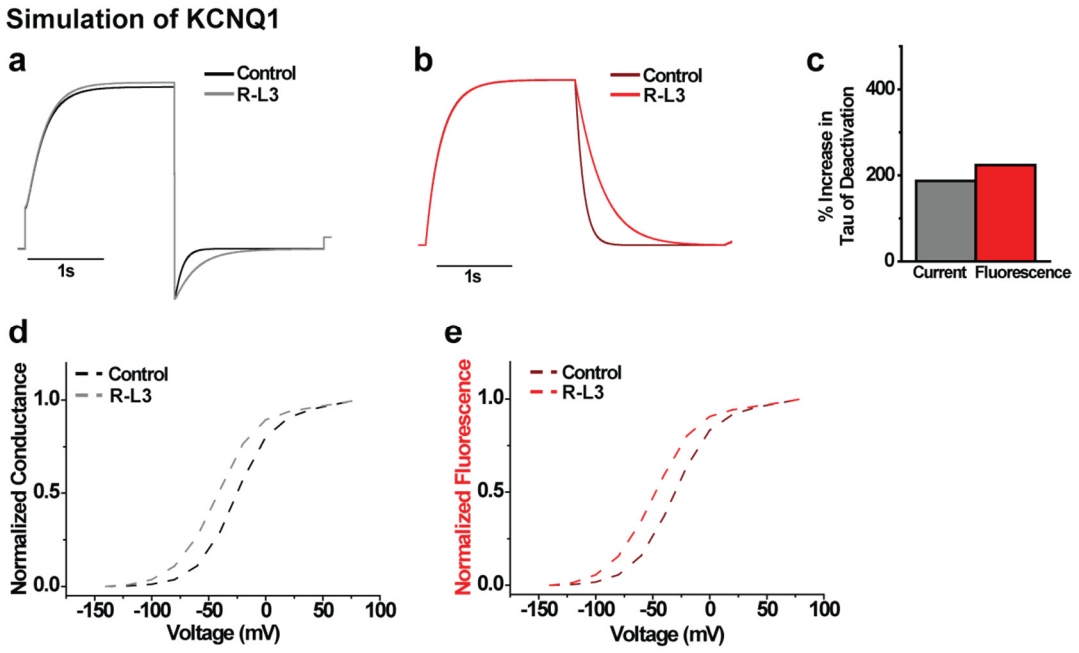

Figure 3.6. Simulating the effects of R-L3 using a kinetic model of KCNQ1. In this simulation, the rate of voltage sensor deactivation was slowed. Pore transitions were not altered. (a-b) Simulated current (a) and fluorescence (b) using the same single pulse protocol as in VCF experiments. (c) Percent increase in time constant of deactivation (tau) at -120 mV. (d-e) Simulated isochronal activation for conductance (d) and fluorescence (e), using the same voltage protocol as in VCF experiments.

Discussion

Slowing of channel deactivation contributes to increased channel function and is an important property of molecular activators. However, given the intricate gating processes of voltage-dependent channels, drugs may alter ionic currents through different mechanism. Here, we have utilized VCF and kinetic modeling to illustrate two KCNQ1 activators with distinct effects on channel gating. Our results suggest that on one hand, ML277 directly slows pore activation and deactivation. On the other hand, R-L3 directly slows voltage sensor deactivation, which indirectly slows current deactivation. These results show that molecular activators can slow KCNQ1 deactivation by different mechanisms and thus provides a key step toward investigating their effectiveness in rescuing distinct loss-of-function mutations. Although the effects of both ML277 and R-L3 diminish with addition of the β-subunit KCNE1 and are therefore unlikely to be clinically useful, our studies provide generalizable insights on mechanisms of gain-of-function that can be applied in future efforts to modulating channel function.

The pore effect of ML277 is supported our mutagenesis experiment, which demonstrates that the KCNQ1 pore domain is required for the action of ML277, including slowing of deactivation. The slowing of pore deactivation indirectly causes a small slowing in voltage sensor deactivation according to our model. This effect is mediated by the coupling between voltage sensor and the pore. While coupling allows S4 activation to control the pore, Zaydman *et al.* previously demonstrated that the reverse process is also possible[95]. They showed that locking KCNQ1's pore in the open conformation stabilized voltage sensor activation. We calculated transition rates in our model to show that in normal KCNQ1 deactivation, most S4 transitions occur while the channel is closed (Supplementary Fig. S6). After slowing pore

closing, the pathway of deactivation is altered such that most S4 deactivation occurs while the channel is open. Because of retrograde coupling, this stabilizes voltage sensors in the activated state and slows voltage sensor deactivation. In fact, when we increased the degree of voltage sensor-pore coupling in our model, we observed a greater slowing in voltage sensor deactivation (Fig. 3.5 g) that is more consistent with our data. Given this, we propose that ML277 may alter voltage sensor-pore coupling in addition to its pore effects. This coupling effect is supported by previous docking and molecular dynamics simulations in which ML277 interacts with the S4-S5 linker[199].

Our VCF results and kinetic model suggest that R-L3 directly slows the deactivation rate of voltage sensors, which indirectly slows current deactivation. This can be explained by examining the transition rates in the model (Supplementary Fig. S6). During KCNQ1 deactivation, the pore normally closes and reopens a number of times as voltage sensors deactivate. Slowing the rate of voltage sensor deactivation increases the number of times the pore reopens, thereby slowing current deactivation. In addition, slowing the rate of voltage sensor deactivation alters the equilibrium between voltage sensor activation and deactivation, thereby explaining the hyperpolarizing shift in the FV. Since voltage sensor movement is coupled to the pore, the GV also left-shifts, resulting in a slight increase in current amplitude. However, given that the increase in amplitude is greater in our experiment compared to our model, an alternative explanation is likely required for this effect. Previous studies have suggested that R-L3 binds to the channel pore. Given this result, it is possible that R-L3 exerts two effects on KCNQ1: an effect on the pore to increase current amplitude, and an effect on voltage sensor movement to slow deactivation. It remains to be explored whether these distinct functional effects result from R-L3 binding to multiple sites on KCNQ1, or from a single binding

site at the channel pore, where it may influence both pore and voltage sensor movement at the same time.

In summary, results from mutagenesis, VCF, and kinetic modeling demonstrate distinct gating effects of two KCNQ1 activators that slow current deactivation. On one hand, ML277 directly slows pore closing, thereby slowing current deactivation. On the other hand, R-L3 slows voltage sensor deactivation, which indirectly slows current deactivation. These findings illustrate distinct mechanisms of channel gain-of-function and pave the way for future development of mechanism-based therapies for the treatment of arrhythmia.

CONCLUSIONS

The slow delayed rectifier potassium current I_{Ks} plays a prominent physiological role by repolarizing the cardiac action potential. Slowing of I_{Ks} deactivation increases channel function and underlies key pathophysiological processes and pharmacological action. My thesis investigated the gating alterations underlying deactivations slowing, utilizing VCF to assay for voltage sensor movement simultaneously with ionic current through the channel pore.

In Chapter 1, we examined the mechanisms of effect for two atrial fibrillation mutations, S140G and V141M, on KCNQ1 gating in the absence of KCNE1. We showed that $KCNQ1^{S140G}$ directly slows voltage sensor deactivation, which indirectly slows current deactivation. On the other hand, $KCNQ1^{V141M}$ has minimal effect on channel gating. These results are consistent with previous structural information on KCNQ1, where S140 faces toward the voltage-sensing domain of the channel, whereas V141 faces away from the channel and toward membrane lipids, in close proximity to the putative location of KCNE1.

In Chapter 2, we examined the gating alterations underlying deactivation slowing by atrial fibrillation mutations in the presence of KCNE1. Surprisingly, both I_{Ks}^{S140G} and I_{Ks}^{V141M} alter the voltage sensor-pore coupling as well as slow the pore closing transition, resulting in pathways of deactivation in which channels can either re-open or stay open. Although I_{Ks}^{S140G} slows voltage sensor deactivation, our experiments and kinetic model show that this is an indirect effect of pore slowing, in contrast to $KCNQ1^{S140G}$. Taken together with results from Chapter 1, these data suggest that KCNE1 plays a critical role in mediating the coupling changes and pore effects in both I_{Ks}^{S140G} and I_{Ks}^{V141M}, leading to deactivation slowing. We proposed a molecular mechanism in which both mutations disrupt the orientation of KCNE1 relative to KCNQ1 and thus impede gate closing. These results imply that KCNE1 could serve as an

important pharmacologic target, either in correcting channel gain-of-function or rescuing channel loss-of-function.

Pharmacologic activators, like atrial fibrillation mutations, can also cause deactivation slowing in KCNQ1. In Chapter 3 we studied the gating mechanisms underlying deactivation slowing by ML277 and R-L3. Our results show their distinct mechanisms of action on channel gating. ML277 slows current activation and deactivation, with minimal effects on voltage sensor movement. These effects are consistent with a direct slowing of pore transitions. On the other hand, R-L3 slows voltage sensor deactivation with a smaller effect on current deactivation. In addition, R-L3 causes a hyperpolarizing shift in voltage-dependence of activation for both voltage sensor movement and conductance. These effects are consistent with a direct slowing of voltage sensor deactivation, which indirectly slows current deactivation. Although the effects of ML277 and R-L3 are abolished by the presence of KCNE1, the gating mechanisms of these drugs in KCNQ1 provide insight on general mechanisms of channel activation that can guide future efforts to modulate channel function.

Many antiarrhythmic agents can induce additional arrhythmia as side effects. To optimize treatment, there is a great interest in understanding mechanism-based pharmacologic rescue of channel dysfunction. The intricate gating mechanisms of voltage-dependent channels allow for different pathways of channel modulation. The combined insights from our studies show that gain-of-function in a voltage-gated channel can be achieved by altering different gating processes: voltage sensor movement, pore opening/closing, and/or the coupling between voltage sensor and the pore. Specific mechanisms of channel gain-of-function may be particularly effective for rescuing a given mechanism of channel loss-of-function. An important

next step is to investigate whether small-molecule activators exhibit mutation-specificity in their abilities to rescue channel function.

Slowing of I_{Ks} deactivation can occur outside the context of atrial fibrillation mutations and molecular activators. As previously discussed, phosphorylation of KCNQ1 during adrenergic stimulation slows I_{Ks} deactivation and allows the cardiac action potential to adapt to elevated heart rates. Dysfunction in adrenergic modification of KCNQ1 is closely associated with congenital LQTS. However, the gating mechanisms underlying deactivation slowing by phosphorylation is unclear. One hypothesis is that the addition of a negatively charged phosphate group influences the electrostatic environment of the voltage sensor, but this remains to be determined. Our VCF and modeling studies provide a paradigm for studying modulation of channel gating and can be extended to examining the effects of phosphorylation.

In summary, we have elucidated gating mechanisms that cause slowing of channel deactivation by atrial fibrillation mutations and small-molecule activators. These results suggest the importance of a β-subunit in modulating pore motions and voltage sensor-pore coupling. In addition, small-molecule activators can increase channel function by distinct gating mechanisms. Taken together, these results provide a key stepping stone in developing mechanism-specific therapies for arrhythmia.

Bibliography

1 Nerbonne, J. M. & Kass, R. S. Molecular physiology of cardiac repolarization. *Physiol Rev* **85**, 1205-1253 (2005).

2 Bohnen, M. S., Peng, G., Robey, S. H., Terrenoire, C., Iyer, V., Sampson, K. J. & Kass, R. S. Molecular Pathophysiology of Congenital Long QT Syndrome. *Physiol Rev* **97**, 89-134, doi:10.1152/physrev.00008.2016 (2017).

3 Noble, D. & Tsien, R. W. Outward membrane currents activated in the plateau range of potentials in cardiac Purkinje fibres. *J.Physiol.(Lond.) J1 - JP* **200**, 205-231 (1969).

4 Sanguinetti, M. C. & Jurkiewicz, N. K. Two components of cardiac delayed rectifier K+ current. Differential sensitivity to block by class III antiarrhythmic agents. *J.Gen.Physiol. J1 - JGP* **96**, 195-215 (1990).

5 Li, G. R., Feng, J., Wang, Z., Fermini, B. & Nattel, S. Adrenergic modulation of ultrarapid delayed rectifier K+ current in human atrial myocytes. *Circ.Res. J1 - CR* **78**, 903-915 (1996).

6 Wang, Z., Fermini, B. & Nattel, S. Rapid and slow components of delayed rectifier current in human atrial myocytes. *Cardiovascular research* **28**, 1540-1546 (1994).

7 Jost, N., Virag, L., Bitay, M., Takacs, J., Lengyel, C., Biliczki, P., Nagy, Z., Bogats, G., Lathrop, D. A., Papp, J. G. & Varro, A. Restricting excessive cardiac action potential and QT prolongation: a vital role for IKs in human ventricular muscle. *Circulation* **112**, 1392-1399, doi:10.1161/CIRCULATIONAHA.105.550111 (2005).

8 Liu, D. W. & Antzelevitch, C. Characteristics of the delayed rectifier current (IKr and IKs) in canine ventricular epicardial, midmyocardial, and endocardial myocytes. A weaker IKs contributes to the longer action potential of the M cell. *Circ.Res. J1 - CR* **76**, 351-365 (1995).

9 Varro, A., Balati, B., Iost, N., Takacs, J., Virag, L., Lathrop, D. A., Csaba, L., Talosi, L. & Papp, J. G. The role of the delayed rectifier component IKs in dog ventricular muscle and Purkinje fibre repolarization. *J Physiol* **523 Pt 1**, 67-81 (2000).

10 Volders, P. G., Sipido, K. R., Carmeliet, E., Spatjens, R. L., Wellens, H. J. & Vos, M. A. Repolarizing K+ currents ITO1 and IKs are larger in right than left canine ventricular midmyocardium. *Circulation J1 - Circ* **99**, 206-210 (1999).

11 Yue, L., Feng, J., Li, G. R. & Nattel, S. Transient outward and delayed rectifier currents in canine atrium: properties and role of isolation methods. *Am J Physiol* **270**, H2157-2168 (1996).

12 Stengl, M., Ramakers, C., Donker, D. W., Nabar, A., Rybin, A. V., Spatjens, R. L., van der Nagel, T., Wodzig, W. K., Sipido, K. R., Antoons, G., Moorman, A. F., Vos, M. A. & Volders, P. G. Temporal patterns of electrical remodeling in canine ventricular

hypertrophy: focus on IKs downregulation and blunted beta-adrenergic activation. *Cardiovascular research* **72**, 90-100, doi:10.1016/j.cardiores.2006.07.015 (2006).

13 Salata, J. J., Jurkiewicz, N. K., Jow, B., Folander, K., Guinosso, P. J., Jr., Raynor, B., Swanson, R. & Fermini, B. IK of rabbit ventricle is composed of two currents: evidence for IKs. *Am J Physiol* **271**, H2477-2489 (1996).

14 Xu, H., Guo, W. & Nerbonne, J. M. Four kinetically distinct depolarization-activated K+ currents in adult mouse ventricular myocytes. **113**, 661-678 (1999).

15 Jervell, A. & Lange-Nielsen, F. Congenital deaf-mutism, functional heart disease with prolongation of the Q-T interval and sudden death. *Am Heart J* **54**, 59-68 (1957).

16 Tranebjaerg, L., Samson, R. A. & Green, G. E. in *GeneReviews(R)* (eds R. A. Pagon *et al.*) (1993).

17 Casimiro, M. C., Knollmann, B. C., Ebert, S. N., Vary, J. C., Jr., Greene, A. E., Franz, M. R., Grinberg, A., Huang, S. P. & Pfeifer, K. Targeted disruption of the Kcnq1 gene produces a mouse model of Jervell and Lange- Nielsen Syndrome. **98**, 2526-2531 (2001).

18 Romano, C., Gemme, G. & Pongiglione, R. [Rare Cardiac Arrhythmias of the Pediatric Age. I. Repetitive Paroxysmal Tachycardia]. *Minerva Pediatr* **15**, 1155-1164 (1963).

19 Ward, O. C. A New Familial Cardiac Syndrome in Children. *J Ir Med Assoc* **54**, 103-106 (1964).

20 Kass, R. S. & Wiegers, S. E. The ionic basis of concentration-related effects of noradrenaline on the action potential of calf cardiac purkinje fibres. *J Physiol* **322**, 541-558 (1982).

21 Walsh, K. B. & Kass, R. S. Regulation of a heart potassium channel by protein kinase A and C. *Science* **242**, 67-69 (1988).

22 Shimizu, W. & Antzelevitch, C. Cellular basis for the ECG features of the LQT1 form of the long-QT syndrome: effects of beta-adrenergic agonists and antagonists and sodium channel blockers on transmural dispersion of repolarization and torsade de pointes. *Circulation* **98**, 2314-2322 (1998).

23 Schwartz, P. J., Priori, S. G., Spazzolini, C., Moss, A. J., Vincent, G. M., Napolitano, C., Denjoy, I., Guicheney, P., Breithardt, G., Keating, M. T., Towbin, J. A., Beggs, A. H., Brink, P., Wilde, A. A., Toivonen, L., Zareba, W., Robinson, J. L., Timothy, K. W., Corfield, V., Wattanasirichaigoon, D., Corbett, C., Haverkamp, W., Schulze-Bahr, E., Lehmann, M. H., Schwartz, K., Coumel, P. & Bloise, R. Genotype-phenotype correlation in the long-QT syndrome: gene-specific triggers for life-threatening arrhythmias. *Circulation* **103**, 89-95 (2001).

24 Payandeh, J., Scheuer, T., Zheng, N. & Catterall, W. A. The crystal structure of a voltage-gated sodium channel. *Nature* **475**, 353-358, doi:10.1038/nature10238 (2011).

25 Gouaux, E. & Mackinnon, R. Principles of selective ion transport in channels and pumps. *Science* **310**, 1461-1465 (2005).

26 Long, S. B., Campbell, E. B. & Mackinnon, R. Crystal structure of a mammalian voltage-dependent Shaker family K+ channel. *Science* **309**, 897-903 (2005).

27 Long, S. B., Campbell, E. B. & Mackinnon, R. Voltage sensor of Kv1.2: structural basis of electromechanical coupling. *Science* **309**, 903-908 (2005).

28 Absalom, N. L., Lewis, T. M. & Schofield, P. R. Mechanisms of channel gating of the ligand-gated ion channel superfamily inferred from protein structure. *Exp Physiol* **89**, 145-153, doi:10.1113/expphysiol.2003.026815 (2004).

29 Delmas, P., Hao, J. & Rodat-Despoix, L. Molecular mechanisms of mechanotransduction in mammalian sensory neurons. *Nat Rev Neurosci* **12**, 139-153, doi:10.1038/nrn2993 (2011).

30 Lu, Z. Mechanism of rectification in inward-rectifier K+ channels. *Annu Rev Physiol* **66**, 103-129, doi:10.1146/annurev.physiol.66.032102.150822 (2004).

31 Sanguinetti, M. C., Curran, M. E., Zou, A., Shen, J., Spector, P. S., Atkinson, D. L. & Keating, M. T. Coassembly of K(V)LQT1 and minK (IsK) proteins to form cardiac I(Ks) potassium channel. *Nature* **384**, 80-83 (1996).

32 Barhanin, J., Lesage, F., Guillemare, E., Fink, M., Lazdunski, M. & Romey, G. K(V)LQT1 and lsK (minK) proteins associate to form the I(Ks) cardiac potassium current. *Nature* **384**, 78-80 (1996).

33 Splawski, I., Shen, J., Timothy, K. W., Lehmann, M. H., Priori, S., Robinson, J. L., Moss, A. J., Schwartz, P. J., Towbin, J. A., Vincent, G. M. & Keating, M. T. Spectrum of mutations in long-QT syndrome genes. KVLQT1, HERG, SCN5A, KCNE1, and KCNE2. *Circulation* **102**, 1178-1185 (2000).

34 Dvir, M., Peretz, A., Haitin, Y. & Attali, B. Recent molecular insights from mutated IKS channels in cardiac arrhythmia. *Curr Opin Pharmacol* **15**, 74-82, doi:10.1016/j.coph.2013.12.004 (2014).

35 Bezanilla, F. How membrane proteins sense voltage. *Nat Rev Mol Cell Biol* **9**, 323-332, doi:10.1038/nrm2376 (2008).

36 Papazian, D. M., Schwarz, T. L., Tempel, B. L., Jan, Y. N. & Jan, L. Y. Cloning of genomic and complementary DNA from Shaker, a putative potassium channel gene from Drosophila. *Science* **237**, 749-753 (1987).

37 Roux, B. & MacKinnon, R. The cavity and pore helices in the KcsA K+ channel: electrostatic stabilization of monovalent cations. *Science* **285**, 100-102 (1999).

38 Zhou, Y., Morais-Cabral, J. H., Kaufman, A. & MacKinnon, R. Chemistry of ion coordination and hydration revealed by a K+ channel-Fab complex at 2.0 A resolution. *Nature* **414**, 43-48, doi:10.1038/35102009 (2001).

39 Tao, X., Hite, R. K. & MacKinnon, R. Cryo-EM structure of the open high-conductance Ca2+-activated K+ channel. *Nature*, doi:10.1038/nature20608 (2016).

40 Lu, Z., Klem, A. M. & Ramu, Y. Ion conduction pore is conserved among potassium channels. *Nature* **413**, 809-813, doi:10.1038/35101535 (2001).

41 Arrigoni, C., Schroeder, I., Romani, G., Van Etten, J. L., Thiel, G. & Moroni, A. The voltage-sensing domain of a phosphatase gates the pore of a potassium channel. *J Gen Physiol* **141**, 389-395, doi:10.1085/jgp.201210940 (2013).

42 Isacoff, E. Y., Jan, L. Y. & Minor, D. L., Jr. Conduits of life's spark: a perspective on ion channel research since the birth of neuron. *Neuron* **80**, 658-674, doi:10.1016/j.neuron.2013.10.040 (2013).

43 Kim, D. M. & Nimigean, C. M. Voltage-Gated Potassium Channels: A Structural Examination of Selectivity and Gating. *Cold Spring Harb Perspect Biol* **8**, doi:10.1101/cshperspect.a029231 (2016).

44 Hodgkin, A. L., Huxley, A. F. & Katz, B. Measurement of current-voltage relations in the membrane of the giant axon of Loligo. *J Physiol* **116**, 424-448 (1952).

45 Hodgkin, A. L. & Huxley, A. F. Currents carried by sodium and potassium ions through the membrane of the giant axon of Loligo. *J Physiol* **116**, 449-472 (1952).

46 Hodgkin, A. L. & Huxley, A. F. The components of membrane conductance in the giant axon of Loligo. *J Physiol* **116**, 473-496 (1952).

47 Hodgkin, A. L. & Huxley, A. F. Propagation of electrical signals along giant nerve fibers. *Proc R Soc Lond B Biol Sci* **140**, 177-183 (1952).

48 Hodgkin, A. L. & Huxley, A. F. The dual effect of membrane potential on sodium conductance in the giant axon of Loligo. *J Physiol* **116**, 497-506 (1952).

49 Hodgkin, A. L. & Huxley, A. F. A quantitative description of membrane current and its application to conduction and excitation in nerve. *J Physiol* **117**, 500-544 (1952).

50 Aggarwal, S. K. & MacKinnon, R. Contribution of the S4 segment to gating charge in the Shaker K+ channel. *Neuron* **16**, 1169-1177 (1996).

51 Seoh, S. A., Sigg, D., Papazian, D. M. & Bezanilla, F. Voltage-sensing residues in the S2 and S4 segments of the Shaker K+ channel. *Neuron* **16**, 1159-1167 (1996).

52 Schoppa, N. E., McCormack, K., Tanouye, M. A. & Sigworth, F. J. The size of gating charge in wild-type and mutant Shaker potassium channels. *Science* **255**, 1712-1715 (1992).

53 Papazian, D. M., Timpe, L. C., Jan, Y. N. & Jan, L. Y. Alteration of voltage-dependence of Shaker potassium channel by mutations in the S4 sequence. *Nature* **349**, 305-310, doi:10.1038/349305a0 (1991).

54 Papazian, D. M., Shao, X. M., Seoh, S. A., Mock, A. F., Huang, Y. & Wainstock, D. H. Electrostatic interactions of S4 voltage sensor in Shaker K+ channel. *Neuron* **14**, 1293-1301 (1995).

55 Larsson, H. P., Baker, O. S., Dhillon, D. S. & Isacoff, E. Y. Transmembrane movement of the shaker K+ channel S4. *Neuron* **16**, 387-397 (1996).

56 Elinder, F., Mannikko, R. & Larsson, H. P. S4 charges move close to residues in the pore domain during activation in a K channel. *J Gen Physiol* **118**, 1-10 (2001).

57 Ahern, C. A. & Horn, R. Focused electric field across the voltage sensor of potassium channels. *Neuron* **48**, 25-29, doi:10.1016/j.neuron.2005.08.020 (2005).

58 Asamoah, O. K., Wuskell, J. P., Loew, L. M. & Bezanilla, F. A fluorometric approach to local electric field measurements in a voltage-gated ion channel. *Neuron* **37**, 85-97 (2003).

59 Chanda, B., Asamoah, O. K., Blunck, R., Roux, B. & Bezanilla, F. Gating charge displacement in voltage-gated ion channels involves limited transmembrane movement. *Nature* **436**, 852-856, doi:10.1038/nature03888 (2005).

60 Posson, D. J., Ge, P., Miller, C., Bezanilla, F. & Selvin, P. R. Small vertical movement of a K+ channel voltage sensor measured with luminescence energy transfer. *Nature* **436**, 848-851, doi:10.1038/nature03819 (2005).

61 Starace, D. M. & Bezanilla, F. A proton pore in a potassium channel voltage sensor reveals a focused electric field. *Nature* **427**, 548-553, doi:10.1038/nature02270 (2004).

62 Tombola, F., Pathak, M. M. & Isacoff, E. Y. Voltage-sensing arginines in a potassium channel permeate and occlude cation-selective pores. *Neuron* **45**, 379-388, doi:10.1016/j.neuron.2004.12.047 (2005).

63 Tombola, F., Pathak, M. M., Gorostiza, P. & Isacoff, E. Y. The twisted ion-permeation pathway of a resting voltage-sensing domain. *Nature* **445**, 546-549, doi:10.1038/nature05396 (2007).

64 Freites, J. A. & Tobias, D. J. Voltage Sensing in Membranes: From Macroscopic Currents to Molecular Motions. *J Membr Biol* **248**, 419-430, doi:10.1007/s00232-015-9805-x (2015).

65 Long, S. B., Tao, X., Campbell, E. B. & MacKinnon, R. Atomic structure of a voltage-dependent K+ channel in a lipid membrane-like environment. *Nature* **450**, 376-382, doi:10.1038/nature06265 (2007).

66 Lorinczi, E., Gomez-Posada, J. C., de la Pena, P., Tomczak, A. P., Fernandez-Trillo, J., Leipscher, U., Stuhmer, W., Barros, F. & Pardo, L. A. Voltage-dependent gating of KCNH potassium channels lacking a covalent link between voltage-sensing and pore domains. *Nat Commun* **6**, 6672, doi:10.1038/ncomms7672 (2015).

67 Mannikko, R., Elinder, F. & Larsson, H. P. Voltage-sensing mechanism is conserved among ion channels gated by opposite voltages. *Nature* **419**, 837-841, doi:10.1038/nature01038 (2002).

68 Armstrong, C. M. Inactivation of the potassium conductance and related phenomena caused by quaternary ammonium ion injection in squid axons. *J Gen Physiol* **54**, 553-575 (1969).

69 Antz, C. & Fakler, B. Fast Inactivation of Voltage-Gated K(+) Channels: From Cartoon to Structure. *News Physiol Sci* **13**, 177-182 (1998).

70 Hoshi, T., Zagotta, W. N. & Aldrich, R. W. Biophysical and molecular mechanisms of Shaker potassium channel inactivation. *Science* **250**, 533-538 (1990).

71 Kurata, H. T. & Fedida, D. A structural interpretation of voltage-gated potassium channel inactivation. *Prog Biophys Mol Biol* **92**, 185-208, doi:10.1016/j.pbiomolbio.2005.10.001 (2006).

72 Hoshi, T. & Armstrong, C. M. C-type inactivation of voltage-gated K+ channels: pore constriction or dilation? *J Gen Physiol* **141**, 151-160, doi:10.1085/jgp.201210888 (2013).

73 Lopez-Barneo, J., Hoshi, T., Heinemann, S. H. & Aldrich, R. W. Effects of external cations and mutations in the pore region on C-type inactivation of Shaker potassium channels. *Receptors Channels* **1**, 61-71 (1993).

74 Smith, P. L., Baukrowitz, T. & Yellen, G. The inward rectification mechanism of the HERG cardiac potassium channel. *Nature* **379**, 833-836, doi:10.1038/379833a0 (1996).

75 Schonherr, R. & Heinemann, S. H. Molecular determinants for activation and inactivation of HERG, a human inward rectifier potassium channel. *J Physiol* **493 (Pt 3)**, 635-642 (1996).

76 Zagotta, W. N., Hoshi, T. & Aldrich, R. W. Shaker potassium channel gating. III: Evaluation of kinetic models for activation. *J Gen Physiol* **103**, 321-362 (1994).

77 Ledwell, J. L. & Aldrich, R. W. Mutations in the S4 region isolate the final voltage-dependent cooperative step in potassium channel activation. *J Gen Physiol* **113**, 389-414 (1999).

78 Horrigan, F. T., Cui, J. & Aldrich, R. W. Allosteric voltage gating of potassium channels I. Mslo ionic currents in the absence of Ca(2+). *J Gen Physiol* **114**, 277-304 (1999).

79 Horrigan, F. T. & Aldrich, R. W. Allosteric voltage gating of potassium channels II. Mslo channel gating charge movement in the absence of Ca(2+). *J Gen Physiol* **114**, 305-336 (1999).

80 Gu, N., Vervaeke, K. & Storm, J. F. BK potassium channels facilitate high-frequency firing and cause early spike frequency adaptation in rat CA1 hippocampal pyramidal cells. *J Physiol* **580**, 859-882, doi:10.1113/jphysiol.2006.126367 (2007).

81 Cox, D. H., Cui, J. & Aldrich, R. W. Allosteric gating of a large conductance Ca-activated K+ channel. *J Gen Physiol* **110**, 257-281 (1997).

82 Altomare, C., Bucchi, A., Camatini, E., Baruscotti, M., Viscomi, C., Moroni, A. & DiFrancesco, D. Integrated allosteric model of voltage gating of HCN channels. *J Gen Physiol* **117**, 519-532 (2001).

83 Barro-Soria, R., Rebolledo, S., Liin, S. I., Perez, M. E., Sampson, K. J., Kass, R. S. & Larsson, H. P. KCNE1 divides the voltage sensor movement in KCNQ1/KCNE1 channels into two steps. *Nat Commun* **5**, 3750, doi:10.1038/ncomms4750 (2014).

84 Zaydman, M. A., Kasimova, M. A., McFarland, K., Beller, Z., Hou, P., Kinser, H. E., Liang, H., Zhang, G., Shi, J., Tarek, M. & Cui, J. Domain-domain interactions determine the gating, permeation, pharmacology, and subunit modulation of the IKs ion channel. *Elife* **3**, e03606, doi:10.7554/eLife.03606 (2014).

85 Wang, Q., Curran, M. E., Splawski, I., Burn, T. C., Millholland, J. M., VanRaay, T. J., Shen, J., Timothy, K. W., Vincent, G. M., de Jager, T., Schwartz, P. J., Toubin, J. A., Moss, A. J., Atkinson, D. L., Landes, G. M., Connors, T. D. & Keating, M. T. Positional cloning of a novel potassium channel gene: KVLQT1 mutations cause cardiac arrhythmias. *Nat Genet* **12**, 17-23 (1996).

86 Takumi, T., Ohkubo, H. & Nakanishi, S. Cloning of a membrane protein that induces a slow voltage-gated potassium current. *Science J1 - sci* **242**, 1042-1045 (1988).

87 Hausdorff, S. F., Goldstein, S. A., Rushin, E. E. & Miller, C. Functional characterization of a minimal K+ channel expressed from a synthetic gene. *Biochemistry* **30**, 3341-3346 (1991).

88 Bendahhou, S., Marionneau, C., Haurogne, K., Larroque, M. M., Derand, R., Szuts, V., Escande, D., Demolombe, S. & Barhanin, J. In vitro molecular interactions and distribution of KCNE family with KCNQ1 in the human heart. *Cardiovascular research* **67**, 529-538 (2005).

89 Sakagami, M., Fukazawa, K., Matsunaga, T., Fujita, H., Mori, N., Takumi, T., Ohkubo, H. & Nakanishi, S. Cellular localization of rat Isk protein in the stria vascularis by immunohistochemical observation. *Hear Res* **56**, 168-172 (1991).

90 Neyroud, N., Tesson, F., Denjoy, I., Leibovici, M., Donger, C., Barhanin, J., Faure, S., Gary, F., Coumel, P., Petit, C., Schwartz, K. & Guicheney, P. A novel mutation in the potassium channel gene KVLQT1 causes the Jervell and Lange-Nielsen cardioauditory syndrome. **15**, 186-189 (1997).

91 Abbott, G. W. Biology of the KCNQ1 Potassium Channel. *New Journal of Science* **2014**, 26, doi:10.1155/2014/237431 (2014).

92 Panaghie, G. & Abbott, G. W. The Role of S4 Charges in Voltage-dependent and Voltage-independent KCNQ1 Potassium Channel Complexes. *J Gen Physiol* (2007).

93 Rocheleau, J. M. & Kobertz, W. R. KCNE peptides differently affect voltage sensor equilibrium and equilibration rates in KCNQ1 K+ channels. *J Gen Physiol* **131**, 59-68, doi:10.1085/jgp.200709816 (2008).

94 Nakajo, K. & Kubo, Y. KCNE1 and KCNE3 stabilize and/or slow voltage sensing S4 segment of KCNQ1 channel. *J Gen Physiol* **130**, 269-281, doi:10.1085/jgp.200709805 (2007).

95 Zaydman, M. A., Silva, J. R., Delaloye, K., Li, Y., Liang, H., Larsson, H. P., Shi, J. & Cui, J. Kv7.1 ion channels require a lipid to couple voltage sensing to pore opening. *Proc Natl Acad Sci U S A* **110**, 13180-13185, doi:10.1073/pnas.1305167110 (2013).

96 Labro, A. J., Boulet, I. R., Choveau, F. S., Mayeur, E., Bruyns, T., Loussouarn, G., Raes, A. L. & Snyders, D. J. The S4-S5 linker of KCNQ1 channels forms a structural scaffold with the S6 segment controlling gate closure. *The Journal of biological chemistry* **286**, 717-725, doi:10.1074/jbc.M110.146977 (2011).

97 Choveau, F. S., Rodriguez, N., Abderemane Ali, F., Labro, A. J., Rose, T., Dahimene, S., Boudin, H., Le Henaff, C., Escande, D., Snyders, D. J., Charpentier, F., Merot, J., Baro, I. & Loussouarn, G. KCNQ1 channels voltage dependence through a voltage-dependent binding of the S4-S5 linker to the pore domain. *J Biol Chem* **286**, 707-716, doi:10.1074/jbc.M110.146324 (2011).

98 Sanguinetti, M. C. Dysfunction of delayed rectifier potassium channels in an inherited cardiac arrhythmia. **868**, 406-413 (1999).

99 Chen, J., Mitcheson, J. S., Tristani-Firouzi, M., Lin, M. & Sanguinetti, M. C. The S4-S5 linker couples voltage sensing and activation of pacemaker channels. *Proc Natl Acad Sci U S A* **98**, 11277-11282. (2001).

100 Ferrer, T., Rupp, J., Piper, D. R. & Tristani-Firouzi, M. The S4-S5 linker directly couples voltage sensor movement to the activation gate in the human ether-a'-go-go-related gene (hERG) K+ channel. *J Biol Chem* **281**, 12858-12864, doi:10.1074/jbc.M513518200 (2006).

101 Haitin, Y. & Attali, B. The C-terminus of Kv7 channels: a multifunctional module. *J Physiol* **586**, 1803-1810, doi:10.1113/jphysiol.2007.149187 (2008).

102 Wiener, R., Haitin, Y., Shamgar, L., Fernandez-Alonso, M. C., Martos, A., Chomsky-Hecht, O., Rivas, G., Attali, B. & Hirsch, J. A. The KCNQ1 (Kv7.1) COOH terminus, a multitiered scaffold for subunit assembly and protein interaction. *J Biol Chem* **283**, 5815-5830, doi:10.1074/jbc.M707541200 (2008).

103 Robbins, J. KCNQ potassium channels: physiology, pathophysiology, and pharmacology. *Pharmacol Ther* **90**, 1-19 (2001).

104 Biervert, C., Schroeder, B. C., Kubisch, C., Berkovic, S. F., Propping, P., Jentsch, T. J. & Steinlein, O. K. A potassium channel mutation in neonatal human epilepsy. *Science* **279**, 403-406 (1998).

105 Singh, N. A., Charlier, C., Stauffer, D., DuPont, B. R., Leach, R. J., Melis, R., Ronen, G. M., Bjerre, I., Quattlebaum, T., Murphy, J. V., McHarg, M. L., Gagnon, D., Rosales, T. O., Peiffer, A., Anderson, V. E. & Leppert, M. A novel potassium channel gene, KCNQ2, is mutated in an inherited epilepsy of newborns. *Nat Genet* **18**, 25-29, doi:10.1038/ng0198-25 (1998).

106 Charlier, C., Singh, N. A., Ryan, S. G., Lewis, T. B., Reus, B. E., Leach, R. J. & Leppert, M. A pore mutation in a novel KQT-like potassium channel gene in an idiopathic epilepsy family. *Nat Genet* **18**, 53-55, doi:10.1038/ng0198-53 (1998).

107 Wang, H. S., Pan, Z., Shi, W., Brown, B. S., Wymore, R. S., Cohen, I. S., Dixon, J. E. & McKinnon, D. KCNQ2 and KCNQ3 potassium channel subunits: molecular correlates of the M-channel. *Science* **282**, 1890-1893 (1998).

108 Timpe, L. C., Schwarz, T. L., Tempel, B. L., Papazian, D. M., Jan, Y. N. & Jan, L. Y. Expression of functional potassium channels from Shaker cDNA in Xenopus oocytes. *Nature* **331**, 143-145, doi:10.1038/331143a0 (1988).

109 Ruscic, K. J., Miceli, F., Villalba-Galea, C. A., Dai, H., Mishina, Y., Bezanilla, F. & Goldstein, S. A. IKs channels open slowly because KCNE1 accessory subunits slow the movement of S4 voltage sensors in KCNQ1 pore-forming subunits. *Proc Natl Acad Sci U S A* **110**, E559-566, doi:10.1073/pnas.1222616110 (2013).

110 Schroeder, B. C., Waldegger, S., Fehr, S., Bleich, M., Warth, R., Greger, R. & Jentsch, T. J. A constitutively open potassium channel formed by KCNQ1 and KCNE3. *Nature* **403**, 196-199, doi:10.1038/35003200 (2000).

111 Barro-Soria, R., Perez, M. E. & Larsson, H. P. KCNE3 acts by promoting voltage sensor activation in KCNQ1. *Proc Natl Acad Sci U S A* **112**, E7286-7292, doi:10.1073/pnas.1516238112 (2015).

112 Cha, A. & Bezanilla, F. Characterizing voltage-dependent conformational changes in the Shaker K+ channel with fluorescence. *Neuron* **19**, 1127-1140 (1997).

113 Mannuzzu, L. M., Moronne, M. M. & Isacoff, E. Y. Direct physical measure of conformational rearrangement underlying potassium channel gating. *Science* **271**, 213-216 (1996).

114 Wang, H. G., Zhu, W., Kanter, R. J., Silva, J. R., Honeywell, C., Gow, R. M. & Pitt, G. S. A novel NaV1.5 voltage sensor mutation associated with severe atrial and ventricular arrhythmias. *J Mol Cell Cardiol* **92**, 52-62, doi:10.1016/j.yjmcc.2016.01.014 (2016).

115 Varga, Z., Zhu, W., Schubert, A. R., Pardieck, J. L., Krumholz, A., Hsu, E. J., Zaydman, M. A., Cui, J. & Silva, J. R. Direct Measurement of Cardiac Na+ Channel Conformations Reveals Molecular Pathologies of Inherited Mutations. *Circ Arrhythm Electrophysiol* **8**, 1228-1239, doi:10.1161/CIRCEP.115.003155 (2015).

116 Pantazis, A., Savalli, N., Sigg, D., Neely, A. & Olcese, R. Functional heterogeneity of the four voltage sensors of a human L-type calcium channel. *Proc Natl Acad Sci U S A* **111**, 18381-18386, doi:10.1073/pnas.1411127112 (2014).

117 Smith, P. L. & Yellen, G. Fast and slow voltage sensor movements in HERG potassium channels. *J Gen Physiol* **119**, 275-293 (2002).

118 Es-Salah-Lamoureux, Z., Fougere, R., Xiong, P. Y., Robertson, G. A. & Fedida, D. Fluorescence-tracking of activation gating in human ERG channels reveals rapid S4 movement and slow pore opening. *PLoS One* **5**, e10876, doi:10.1371/journal.pone.0010876 (2010).

119 Thouta, S., Sokolov, S., Abe, Y., Clark, S. J., Cheng, Y. M. & Claydon, T. W. Proline scan of the HERG channel S6 helix reveals the location of the intracellular pore gate. *Biophys J* **106**, 1057-1069, doi:10.1016/j.bpj.2014.01.035 (2014).

120 Bruening-Wright, A., Elinder, F. & Larsson, H. P. Kinetic relationship between the voltage sensor and the activation gate in spHCN channels. *J Gen Physiol* **130**, 71-81, doi:10.1085/jgp.200709769 (2007).

121 Osteen, J. D., Barro-Soria, R., Robey, S., Sampson, K. J., Kass, R. S. & Larsson, H. P. Allosteric gating mechanism underlies the flexible gating of KCNQ1 potassium channels. *Proc Natl Acad Sci U S A* **109**, 7103-7108, doi:10.1073/pnas.1201582109 (2012).

122 Liin, S. I., Barro-Soria, R. & Larsson, H. P. The KCNQ1 channel - remarkable flexibility in gating allows for functional versatility. *J Physiol* **593**, 2605-2615, doi:10.1113/jphysiol.2014.287607 (2015).

123 McLaughlin, S., Wang, J., Gambhir, A. & Murray, D. PIP(2) and proteins: interactions, organization, and information flow. *Annu Rev Biophys Biomol Struct* **31**, 151-175, doi:10.1146/annurev.biophys.31.082901.134259 (2002).

124 Loussouarn, G., Park, K. H., Bellocq, C., Baro, I., Charpentier, F. & Escande, D. Phosphatidylinositol-4,5-bisphosphate, PIP2, controls KCNQ1/KCNE1 voltage-gated

potassium channels: a functional homology between voltage-gated and inward rectifier K+ channels. *EMBO J* **22**, 5412-5421, doi:10.1093/emboj/cdg526 (2003).

125 Hilgemann, D. W. & Ball, R. Regulation of cardiac Na+,Ca2+ exchange and KATP potassium channels by PIP2. *Science* **273**, 956-959 (1996).

126 Huang, C. L., Feng, S. & Hilgemann, D. W. Direct activation of inward rectifier potassium channels by PIP2 and its stabilization by Gbetagamma. *Nature* **391**, 803-806, doi:10.1038/35882 (1998).

127 Bian, J., Cui, J. & McDonald, T. V. HERG K(+) channel activity is regulated by changes in phosphatidyl inositol 4,5-bisphosphate. *Circ Res* **89**, 1168-1176 (2001).

128 Wu, L., Bauer, C. S., Zhen, X. G., Xie, C. & Yang, J. Dual regulation of voltage-gated calcium channels by PtdIns(4,5)P2. *Nature* **419**, 947-952, doi:10.1038/nature01118 (2002).

129 Chuang, H. H., Prescott, E. D., Kong, H., Shields, S., Jordt, S. E., Basbaum, A. I., Chao, M. V. & Julius, D. Bradykinin and nerve growth factor release the capsaicin receptor from PtdIns(4,5)P2-mediated inhibition. *Nature* **411**, 957-962, doi:10.1038/35082088 (2001).

130 Kasimova, M. A., Zaydman, M. A., Cui, J. & Tarek, M. PIP(2)-dependent coupling is prominent in Kv7.1 due to weakened interactions between S4-S5 and S6. *Sci Rep* **5**, 7474, doi:10.1038/srep07474 (2015).

131 Chen, L., Zhang, Q., Qiu, Y., Li, Z., Chen, Z., Jiang, H., Li, Y. & Yang, H. Migration of PIP2 lipids on voltage-gated potassium channel surface influences channel deactivation. *Sci Rep* **5**, 15079, doi:10.1038/srep15079 (2015).

132 Zaydman, M. A. & Cui, J. PIP2 regulation of KCNQ channels: biophysical and molecular mechanisms for lipid modulation of voltage-dependent gating. *Front Physiol* **5**, 195, doi:10.3389/fphys.2014.00195 (2014).

133 Telezhkin, V., Reilly, J. M., Thomas, A. M., Tinker, A. & Brown, D. A. Structural requirements of membrane phospholipids for M-type potassium channel activation and binding. *J Biol Chem* **287**, 10001-10012, doi:10.1074/jbc.M111.322552 (2012).

134 Li, Y., Zaydman, M. A., Wu, D., Shi, J., Guan, M., Virgin-Downey, B. & Cui, J. KCNE1 enhances phosphatidylinositol 4,5-bisphosphate (PIP2) sensitivity of IKs to modulate channel activity. *Proc Natl Acad Sci U S A* **108**, 9095-9100, doi:10.1073/pnas.1100872108 (2011).

135 Chung, D. Y., Chan, P. J., Bankston, J. R., Yang, L., Liu, G., Marx, S. O., Karlin, A. & Kass, R. S. Location of KCNE1 relative to KCNQ1 in the I(KS) potassium channel by disulfide cross-linking of substituted cysteines. *Proc Natl Acad Sci U S A* **106**, 743-748, doi:0811897106 [pii]

10.1073/pnas.0811897106 (2009).

136 Shamgar, L., Haitin, Y., Yisharel, I., Malka, E., Schottelndreier, H., Peretz, A., Paas, Y. & Attali, B. KCNE1 constrains the voltage sensor of Kv7.1 K+ channels. *PLoS ONE* **3**, e1943, doi:10.1371/journal.pone.0001943 (2008).

137 Kang, C., Tian, C., Sonnichsen, F. D., Smith, J. A., Meiler, J., George, A. L., Jr., Vanoye, C. G., Kim, H. J. & Sanders, C. R. Structure of KCNE1 and implications for how it modulates the KCNQ1 potassium channel. *Biochemistry* **47**, 7999-8006, doi:10.1021/bi800875q (2008).

138 Osteen, J. D., Gonzalez, C., Sampson, K. J., Iyer, V., Rebolledo, S., Larsson, H. P. & Kass, R. S. KCNE1 alters the voltage sensor movements necessary to open the KCNQ1 channel gate. *Proceedings of the National Academy of Sciences of the United States of America* **107**, 22710-22715, doi:10.1073/pnas.1016300108 (2010).

139 Xu, X., Jiang, M., Hsu, K. L., Zhang, M. & Tseng, G. N. KCNQ1 and KCNE1 in the IKs channel complex make state-dependent contacts in their extracellular domains. *J Gen Physiol* **131**, 589-603, doi:jgp.200809976 [pii]

10.1085/jgp.200809976 (2008).

140 Melman, Y. F., Um, S. Y., Krumerman, A., Kagan, A. & McDonald, T. V. KCNE1 binds to the KCNQ1 pore to regulate potassium channel activity. *Neuron* **42**, 927-937 (2004).

141 Panaghie, G., Tai, K. K. & Abbott, G. W. Interaction of KCNE subunits with the KCNQ1 K+ channel pore. *J Physiol* **570**, 455-467 (2006).

142 Lvov, A., Gage, S. D., Berrios, V. M. & Kobertz, W. R. Identification of a protein-protein interaction between KCNE1 and the activation gate machinery of KCNQ1. *J Gen Physiol* **135**, 607-618, doi:10.1085/jgp.200910386 (2010).

143 Haitin, Y., Wiener, R., Shaham, D., Peretz, A., Cohen, E. B., Shamgar, L., Pongs, O., Hirsch, J. A. & Attali, B. Intracellular domains interactions and gated motions of I(KS) potassium channel subunits. *Embo J* **28**, 1994-2005 (2009).

144 Zheng, R., Thompson, K., Obeng-Gyimah, E., Alessi, D., Chen, J., Cheng, H. & McDonald, T. V. Analysis of the interactions between the C-terminal cytoplasmic domains of KCNQ1 and KCNE1 channel subunits. *The Biochemical journal* **428**, 75-84 (2010).

145 Morin, T. J. & Kobertz, W. R. Counting membrane-embedded KCNE beta-subunits in functioning K+ channel complexes. *Proc Natl Acad Sci U S A* **105**, 1478-1482, doi:0710366105 [pii]

10.1073/pnas.0710366105 (2008).

146 Plant, L. D., Xiong, D., Dai, H. & Goldstein, S. A. Individual IKs channels at the surface of mammalian cells contain two KCNE1 accessory subunits. *Proc Natl Acad Sci U S A* **111**, E1438-1446, doi:10.1073/pnas.1323548111 (2014).

147 Wang, W., Xia, J. & Kass, R. S. MinK-KvLQT1 fusion proteins, evidence for multiple stoichiometries of the assembled IsK channel. *J Biol Chem* **273**, 34069-34074 (1998).

148 Nakajo, K., Ulbrich, M. H., Kubo, Y. & Isacoff, E. Y. Stoichiometry of the KCNQ1 - KCNE1 ion channel complex. *Proc Natl Acad Sci U S A* **107**, 18862-18867, doi:1010354107 [pii]

10.1073/pnas.1010354107 (2010).

149 Murray, C. I., Westhoff, M., Eldstrom, J., Thompson, E., Emes, R. & Fedida, D. Unnatural amino acid photo-crosslinking of the IKs channel complex demonstrates a KCNE1:KCNQ1 stoichiometry of up to 4:4. *Elife* **5**, doi:10.7554/eLife.11815 (2016).

150 Tinel, N., Diochot, S., Borsotto, M., Lazdunski, M. & Barhanin, J. KCNE2 confers background current characteristics to the cardiac KCNQ1 potassium channel. **19**, 6326-6330 (2000).

151 Grunnet, M., Jespersen, T., Rasmussen, H. B., Ljungstrom, T., Jorgensen, N. K., Olesen, S. P. & Klaerke, D. A. KCNE4 is an inhibitory subunit to the KCNQ1 channel. *J Physiol* **542**, 119-130 (2002).

152 Wu, D., Delaloye, K., Zaydman, M. A., Nekouzadeh, A., Rudy, Y. & Cui, J. State-dependent electrostatic interactions of S4 arginines with E1 in S2 during Kv7.1 activation. *J Gen Physiol* **135**, 595-606, doi:10.1085/jgp.201010408 (2010).

153 Cui, J. Voltage-Dependent Gating: Novel Insights from KCNQ1 Channels. *Biophys J* **110**, 14-25, doi:10.1016/j.bpj.2015.11.023 (2016).

154 Marx, S. O., Kurokawa, J., Reiken, S., Motoike, H., D'Armiento, J., Marks, A. R. & Kass, R. S. Requirement of a macromolecular signaling complex for beta adrenergic receptor modulation of the KCNQ1-KCNE1 potassium channel. *Science* **295**, 496-499 (2002).

155 Li, Y., Chen, L., Kass, R. S. & Dessauer, C. W. The A-kinase anchoring protein Yotiao facilitates complex formation between adenylyl cyclase type 9 and the IKs potassium channel in heart. *The Journal of biological chemistry* **287**, 29815-29824, doi:10.1074/jbc.M112.380568 (2012).

156 Terrenoire, C., Houslay, M. D., Baillie, G. S. & Kass, R. S. The cardiac IKs potassium channel macromolecular complex includes the phosphodiesterase PDE4D3. *J Biol Chem* **284**, 9140-9146, doi:M805366200 [pii]

10.1074/jbc.M805366200 (2009).

157 Kurokawa, J., Chen, L. & Kass, R. S. Requirement of subunit expression for cAMP-mediated regulation of a heart potassium channel. *Proc Natl Acad Sci U S A* **100**, 2122-2127 (2003).

158 Chen, L., Kurokawa, J. & Kass, R. S. Phosphorylation of the A-kinase-anchoring protein Yotiao contributes to protein kinase A regulation of a heart potassium channel. *J Biol Chem* **280**, 31347-31352 (2005).

159 Moss, A. J. & Kass, R. S. Long QT syndrome: from channels to cardiac arrhythmias. *J Clin Invest* **115**, 2018-2024 (2005).

160 Alders, M. & Christiaans, I. in *GeneReviews(R)* (eds R. A. Pagon *et al.*) (1993).

161 Ackerman, M. J., Priori, S. G., Willems, S., Berul, C., Brugada, R., Calkins, H., Camm, A. J., Ellinor, P. T., Gollob, M., Hamilton, R., Hershberger, R. E., Judge, D. P., Le Marec, H., McKenna, W. J., Schulze-Bahr, E., Semsarian, C., Towbin, J. A., Watkins, H., Wilde, A., Wolpert, C., Zipes, D. P., Heart Rhythm, S. & European Heart Rhythm, A. HRS/EHRA expert consensus statement on the state of genetic testing for the channelopathies and cardiomyopathies: this document was developed as a partnership between the Heart Rhythm Society (HRS) and the European Heart Rhythm Association (EHRA). *Europace* **13**, 1077-1109, doi:10.1093/europace/eur245 (2011).

162 Jons, C., Moss, A. J., Lopes, C. M., McNitt, S., Zareba, W., Goldenberg, I., Qi, M., Wilde, A. A., Shimizu, W., Kanters, J. K., Towbin, J. A., Ackerman, M. J. & Robinson, J. L. Mutations in conserved amino acids in the KCNQ1 channel and risk of cardiac events in type-1 long-QT syndrome. *J Cardiovasc Electrophysiol* **20**, 859-865, doi:10.1111/j.1540-8167.2009.01455.x (2009).

163 Burgess, D. E., Bartos, D. C., Reloj, A. R., Campbell, K. S., Johnson, J. N., Tester, D. J., Ackerman, M. J., Fressart, V., Denjoy, I., Guicheney, P., Moss, A. J., Ohno, S., Horie, M. & Delisle, B. P. High-risk long QT syndrome mutations in the Kv7.1 (KCNQ1) pore disrupt the molecular basis for rapid K(+) permeation. *Biochemistry* **51**, 9076-9085, doi:10.1021/bi3009449 (2012).

164 Aidery, P., Kisselbach, J., Schweizer, P. A., Becker, R., Katus, H. A. & Thomas, D. Impaired ion channel function related to a common KCNQ1 mutation - implications for risk stratification in long QT syndrome 1. *Gene* **511**, 26-33, doi:10.1016/j.gene.2012.09.041 (2012).

165 Barsheshet, A., Goldenberg, I., J, O. U., Moss, A. J., Jons, C., Shimizu, W., Wilde, A. A., McNitt, S., Peterson, D. R., Zareba, W., Robinson, J. L., Ackerman, M. J., Cypress, M., Gray, D. A., Hofman, N., Kanters, J. K., Kaufman, E. S., Platonov, P. G., Qi, M., Towbin, J. A., Vincent, G. M. & Lopes, C. M. Mutations in cytoplasmic loops of the KCNQ1 channel and the risk of life-threatening events: implications for mutation-specific response to beta-blocker therapy in type 1 long-QT syndrome. *Circulation* **125**, 1988-1996, doi:10.1161/CIRCULATIONAHA.111.048041 (2012).

166 Chen, L., Marquardt, M. L., Tester, D. J., Sampson, K. J., Ackerman, M. J. & Kass, R. S. Mutation of an A-kinase-anchoring protein causes long-QT syndrome. *Proc Natl Acad Sci U S A* (2007).

167 Naccarelli, G. V., Varker, H., Lin, J. & Schulman, K. L. Increasing prevalence of atrial fibrillation and flutter in the United States. *Am J Cardiol* **104**, 1534-1539, doi:10.1016/j.amjcard.2009.07.022 (2009).

168 Mahida, S., Lubitz, S. A., Rienstra, M., Milan, D. J. & Ellinor, P. T. Monogenic atrial fibrillation as pathophysiological paradigms. *Cardiovascular research* **89**, 692-700, doi:10.1093/cvr/cvq381 (2011).

169 Patel, C., Yan, G. X. & Antzelevitch, C. Short QT syndrome: from bench to bedside. *Circ Arrhythm Electrophysiol* **3**, 401-408, doi:10.1161/CIRCEP.109.921056 (2010).

170 Wan, E., Abrams, J., Weinberg, R. L., Katchman, A. N., Bayne, J., Zakharov, S. I., Yang, L., Morrow, J. P., Garan, H. & Marx, S. O. Aberrant sodium influx causes cardiomyopathy and atrial fibrillation in mice. *J Clin Invest* **126**, 112-122, doi:10.1172/JCI84669 (2016).

171 Xia, M., Jin, Q., Bendahhou, S., He, Y., Larroque, M. M., Chen, Y., Zhou, Q., Yang, Y., Liu, Y., Liu, B., Zhu, Q., Zhou, Y., Lin, J., Liang, B., Li, L., Dong, X., Pan, Z., Wang, R., Wan, H., Qiu, W., Xu, W., Eurlings, P., Barhanin, J. & Chen, Y. A Kir2.1 gain-of-function mutation underlies familial atrial fibrillation. *Biochem Biophys Res Commun* **332**, 1012-1019, doi:10.1016/j.bbrc.2005.05.054 (2005).

172 Antzelevitch, C., Pollevick, G. D., Cordeiro, J. M., Casis, O., Sanguinetti, M. C., Aizawa, Y., Guerchicoff, A., Pfeiffer, R., Oliva, A., Wollnik, B., Gelber, P., Bonaros, E. P., Jr., Burashnikov, E., Wu, Y., Sargent, J. D., Schickel, S., Oberheiden, R., Bhatia, A., Hsu, L. F., Haissaguerre, M., Schimpf, R., Borggrefe, M. & Wolpert, C. Loss-of-function mutations in the cardiac calcium channel underlie a new clinical entity characterized by ST-segment elevation, short QT intervals, and sudden cardiac death. *Circulation* **115**, 442-449, doi:10.1161/CIRCULATIONAHA.106.668392 (2007).

173 Brugada, R., Hong, K., Dumaine, R., Cordeiro, J., Gaita, F., Borggrefe, M., Menendez, T. M., Brugada, J., Pollevick, G. D., Wolpert, C., Burashnikov, E., Matsuo, K., Wu, Y. S., Guerchicoff, A., Bianchi, F., Giustetto, C., Schimpf, R., Brugada, P. & Antzelevitch, C. Sudden death associated with short-QT syndrome linked to mutations in HERG. *Circulation* **109**, 30-35, doi:10.1161/01.CIR.0000109482.92774.3A (2004).

174 Chen, Y. H., Xu, S. J., Bendahhou, S., Wang, X. L., Wang, Y., Xu, W. Y., Jin, H. W., Sun, H., Su, X. Y., Zhuang, Q. N., Yang, Y. Q., Li, Y. B., Liu, Y., Xu, H. J., Li, X. F., Ma, N., Mou, C. P., Chen, Z., Barhanin, J. & Huang, W. KCNQ1 gain-of-function mutation in familial atrial fibrillation. *Science* **299**, 251-254, doi:10.1126/science.1077771 (2003).

175 Hong, K., Piper, D. R., Diaz-Valdecantos, A., Brugada, J., Oliva, A., Burashnikov, E., Santos-de-Soto, J., Grueso-Montero, J., Diaz-Enfante, E., Brugada, P., Sachse, F.,

Sanguinetti, M. C. & Brugada, R. De novo KCNQ1 mutation responsible for atrial fibrillation and short QT syndrome in utero. *Cardiovascular research* **68**, 433-440, doi:10.1016/j.cardiores.2005.06.023 (2005).

176 Das, S., Makino, S., Melman, Y. F., Shea, M. A., Goyal, S. B., Rosenzweig, A., Macrae, C. A. & Ellinor, P. T. Mutation in the S3 segment of KCNQ1 results in familial lone atrial fibrillation. *Heart Rhythm* **6**, 1146-1153, doi:10.1016/j.hrthm.2009.04.015 (2009).

177 Terrenoire, C., Clancy, C. E., Cormier, J. W., Sampson, K. J. & Kass, R. S. Autonomic control of cardiac action potentials: role of potassium channel kinetics in response to sympathetic stimulation. *Circ Res* **96**, e25-34, doi:10.1161/01.RES.0000160555.58046.9a (2005).

178 Sampson, K. J., Terrenoire, C., Cervantes, D. O., Kaba, R. A., Peters, N. S. & Kass, R. S. Adrenergic regulation of a key cardiac potassium channel can contribute to atrial fibrillation: evidence from an I Ks transgenic mouse. *J Physiol* **586**, 627-637, doi:10.1113/jphysiol.2007.141333 (2008).

179 Abitbol, I., Peretz, A., Lerche, C., Busch, A. E. & Attali, B. Stilbenes and fenamates rescue the loss of I(KS) channel function induced by an LQT5 mutation and other IsK mutants. **18**, 4137-4148 (1999).

180 Yu, H., Lin, Z., Mattmann, M. E., Zou, B., Terrenoire, C., Zhang, H., Wu, M., McManus, O. B., Kass, R. S., Lindsley, C. W., Hopkins, C. R. & Li, M. Dynamic subunit stoichiometry confers a progressive continuum of pharmacological sensitivity by KCNQ potassium channels. *Proc Natl Acad Sci U S A* **110**, 8732-8737, doi:10.1073/pnas.1300684110 (2013).

181 Nakajo, K. & Kubo, Y. Steric hindrance between S4 and S5 of the KCNQ1/KCNE1 channel hampers pore opening. *Nat Commun* **5**, 4100, doi:10.1038/ncomms5100 (2014).

182 Eyring, H. The Activated Complex in Chemical Reactions. *J Chem Phys* **3**, 107-115, doi:10.1063/1.1749604 (1935).

183 Colquhoun, D., Dowsland, K. A., Beato, M. & Plested, A. J. How to impose microscopic reversibility in complex reaction mechanisms. *Biophys J* **86**, 3510-3518, doi:10.1529/biophysj.103.038679 (2004).

184 Corana, A., Marchesi, M., Martini, C. & Ridella, S. Minimizing Multimodal Functions of Continuous-Variables with the Simulated Annealing Algorithm. *Acm T Math Software* **13**, 262-280, doi:Doi 10.1145/29380.29864 (1987).

185 Splawski, I., Tristani-Firouzi, M., Lehmann, M. H., Sanguinetti, M. C. & Keating, M. T. Mutations in the hminK gene cause long QT syndrome and suppress IKs function. *Nat Genet* **17**, 338-340, doi:10.1038/ng1197-338 (1997).

186 Bellocq, C., van Ginneken, A. C., Bezzina, C. R., Alders, M., Escande, D., Mannens, M. M., Baro, I. & Wilde, A. A. Mutation in the KCNQ1 gene leading to the short QT-

interval syndrome. *Circulation* **109**, 2394-2397, doi:10.1161/01.CIR.0000130409.72142.FE (2004).

187 Campbell, C. M., Campbell, J. D., Thompson, C. H., Galimberti, E. S., Darbar, D., Vanoye, C. G. & George, A. L., Jr. Selective targeting of gain-of-function KCNQ1 mutations predisposing to atrial fibrillation. *Circ Arrhythm Electrophysiol* **6**, 960-966, doi:10.1161/CIRCEP.113.000439 (2013).

188 Labro, A. J., Boulet, I. R., Choveau, F. S., Mayeur, E., Bruyns, T., Loussouarn, G., Raes, A. L. & Snyders, D. J. The S4-S5 linker of KCNQ1 channels forms a structural scaffold with the S6 segment controlling gate closure. *J Biol Chem* **286**, 717-725, doi:10.1074/jbc.M110.146977 (2011).

189 Restier, L., Cheng, L. & Sanguinetti, M. C. Mechanisms by which atrial fibrillation-associated mutations in the S1 domain of KCNQ1 slow deactivation of IKs channels. *J Physiol* **586**, 4179-4191, doi:10.1113/jphysiol.2008.157511 (2008).

190 Chan, P. J., Osteen, J. D., Xiong, D., Bohnen, M. S., Doshi, D., Sampson, K. J., Marx, S. O., Karlin, A. & Kass, R. S. Characterization of KCNQ1 atrial fibrillation mutations reveals distinct dependence on KCNE1. *J Gen Physiol* **139**, 135-144, doi:10.1085/jgp.201110672 (2012).

191 Murata, Y., Iwasaki, H., Sasaki, M., Inaba, K. & Okamura, Y. Phosphoinositide phosphatase activity coupled to an intrinsic voltage sensor. *Nature* **435**, 1239-1243, doi:10.1038/nature03650 (2005).

192 Smith, J. A., Vanoye, C. G., George, A. L., Jr., Meiler, J. & Sanders, C. R. Structural models for the KCNQ1 voltage-gated potassium channel. *Biochemistry* **46**, 14141-14152, doi:10.1021/bi701597s (2007).

193 Osteen, J. D., Gonzalez, C., Sampson, K. J., Iyer, V., Rebolledo, S., Larsson, H. P. & Kass, R. S. KCNE1 alters the voltage sensor movements necessary to open the KCNQ1 channel gate. *Proc Natl Acad Sci U S A* **107**, 22710-22715, doi:10.1073/pnas.1016300108 (2010).

194 Abitbol, I., Peretz, A., Lerche, C., Busch, A. E. & Attali, B. Stilbenes and fenamates rescue the loss of I(KS) channel function induced by an LQT5 mutation and other IsK mutants. *EMBO J* **18**, 4137-4148, doi:10.1093/emboj/18.15.4137 (1999).

195 Unsold, B., Kerst, G., Brousos, H., Hubner, M., Schreiber, R., Nitschke, R., Greger, R. & Bleich, M. KCNE1 reverses the response of the human K+ channel KCNQ1 to cytosolic pH changes and alters its pharmacology and sensitivity to temperature. *Pflugers Arch* **441**, 368-378 (2000).

196 Kowey, P. R. Pharmacological effects of antiarrhythmic drugs. Review and update. *Arch Intern Med* **158**, 325-332 (1998).

197 Roden, D. M. Personalized medicine to treat arrhythmias. *Curr Opin Pharmacol* **15**, 61-67, doi:10.1016/j.coph.2013.11.013 (2014).

198 Yu, H., Lin, Z., Xu, K., Huang, X., Long, S., Wu, M., McManus, O. B., Le Engers, J., Mattmann, M. E., Engers, D. W., Le, U. M., Lindsley, C. W., Hopkins, C. R. & Li, M. in *Probe Reports from the NIH Molecular Libraries Program* (2010).

199 Xu, Y., Wang, Y., Zhang, M., Jiang, M., Rosenhouse-Dantsker, A., Wassenaar, T. & Tseng, G. N. Probing binding sites and mechanisms of action of an I(Ks) activator by computations and experiments. *Biophys J* **108**, 62-75, doi:10.1016/j.bpj.2014.10.059 (2015).

200 Salata, J. J., Jurkiewicz, N. K., Wang, J., Evans, B. E., Orme, H. T. & Sanguinetti, M. C. A novel benzodiazepine that activates cardiac slow delayed rectifier K+ currents. *Mol Pharmacol* **54**, 220-230 (1998).

Appendix: Supplementary Figures and Tables

A number of control experiments and supporting data are shown here. Figure S1 demonstrates that the current generated by VCF KCNQ1 constructs co-expressed with KCNE1 can be blocked by Chromanol 293B. Figure S2 shows that UCL2077, as previously shown, effectively inhibits I_{Ks} current. In addition, the drug reduces the second component of fluorescence that is associated with channel opening. Figure S3 compares the kinetics of fluorescence activation and deactivation between previously published VCF recordings and our kinetic model of I_{Ks}. Figure S4 illustrates current traces and Rb^+/K^+ permeability ratios for true wildtype KCNQ1 and I_{Ks}. The Rb^+/K^+ ratio for KCNQ1 is higher than for I_{Ks}, similar to the VCF constructs. Figure S5 provides rate constants at -100 mV to help illustrate the deactivation pathways for our kinetic models of KCNQ1, I_{Ks}, and atrial fibrillation mutants. Figure S6 provides rate constants at -120 mV to help illustrate deactivation pathways for our kinetic models of KCNQ1 in the absence and presence of molecular activators. Figure S7 provides the model schematic; accompanying rate parameters are presented in Tables S1-S3.

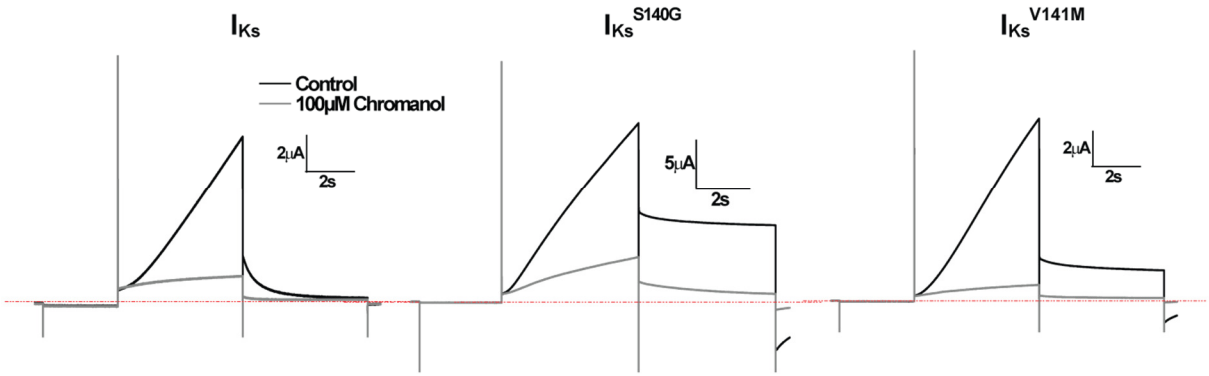

Figure S1. Chromanol 293B block of I_{Ks} and mutants. Single pulse current recordings are shown for I_{Ks}, I_{Ks}^{S140G}, and I_{Ks}^{V141M} in control condition and following application of 100 μM Chromanol 293B, with the same KCNQ1 constructs as used in VCF experiments.

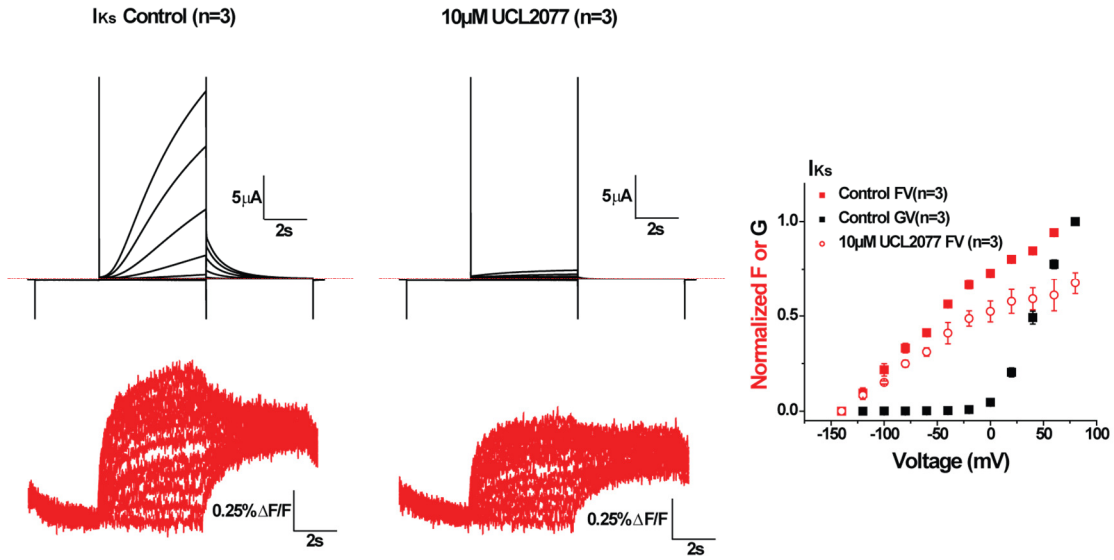

Figure S2. Effect of UCL2077 on I_{Ks} isochronal activation. Cells were held at -110 mV, prepulsed to -140 mV to deactivate channels, followed by test pulses between +80 mV and -140 mV in intervals of 20 mV, and then repolarized to -40 mV. Fluorescence traces are shown in red whereas current traces are shown in black. Plots of isochronal activation for fluorescence and conductance are shown on the right.

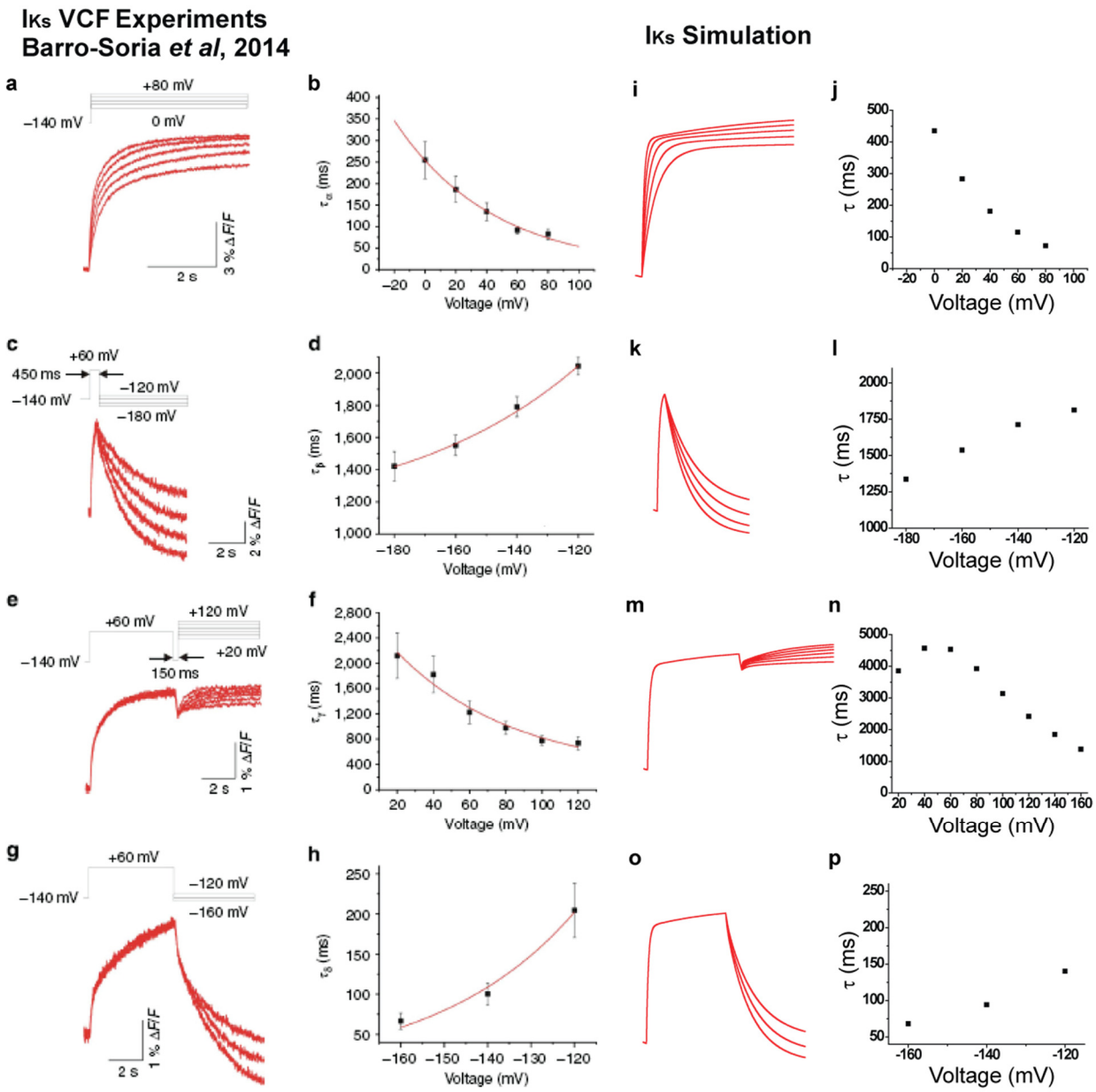

Figure S3. Comparing previous VCF experimental results with simulation of I_{Ks}. (a-h) Fluorescence traces recorded under four voltage protocols and corresponding plots of voltage-dependence of time constants for activation (b, f) and deactivation (d, h). (i-p) Simulated fluorescence traces and voltage-dependence of time constants based on the kinetic model of I_{Ks}. Panels (a-h) from Barro-Soria, R. *et al.*, 2014.

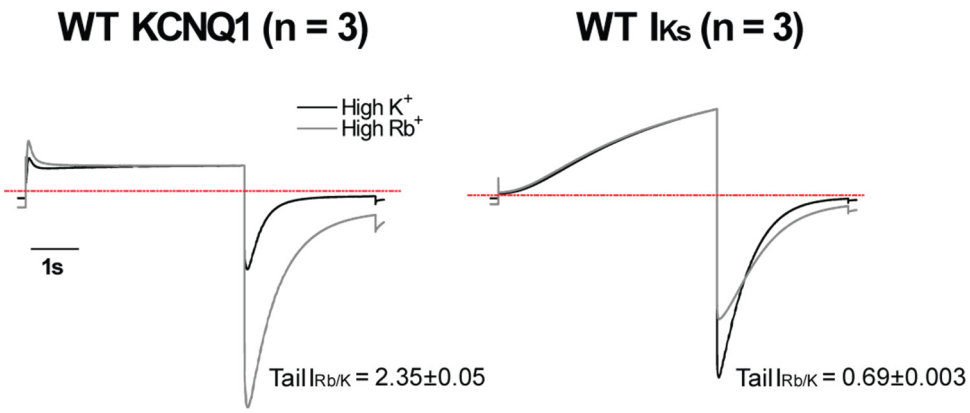

Figure S4. Determining Rb^+/K^+ permeability ratio for true wildtype KCNQ1 and I_{Ks}. Averaged current traces are shown, recorded in external solutions containing 100 mM K^+ or Rb^+.

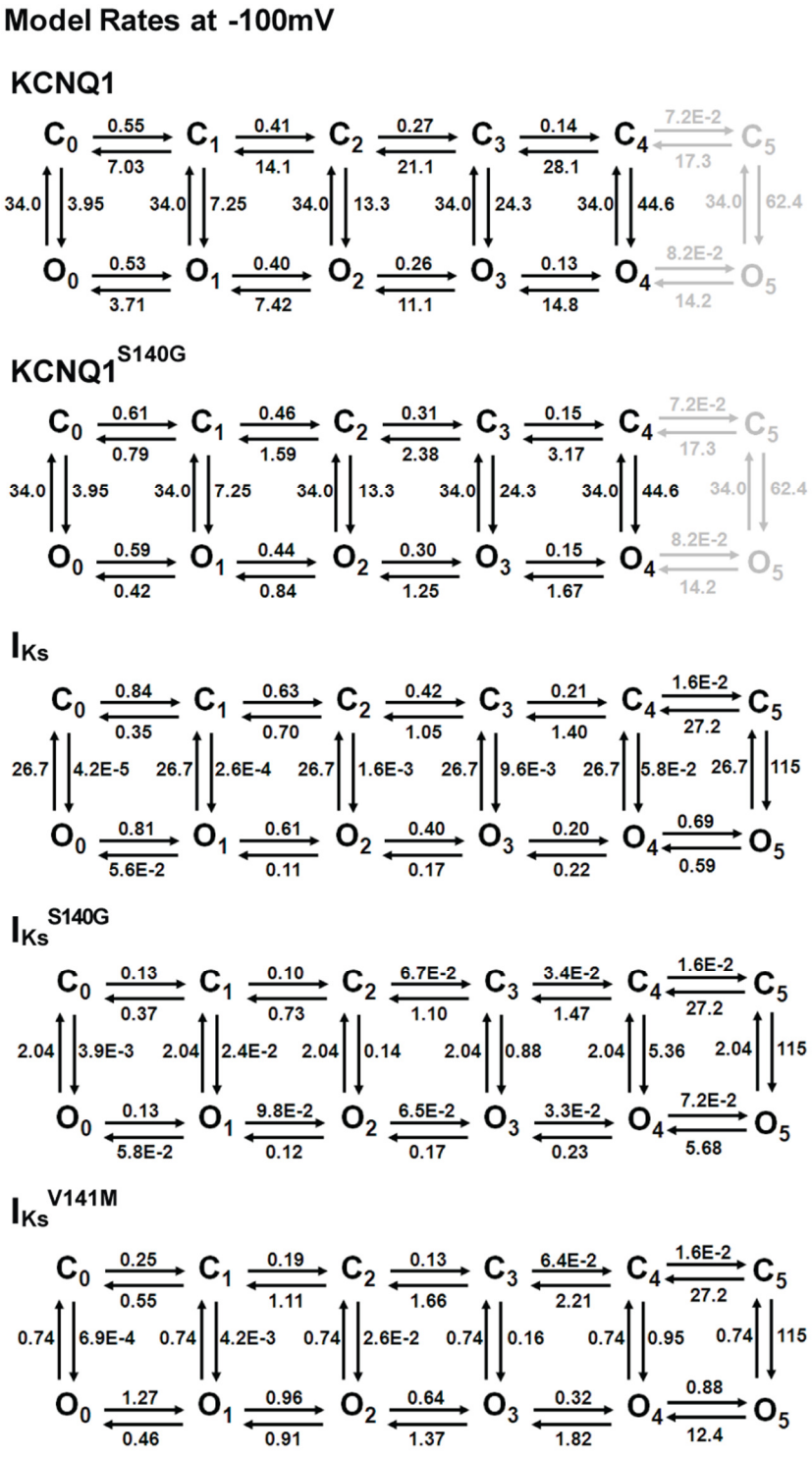

Figure S5. Model rate constants at -100 mV for atrial fibrillation mutations. Rate constants (in s^{-1}) are calculated from model parameters for KCNQ1, I_{Ks}, and mutants. For KCNQ1, the probability of channels existing in fully activated voltage sensor states (transparent) is low.

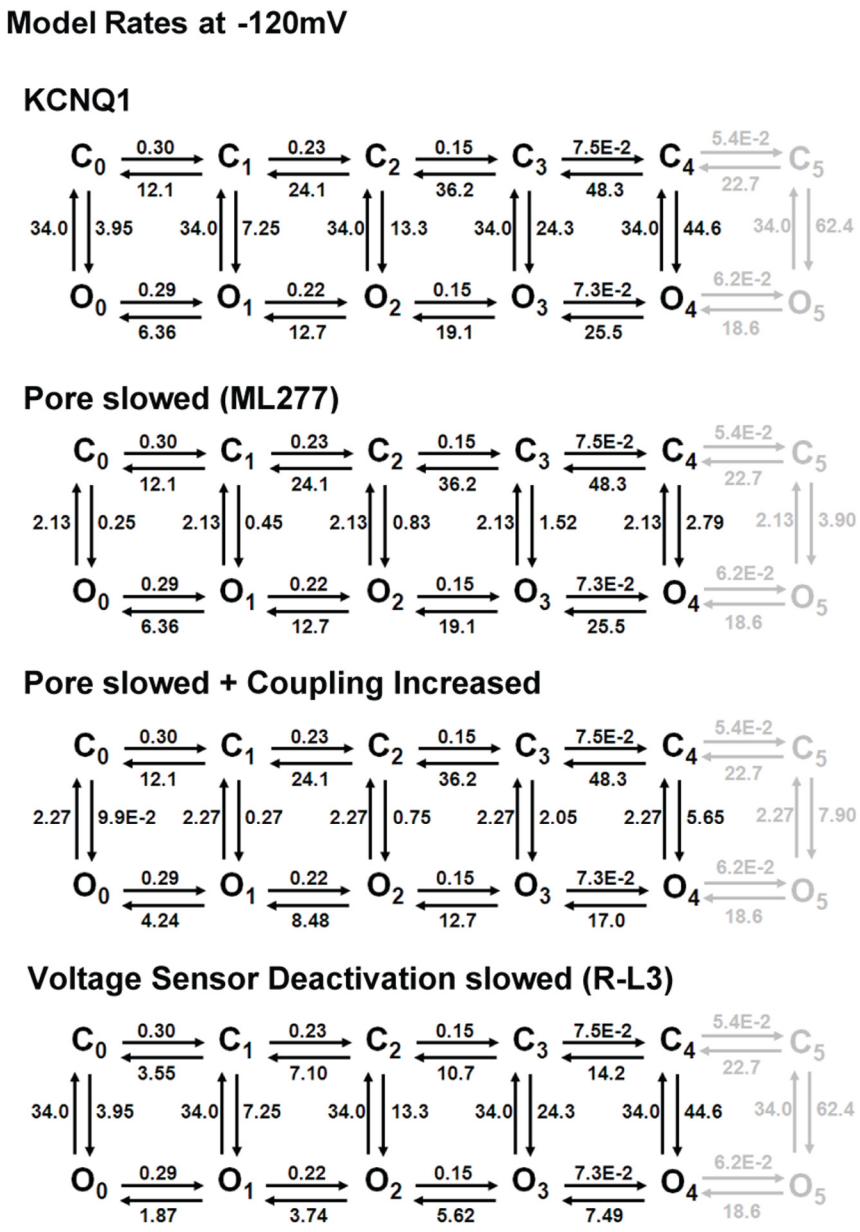

Figure S6. Model rate constants at -120 mV for molecular activators. Rate constants (in s^{-1}) are calculated from model parameters for KCNQ1 in the absence and presence of activators. The probability of channels existing in fully activated voltage sensor states (transparent) is low.

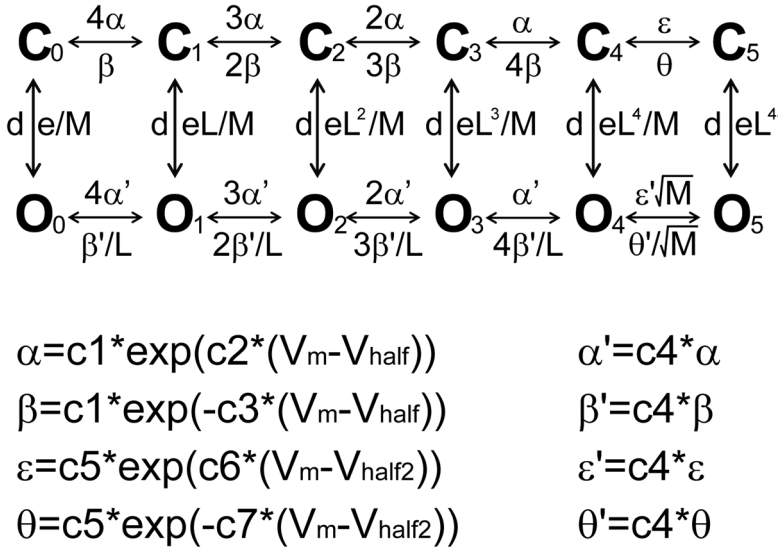

Figure S7. Model schematic.

	KCNQ1	Q1^{S140G}	Units
c1	1.079	0.3624	s^{-1}
c2	0.02977	0.02977	mV^{-1}
c3	0.02700	0.02700	mV^{-1}
c4	0.9659	0.9659	
d	34.03	34.03	s^{-1}
e	5.533	5.533	s^{-1}
vHalf	-30.56	-70.99	mV
L	1.833	1.833	
c5	1.187	1.187	s^{-1}
c6	0.01413	0.01413	mV^{-1}
c7	0.01354	0.01354	mV^{-1}
vHalf2	98.11	98.11	mV
M	1.399	1.399	
fl	0.8559	0.8559	

Table S1. Simulation parameters for KCNQ1 in the absence of KCNE1. Values altered to simulate KCNQ1^{S140G} are highlighted in yellow. The parameter fl represents the fractional fluorescence of the first component of fluorescence.

	I_{Ks}	I_{Ks}^{S140G}	I_{Ks}^{V141M}	Units
c1	0.3037	0.1890	0.3037	s^{-1}
c2	0.02320	0.02320	0.023120	mV^{-1}
c3	0.008915	0.008915	0.008915	mV^{-1}
c4	0.9659	0.9659	5	
d	26.67	2.036	0.7434	s^{-1}
e	0.08381	0.08381	0.08381	s^{-1}
vHalf	-83.97	-25.68	-32.66	mV
L	6.08	6.08	6.08	
c5	0.2083	0.2083	0.2083	s^{-1}
c6	0.01467	0.01467	0.01467	mV^{-1}
c7	0.02793	0.02793	0.02793	mV^{-1}
vHalf2	74.42	74.42	74.42	mV
M	1971	21.37	120.0	
fl	0.8559	0.8559	0.8559	

Table S2. Simulation parameters for I_{Ks}. Values altered to simulate mutants are highlighted in yellow. The parameter fl represents the fractional fluorescence of the first component of fluorescence.

	KCNQ1	Pore slowed (ML277)	VSD deactivation slowed (R-L3)	Pore slowed + increased coupling	Units
c1	1.079	1.079	0.5681	1.079	s^{-1}
c2	0.02977	0.02977	0.02977	0.02977	mV^{-1}
c3	0.02700	0.02700	0.02700	0.02700	mV^{-1}
c4	0.9659	0.9659	0.9659	0.9659	
d	34.03	2.127	34.03	2.267	s^{-1}
e	5.533	0.3458	5.533	0.1383	s^{-1}
vHalf	-30.56	-30.56	-52.12	-30.56	mV
L	1.833	1.833	1.833	2.749	
c5	1.187	1.187	1.187	1.187	s^{-1}
c6	0.01413	0.01413	0.01413	0.01413	mV^{-1}
c7	0.01354	0.01354	0.01354	0.01354	mV^{-1}
vHalf2	98.11	98.11	98.11	98.11	mV
M	1.399	1.399	1.399	1.399	
fl	0.8559	0.8559	0.8559	0.8559	
I amplitude	1	1.95	1	1.56	

Table S3. Simulation parameters for KCNQ1 and response to molecular activators. Values altered to simulate drug effects are highlighted in yellow. The parameter fl represents the fractional fluorescence of the first component of fluorescence.